UNIVERSITY OF OKLAHOMA

GRADUATE COLLEGE

CARBONACEOUS NANOSIZED SURFACTANT CARRIERS AND OIL-INDUCED VISCOELASTIC FLUID FOR POTENTIAL EOR APPLICATIONS

A DISSERTATION

SUBMITTED TO THE GRADUATE FACULTY

in partial fulfillment of the requirements for the

Degree of

DOCTOR OF PHILOSOPHY

By

CHANGLONG CHEN
Norman, Oklahoma
2018

CARBONACEOUS NANOSIZED SURFACTANT CARRIERS AND OIL-INDUCED VISCOELASTIC FLUID FOR POTENTIAL EOR APPLICATIONS

A DISSERTATION APPROVED FOR THE
MEWBOURNE SCHOOL OF PETROLEUM AND GEOLOGICAL ENGINEERING

BY

_____
Dr. Bor-Jier Shiau, Chair

_____
Dr. Jeffrey H. Harwell

_____
Dr. Ahmad Jamili

_____
Dr. Rouzbeh G. Moghanloo

_____
Dr. Xingru Wu

To my wife Lian, and my daughter Yiyun.

Acknowledgements

First of all, I would like to thank my advisors Dr. Bor-Jier Shiau and Dr. Jeffrey H. Harwell for their guidance and advice throughout my Ph.D study. Their encouragements and inspirations allowed me to expand my knowledge in the field of colloidal and interface science. I also thank them for offering me the chance and freedom to research the topic I am interested in. I would not have been able to accomplish this study without their invaluably constructive criticism, friendly advice and continuous support.

I want to express my sincere gratitude to my committee members, Dr. Ahmad Jamili, Dr. Rouzbeh G. Moghanloo, and Dr. Xingru Wu. I thank you all for taking time to supervise my research work and provide insightful comments and suggestions. I also would like to thank Dr. Brian P. Grady for his insightful discussions on rheology which facilitated my understanding of wormlike micelles.

I feel grateful to all my colleagues, Dr. Mohannad Kadhum, Dr. Javen Weston, Dr. Ngoc Hong Pham, Dr. Chien-Yuan Su, Dr. Shengbo Wang, Dr. Sangho Bang, Dr. Wei Tian, Dr. Shuoshi Wang, Zahra Sharashoob, and Maria Castillo Sanchez for their scientific discussions, advice and contributions to my research. Special thanks go to Shengbo and Shuoshi, who helped me through the struggling time in my research. Without them, the time in laboratory would not have been as pleasant as they were.

I am indebted to the Advanced Energy Consortium (AEC), who provided funding to explore MWNT's potential as surfactant carrier in reservoir applications. Also, I greatly appreciate OUHSC College of Pharmacy for sharing dynamic light scattering equipment with me, and Dr. Michael S. Detamore in Stephenson School of Biomedical Engineering to allow me using rheometer in his lab.

Finally, I would like to thank my parents and my family for their unconditional love and supports. And I would also like to thank all my friends in Norman who made my life enjoyable and memorable.

Table of Contents

List of Tables

List of Figures

Abstract

This dissertation aims to advance the conventional tertiary oil recovery method, surfactant flooding process. Via injecting a finite slug of surfactant-only or mixture of surfactant/polymer solution into reservoir, surfactants are capable to dramatically reduce the residual oil/water interfacial tension (IFT) thus mobilize trapped oil. Despite the technical viability of surfactant flooding, this approach has some difficulties to be realized at large field scale, such as substantial adsorption loss, and unfavorable sweep efficiency of surfactant-only slug.

This dissertation examined the feasibility of using carbonaceous nanoparticles, multiwalled carbon nanotube (MWNT), and carbon black as potential surfactant carriers in enhanced oil recovery. Stability of MWNT dispersion at high temperature high salinity levels, typical encountered in reservoir, as well as transport and fate of these stable nano-fluids in porous medium were first examined as a prerequisite for any field applications. MWNTs exhibited exceptional stability in 10 wt% brine by dispersing them with nonionic surfactant such as alkylphenol polyethoxylates with a large number of ethylene oxide (EO) groups. In the sandpack column test, a binary surfactant formulation, which consisted of a nonionic surfactant and an anionic surfactant in the proper ratios, exhibited an excellent capability to propagate MWNT, with 96% of the injected nanotubes recovered in the effluent. Chapter 2 presents the details of MWNT stability and transport in porous medium, which was previously published on Energy & Fuels.

A successful surfactant delivery agent requires that surfactant ought to be released from the carriers once contact the target oil. In Chapter 3, batch adsorption tests indicated that competitive adsorption of surfactant on nanoparticles was beneficial to decrease

adsorptive loss on Ottawa sand at equilibrium concentration below critical micelle concentration; microemulsions phase behavior proved spontaneous release of loaded surfactants from the treated MWNTs surfaces to oil/water interface; sand pack column tests carried out for an optimum surfactant formulation affirmed the advantage of adding nanoparticles into surfactant slug, as injection of MWNT-surfactant blend achieved faster and higher tertiary recovery than surfactant-only formulation. Chapter 3 was previously published on Fuel.

An episode in the research of stable carbonaceous nanoparticles dispersion, reversed binary micellar interactions between anionic surfactant alpha olefin sulfonate (AOS) and nonionic surfactant nonylphenol polyethylene glycol ether (NPEs) were observed depending on the addition of electrolytes. In the absence of additional electrolytes, NPEs exhibited substantially higher activity in micelles than bulk solution; with growth of EO groups, shrinkage on the scale of synergistic interaction was evidenced. In contrary, with swamping amount of electrolytes, synergistic interactions enlarged with the rise of EO groups, and AOS activity in mixed micelles was found depending on both EO length and bulk mole fraction (α_A). These findings are summarized in Chapter 4 and have been published on Colloids and Surfaces A: Physicochemical and Engineering Aspects.

Chapter 5 discovered an oil-induced viscoelastic wormlike micellar solution. Wormlike micellar solution blends are important for industrial products where the high viscosity and elastic properties are exploited. However, wormlike surfactant micelles are extremely susceptible to oils; solubilization of paraffinic oils inside the micelle core leads to a disruption of wormlike micelles and loss of viscoelasticity. Oil-induced viscoelastic micellar fluid system is promising for various reservoir applications, such as proppant

carrying fluids in hydraulic fracturing, and chemical slugs with built-in viscosity control in enhanced oil recovery.

Chapter 6 presents some concluding remarks of this work and recommendations for the future studies.

Chapter 1 Overview

1.1 Fundamentals of enhanced oil recovery

Along the production history of a hydrocarbon reservoir, the stages of production can be categorized into primary recovery, secondary recovery, and tertiary recovery. First two stages, also known as conventional recovery, basically rely on the natural drive mechanism and artificial reservoir pressure maintenance, respectively. Conventional ultimate oil recovery is about 35%.[1] Any techniques applied after secondary stage to produce oil unrecoverable by conventional means is classified tertiary recovery, also known as enhanced oil recovery (EOR).Three basic EOR process are thermal recovery, including steam flood, in-situ combustion, and steam assisted gravity drainage; solvent method including injection of miscible CO_2, hydrocarbon, nitrogen, and immiscible gases; and chemical flood, such as surfactant, polymer, and alkaline flood. EOR can achieve another 5% to 15% OOIP in a reservoir depending on the methods used.[2]

1.1.1 Oil recovery efficiency

Total oil recovery efficiency E_R, is the amount of the oil displaced divided by the initial oil in place in the swept portion of the reservoir. It is expressed as:

$$E_R = E_D \times E_V \tag{1.1}$$

Where E_V is macroscopic displacement efficiency, and E_D is microscopic displacement efficiency. The former one is defined as the fraction of the reservoir volume swept by the displacing fluid. E_V is expressed as the product of areal sweep efficiency E_A, and vertical sweep efficiency E_z,

$$E_V = E_A \times E_Z \tag{1.2}$$

E_D is defined as the volume of oil displaced from the invaded region divided by the volume of the oil initially in place in the invaded region as,[3]

$$E_D = 1 - \frac{S_{or}}{S_{oi}} \tag{1.3}$$

Where S_{or} is the residual oil saturation in the swept region, and S_{oi} is the initial oil saturation in the swept region. Clearly, increasing either E_V or E_D is beneficial to give rise to a higher ultimate oil recovery, and these are two principal mechanisms behind chemical flood. Higher E_V is achievable via polymer flooding to provide favorable mobility control, while higher E_D can be attained by injecting surfactants or alkali to reduce oil water interfacial tension (IFT).

1.1.2 Mobility and mobility ratio

The mobility of a fluid, λ, is defined as the ratio of its effective permeability to its viscosity, expressed as:

$$\lambda_i = \frac{\mathrm{k}_i}{\mu_i} \tag{1.4}$$

Where k_i is the effective permeability of the fluid, and μ_i is viscosity. Mobility ratio, M, is simply the ratio of the mobility of the displacing phase to the mobility of the displaced phase. For water displacing oil in water flooding, it is given by:

$$\mathrm{M} = \frac{\lambda_w}{\lambda_o} = \frac{\mathrm{k}_w}{\mathrm{k}_o} * \frac{\mu_o}{\mu_w} \tag{1.5}$$

Where the notation w, and o indicates water and oil phase respectively. From the definition, the displacement process is favorable if $M \leq 1$, i.e., the displaced fluid is more mobile than the displacing fluid. And the process is considered unfavorable if $M > 1$, i.e.,

the displaced fluid is less mobile than the displacing fluid. High mobility ratio could lead to viscous fingering, which can bypass a significant amount of oil.[4]

1.1.3 Capillary pressure and capillary number

Capillary pressure, p_c, is the difference in pressure of the non-wetting phase and the pressure of the wetting phase. This is represented as:

$$p_c = p_{nw} - p_w = \frac{2\sigma * \cos\theta}{r} \tag{1.6}$$

Where p_{nw}, and p_w are the pressure of non-wetting and wetting phase, respectively. σ is the water and oil interfacial tension, θ is the contact angle, and r is the effective radius of the interface. Consider a water wetting reservoir, capillary pressure could increase significantly at the pore neck, where the effective radius is extremely small, therefore, stop the oil drop from passing through the pore neck. When ultralow IFT (<0.001mN/m) is achieved, e.g., via using surfactant, the capillary pressure can reduce to a sufficient low level (four to five orders of magnitudes lower) to allow oil drop to deform then pass through the pore neck.[1]

Capillary number is defined as the ratio of viscous force (mobilizes oil) to capillary force (traps oil) by,

$$\mathrm{N}_c = \frac{v * \mu}{\sigma} \tag{1.7}$$

Where v is interstitial velocity, μ is viscosity of displacing fluid, and σ is the IFT between water and oil. Capillary number can be increased by either increasing the viscous forces or decreasing the IFT using surfactants, the latter one being a more effective and practical way to increase the capillary number by several orders of magnitude.

1.2 Surfactants, micelles, and microemulsions

Surfactants are substance, which consists of a hydrophobic hydrocarbon tail and a hydrophilic head, thus they are soluble in both oil and water phase. Surfactant has the propensity to adsorb onto the surfaces or interfaces of the system and reduce the surface or interfacial free energies of those surfaces or interfaces.[5]

Depends on the charge of head groups, surfactants are classified as anionic, cationic, nonionic, and zwitterionic. In chemical EOR, anionic surfactants are most widely used because they exhibit relatively low adsorption at neutral to high pH on both sandstones and carbonates, can be tailored to a wide range of conditions, and are widely available at relative low cost. Nonionic surfactants are used as cosurfactants to improve the behavior of surfactant system due to their excellent tolerance to salinity and hardness brine.[4]

1.2.1 Micelles and packing parameter

In the surfactant solution, once the concentration is sufficiently high, surfactant molecules will form aggregates called micelles. The concentration of surfactants above which micelles form is called the critical micelle concentration (CMC); above CMC all additional surfactants added to the system go to micelles.

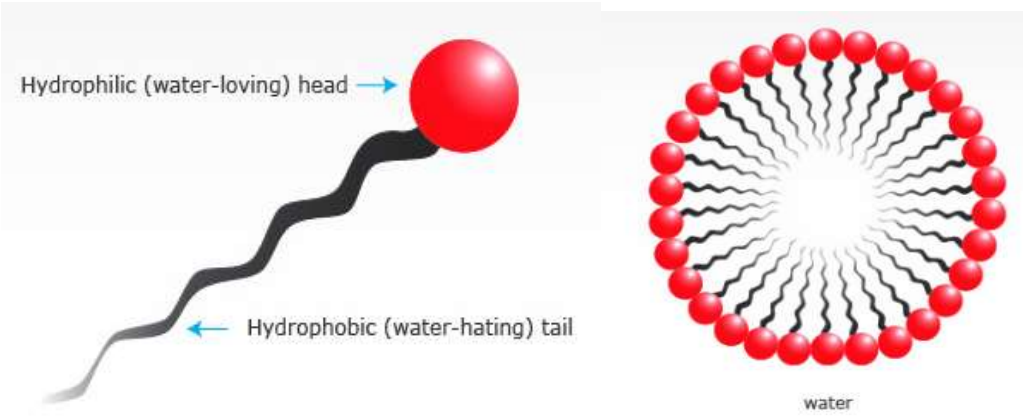

Figure 1.1. Surfactant monomer (left) and micelle (right)

Figure 1.1 shows a normal micelle, which forms in water solution, with hydrophobic hydrocarbon groups in the interior and hydrophilic head groups exposed to the external aqueous solution. Reverse micelles form in nonpolar solvents, with hydrophilic head groups oriented in the interior, and hydrophobic hydrocarbon groups exposed to the similar groups of the surrounding solvent.

Based upon the geometry of various micellar shapes and the space occupied by the hydrophilic and hydrophobic groups of the surfactant molecules, the micelle shape can be estimated by critical packing parameter (CP),[6]

$$\mathrm{CP} = \frac{V}{a_o * l_c} \tag{1.8}$$

Where V is the volume occupied by the hydrophobic groups in the micellar core, l_c is the length of the hydrophobic group in the core, and a_o is the cross-sectional area occupied by the hydrophilic group at the micelle–solution interface. The major types of micelles appear to be (1) relatively small spherical structures ($0 < \mathrm{CP} < 1/3$), (2) elongated cylindrical, rodlike micelles ($1/3 < \mathrm{CP} < 1/2$), (3) large, flat lamellar micelles ($1/2 < \mathrm{CP} < 1$), and (4) reverse micelles in nonpolar phase ($\mathrm{CP} > 1$).

Micelle structure could be tuned via altering the electrolyte content, temperature, pH, and the presence of additives in the solution. For instance, increase electrolyte content of an ionic surfactant solution will lead to a reduced a_0 due to compression of the electrical double layer. The reduction of a_0 will promote change in the shape of the micelle from spherical to cylindrical. For polyoxyethylene (POE) nonionic surfactants, an increase in temperature also cause a change in shape due to increased dehydration of the POE chain.

1.2.2 Microemulsions

To effectively displace the oil in the capillaries of reservoir rocks, IFT of 10^{-3} mN/m is generally required,[7] and microemulsion phase behavior is often conducted to design surfactant formulations with such ultralow IFT. Microemulsion is an isotropic liquid mixture of oil, water and surfactant, in thermodynamically equilibrium. Dependent on types and concentrations of surfactants and co-surfactants, species of oil, salinity and hardness of water, and temperature, different type of microemulsions may form among oil/water/surfactant system.

Winsor I microemulsions are oil in water microemulsions, in that oil is solubilized in normal micelles in the water phase; Winsor II microemulsions are water in oil microemulsion, in that water is solubilized in reverse micelles in the oil phase. And Winsor III microemulsions, also known as middle phase microemulsions, are characterized by a bi-continuous structure containing most of the surfactant in equilibrium with both excess water and excess oil phase. Winsor III microemulsions solubilize equal amount of oil and brine.[8, 9]

R ratio is a criterion to estimate the interaction of the adsorbed surfactant at the interface with the neighboring oil and water molecules by,[8]

$$R = \frac{A_{CO} - A_{oo}}{A_{Cw} - A_{ww}} \tag{1.9}$$

where A_{CO} and A_{CW} are the interaction of surfactant molecules per unit area at the interface with oil and water, respectively; A_{OO} the interaction between two oil molecules; and A_{WW} the interaction between two water molecules. $R<1$, $R = 1$ and $R>1$ correspond to Winsor I, Winsor III, and Winsor II microemulsion, respectively. Via increasing salinity in ionic surfactants or temperature in nonionic surfactants, the microemulsion

system changes from Winsor I, to Winsor III and to Winsor II and the oil/water IFT goes through a minimum value at optimal condition where R = 1.

1.2.3 Hydrophilic-Lipophilic Deviation

Phase behavior of water, oil and surfactant is one of the most important factors that determine the efficiency of chemical flood using surfactants.[10] In order to describe the behavior of surfactant induced microemulsions, Salager proposed a model called hydrophilic–lipophilic deviation (HLD) model to measure the departure from optimum formulation.[7] For ionic surfactants, HLD is written as:

$$\mathrm{HLD} = \ln S - \mathrm{K} * \mathrm{EACN} - \mathrm{f(A)} + \mathrm{Cc} - \alpha_{\mathrm{T}}\Delta\mathrm{T} \qquad (1.10)$$

Where S is the salinity of the system in grams of electrolyte per 100 ml, k is an empirical constant, $EACN$ is the equivalent alkane carbon number of the oil phase, Cc is a constant characterizing the hydrophilicity/lipophilicity of the surfactant, $f(A)$ is a function of added alcohol, α_T is an empirical constant, and $\Delta(T)$ is the temperature deviation from a reference temperature of 25 °C. Negative, zero, or positive HLD values indicate the formation of Winsor I, Winsor III or Winsor II microemulsions, respectively.

1.3 Objectives of this dissertation

Surfactant flooding was proven for decades a technically viable method from extensive laboratory efforts and numerous pilot tests, however, large field scale implementations have yet been realized due to the complexity of chemical flooding design and in many instances excessive adsorption of surfactant on formation rocks which adversely challenges economic viability of the projects. The adsorption of surfactant onto reservoir rock materials is a complex function of surfactant type, equivalent weight, and

concentration; in-situ mineral composition, and clay content; reservoir temperature; and flow rate of the solution.[4] Mechanisms of anionic surfactants adsorb onto the solid substrates from aqueous solution can in general be categorized as: ion exchange, ion pairing, hydrophobic bonding, adsorption by polarization of π electrons, and adsorption by dispersion forces.[11]

Large volume of literature has documented that surfactant adsorption onto reservoir rock material can vary from 0.2 mg/g to as high as 1.0 mg/g (mass of surfactant per mass of rock).[11, 12] Substantial adsorption loss of surfactants onto mineral surface could drastically worsen the required ultralow IFT and lead to a huge wastage on chemicals as well as manpower. Thus, a proper control of adsorption of surfactant in chemical flooding is of great importance to achieve a successful recovery operation.

Besides, surfactant is seldomly used alone in chemical flooding. Typically, a combination of a surfactant slug and a subsequent polymer slug (SP) are injected inside oil reservoir to provide both microscopic displacement efficiency as well as macroscopic sweep efficiency. However, operation with multiple slugs inevitably add the technical complexity, such as formulation compatibility with high salinity brine, e.g. TDS > 150,000 ppm in Texas and Oklahoma area, as well as huge chemical costs. Thus, a single-step process via injecting displacing agent that offers both the ultra-low interfacial tension and highly favorable mobility characteristic shall be of great interest for oilfield applications.

This dissertation aims to provide alternatives in reducing surfactant adsorption loss and improving sweep efficiency in conventional surfactant flooding process.

Carbonaceous nanoparticles, i.e., carbon nanotubes and carbon blacks were exploited as surfactant carriers in tertiary oil recovery. Carbon nanotube is allotrope of carbon with a cylindrical nanostructure, whereas carbon black is a form of paracrystalline carbon that generally produced by the incomplete combustion of heavy petroleum products. These nanosized particles are very promising material that could be applied in oil industry due to their outstanding physical and chemical properties. The superior characteristics of carbonaceous nanoparticles involve that other hydrophobic compounds or the hydrophobic moiety of an amphiphilic molecule, e.g. long surfactant tail, will strongly attract to these nanoparticle surfaces because of the entropy-driven hydrophobic interactions. Besides, enormous specific surface area of these nanoparticles (close to 250 m^2/g for nanotubes in this study) could afford substantial amount of hydrophobic molecules to be loaded onto their surfaces thus being delivered to target zone.

A single slug of oil-induced viscoelastic formulation reformed form Winsor III microemulsion was investigated as potential alternative in surfactant flooding process. Contrary to typical oleo-responsive wormlike micelles, that worms break with addition of oil, solubilized oil is capable to give rise to an exceptional viscoelastic behavior in oil-induced wormlike micellar solution. This unique formulation has the potential to drastically improve both the volumetric sweep efficiency and microscopic displacement efficiency. Injection of a single viscoelastic slug instead of multiple slugs as in traditional SP flooding has the potential of saving both operating time and chemical expenses for tertiary oil recovery operations, thus is of great significance in oilfield applications.

Reference

1. Lake, L. W.; Johns, R. T.; Rossen, W. R.; Pope, G. A., Fundamentals of enhanced oil recovery. **2014**.

2. Sheng, J., *Modern chemical enhanced oil recovery: theory and practice*. Gulf Professional Publishing: 2010.

3. Ezekwe, N., *Petroleum reservoir engineering practice*. Pearson Education: 2010.

4. Green, D. W.; Willhite, G. P., *Enhanced oil recovery*. Henry L. Doherty Memorial Fund of AIME, Society of Petroleum Engineers Richardson, TX: 1998; Vol. 6.

5. Rosen, M. J.; Kunjappu, J. T., *Surfactants and interfacial phenomena*. John Wiley & Sons: 2012.

6. Israelachvili, J. N., *Intermolecular and surface forces*. Academic press: 2011.

7. Salager, J.-L.; Forgiarini, A. M.; Bullón, J., How to attain ultralow interfacial tension and three-phase behavior with surfactant formulation for enhanced oil recovery: a review. Part 1. Optimum formulation for simple surfactant–oil–water ternary systems. *Journal of Surfactants and Detergents* **2013,** 16, (4), 449-472.

8. Winsor, P., Binary and multicomponent solutions of amphiphilic compounds. Solubilization and the formation, structure, and theoretical significance of liquid crystalline solutions. *Chemical reviews* **1968,** 68, (1), 1-40.

9. Bourrel, M.; Schechter, R. S., *Microemulsions and related systems: formulation, solvency, and physical properties*. Editions Technip: 2010.

10. Hirasaki, G.; Zhang, D. L., Surface chemistry of oil recovery from fractured, oil-wet, carbonate formations. *Spe Journal* **2004,** 9, (02), 151-162.

11. Paria, S.; Khilar, K. C., A review on experimental studies of surfactant adsorption at the hydrophilic solid–water interface. *Advances in colloid and interface science* **2004,** 110, (3), 75-95.

12. Novosad, J., Surfactant retention in berea sandstone-effects of phase behavior and temperature. *Society of Petroleum Engineers Journal* **1982,** 22, (06), 962-970.

Chapter 2 Surfactant-Only Stabilized Dispersions of Multiwalled Carbon Nanotubes in High-Electrolyte-Concentration Brines

Abstract

Multiwalled carbon nanotubes (MWNTs) exhibit promising properties for potential applications in oil production. Because of their substantial surface area, they could be used as carriers for catalysts or chemicals into subsurface oil and gas zones to change the properties of reservoir fluids or rock. A prerequisite for utilizing the MWNT in reservoir applications is to generate stable aqueous-phase dispersions that are well-dispersed and able to propagate successfully through the reservoir medium. In this study, different types of surfactants were investigated for their ability to disperse MWNTs in high-ionic-strength solutions typical of oil reservoirs up to 10% American Petroleum Institute (API) brine (8 wt% NaCl and 2 wt% $CaCl_2$). Stable nanotube dispersions in deionized water were achieved with the anionic surfactants evaluated. Compression of the electrical double layer, however, at high ionic strength, e.g., > 3 wt% electrolytes, led to rapid aggregation of the anionic surfactant-aided nanotube dispersion. This study showed that by dispersing nanotubes in nonionic surfactant such as alkylphenol polyethoxylates with a large number of ethylene oxide (EO) groups, stable MWNT dispersions were obtained in 10 wt% brine. In the sandpack column test, a binary surfactant formulation, which consisted of a nonionic surfactant and an anionic surfactant in the proper ratios, exhibited an excellent capability to propagate MWNT, with 96% of the injected nanotubes recovered in the effluent. The adsorption density of surfactants onto MWNT was determined to be 9 molecules/nm^2 from the shift of the CMC value in the surface tension

measurement. This study reveals that steric repulsion between the nanotubes could eliminate the aggregation of dispersed MWNT under the high-electrolyte-concentration condition, whereas nanotube-nanotube, and nanotube-sand surface electrical repulsion could assist in the transport of the MWNT dispersion through porous media.

2.1 Introduction

Multiwalled carbon nanotubes (MWNTs) are a very promising material that could be utilized in many applications due to their outstanding physical and chemical properties.[1] One attractive characteristic of nanoparticles, an application of which we explore in this paper, is their high specific surface area (220-300 m^2/g for the MWNTs used in this study).

Stable dispersions of nanotubes using a wide range of surfactants has been achieved previously in deionized water.[2-10] The mechanisms to stabilize suspended nanotubes rely on either electrostatic repulsion induced by adsorbed ionic surfactants or steric repulsion by nonionic surfactants, to overcome the van der Waals attraction between nanotubes.[3, 7-10] In general, surfactants disperse the nanotubes if they contain alkyl chains equal to and longer than a decyl group, regardless of the functionality of their hydrophilic heads.[2] Among ionic surfactants, sodium dodecylbenzene sulfonate (SDBS) is reported to exhibit a high dispersive efficiency.[4, 5] A detailed investigation of SDBS in dispersing nanotubes revealed that, at saturation, surfactants form a monolayer covering the nanotube surface with the tails oriented perpendicular to the surface. In addition, the presence of micelles was suggested not to be a requirement to form nanotube suspension.[6] For nonionic surfactants, it was reported that surfactants with higher molecular weight could suspend more nanotubes because of improved steric stabilization.[5] Study of Triton X-series

surfactants found that the quantity of nanotubes suspended in water were positively related to the adsorption capacities of the surfactants, but negatively with the hydrophilic fraction ratio of surfactants.[7]

Although a number of papers have shown stable nanotube dispersions created in deionized water with surfactants, to our knowledge, no study examined dispersion stability at elevated salinity conditions.

This work focuses on generating stable MWNT dispersions using surfactants at high electrolyte concentration that mimic common oil reservoir conditions. Both ionic and nonionic surfactant were examined under high ionic strength, up to 10 wt% American Petroleum Institute (API) brine (8 wt% NaCl and 2 wt% $CaCl_2$). Effects of the surfactant head group on dispersion stability were studied with several anionic surfactants possessing similar alkyl chains, approximately a dodecyl group. Extended surfactants with different propylene oxide (PO) lengths and internal olefin sulfonate (IOS) were used to compare the effect of hydrophobic tail. A series of nonionic surfactants acquired with the same hydrophobic group (4-(2,4-dimethylheptan-3-yl)phenol), but different lengths of hydrophilic polyethoxyl chain (10 EO, 20 EO, 30 EO, and 40 EO) were selected to investigate the effect of ethoxylate (EO) groups on dispersion stability in API brine.

In the surfactant solution, once the concentration is sufficiently high, surfactant molecules will form aggregates called micelles. The micelles are in an equilibrium state where surfactant molecules existing as monomers; components of the micelles are exchanging with each other and the monomers at the timescale of microseconds.[11] In the presence of MWNTs, one more equilibrium is introduced: exchange between surfactants adsorbed onto MWNTs. Since both equilibria would occur in the solution with MWNT and

micelles present simultaneously, the apparent critical micelle concentration (CMC) should be altered by the amount of surfactant adsorbed on the MWNT;[6] surfactant adsorbed on the MWNT does not contribute to the monomer concentration in solution. In this study, the adsorption capacity of the MWNT is estimated by measuring the change in the apparent CMC of the surfactant solution in the presence of the MWNT.

Once stable dispersions of MWNT in high electrolyte concentration solutions were realized, propagation studies using sand packs were conducted to explore the transport behavior of the dispersed MWNT. The main limitations for transport of carbon nanotubes in water-saturated porous media are surface retention and physical trapping[12, 13] which could be controlled by properties of MWNTs, such as material shape, size,[14, 15] and surface coating,[16, 17] as well as various physicochemical and hydrogeological parameters of the porous media, such as the solution ionic strength,[15, 18] pore water velocity,[19, 20] grain size,[21, 22] and grain roughness.[23, 24]

Early studies on the transport of nanotubes agreed that physical straining played an important role in the retention of these nanomaterials in porous media, where less mobility was observed for larger size nanotubes or in less permeable porous media.[14, 15, 21] Study found that nanotubes longer than 8 μm were preferentially retained in 40-50 mesh quartz sand.[14] However, the opposite phenomenon has also been reported, where smaller MWNT were retained to a greater extent in porous media than larger MWNT. A suggested possible reason of this unusual observation was increase in Brownian motion leading to more MWNT collisions with the porous media with decreasing size.[25]

It is well known that increasing concentrations of ions in solution facilitate deposition of mobilized colloids onto mineral surfaces due to compression the electric double layer.[26-

[28] Studies on carbon nanotubes dispersion, using both covalent and non-covalent approaches, also revealed that solution chemistry is a dominant factor controlling nanotube mobility in porous media.[15, 29-31] Research on carboxyl-functionalized single-walled carbon nanotubes (SWNT) suggested that deposition of nanomaterials onto porous medium surfaces is a key process controlling their transport in aquatic systems, with increasing solution ionic strength resulting in higher SWNT retention.[18] Divalent cations have been proved to be more effective in increasing SWNT retention than monovalent cations, where the deposition rate coefficient basically did not change appreciably above 0.1 mM $CaCl_2$ or 0.3 mM KCl.[15] SDBS coated carbon nanotubes showed excellent mobility in quartz sand pack due to increased electrostatic repulsion between nanotubes and porous media;[17, 32-34] however, when solution Ca^{2+} concentration increased from 0 to 0.88 mM, the retention of SDBS dispersed MWNTs drastically increased from 20% to 64% in quartz sand packs.[29] A recent study from our group proposed a mixed polymer system for stabilizing MWNT at high ionic strength and minimizing adsorption on the sand surfaces during propagation. In this study it was concluded that the primary dispersant, a low molecular weight polyvinyl pyrrolidone, helps disaggregation by effectively wrapping individual nanotubes, while the secondary dispersant, hydroxyethyl cellulose, inhibits the reaggregation in saline solutions[35] by introducing steric repulsion between the dispersed tubes.

Although numerous studies have shown functionalized or surfactant assisted nanotubes are highly mobile in the columns under DI water conditions, it should be anticipated that a slight increase of solution ionic strength to 10 mM could dramatically reduce mobility.

It has also been shown that in most cases MWNT attachment to the porous media was irreversible.[15, 29]

Using a procedure developed previously, MWNT dispersions used in this study are first dispersed by sonication in a solution of the primary dispersant, centrifuged, and then filtered through a one-micron glass fiber filter.[35] Only the resultant dispersion was injected into the sand pack. This procedure removes any undispersed nanotubes that can become trapped in pore throats due to physical straining, which effectively creates a filter cake at the pore throat, trapping any nanotubes subsequently reaching that location, and preventing propagation of the nanotubes. Once physical trapping has been eliminated by this preparation procedure, the dominant remaining limitations for effective MWNT propagation would be surface retention/adsorption of nanotubes onto mineral surfaces. Coating nanotubes with a physically adsorbed surfactant layer provides them with surface hydrophilicity and enables them to be dispersed in aqueous solution; additionally, steric and electrostatic repulsion of the adsorbed surfactant layer from the mineral surface prevents excessive nanotube retention. Hence, to a large extent, the retention and adsorption of MWNT in reservoir rock depends on the dispersant added to stabilize MWNT.

This work evaluates the performance of a series of surfactant-dispersed MWNTs, while varying ionic surfactant, nonionic surfactant, and anionic-nonionic surfactant mixture ratios, in terms of their ability to transport MWNTs through a porous medium in one-dimensional column tests. It will be shown that stable MWNT dispersions using binary surfactant systems exhibit a robust ability to propagate through porous media under conditions of high electrolyte concentration. The surfactant system includes a nonionic

surfactant possessing certain EO groups, together with an associated anionic surfactant, kept at a proper ratio. Our hypothesis is that the polyethoxylated nonionic surfactant provides steric repulsion between the nanotubes that eliminates coagulation of dispersed nanotubes in high electrolyte concentration condition, while anionic surfactant, with negatively charged head group, promote tube-tube, and tube-sand surface electrical repulsion, and hence ensures the MWNT dispersion transport in porous media.

2.2 Experiments

2.2.1 Materials

i. Nanomaterials

MWNTs used in this study were provided by SouthWest Nanotechnologies Inc. (SWeNT), Norman OK. In the manufacturing process nanotube growth is controlled to the desired length of approximately 1 micron (μm) with an average outer diameter of approximately 10 nanometers (nm) (SWeNT product SMW100). Transmission electron microscopy (TEM) images of the nanotube has been shown elsewhere.[36]

ii. Surfactants

Two sodium laureth sulfates ($C_{12}EOSO_4Na$, $C_{12}(EO)_3SO_4Na$), were manufactured and provided by Stepan Company (Northfield, IL) as 25.3 wt%, and 60 wt% active solutions respectively. Sodium dodecyl diphenyloxide disulfonate (SDDPDS; $C_{12}PhOPh(SO_3)_2Na_2$) exhibits very high solubility in water, including in high salinity brine. SDDPDS was purchased from Pilot Chemical Company (Cincinnati, OH) and received as 45 wt% active in solution. Alkyl propoxy sulfates (or so called extended surfactants), $C_{12,13}(PO)_4SO_4Na$ and $C_{12,13}(PO)_8SO_4Na$, contain alkyl chain of 12-13

carbons, with 4 and 8 propylene oxide units (PO), respectively. Both were provided by Sasol North America Inc. (Lake Charles, LA) as 86 wt% active solutions. One internal olefin sulfonate (IOS) surfactant,[37] with an average alkyl chain length of 19-23 carbons, was provided by Shell (Houston, TX) as 26.8 wt% active solution in water. Three nonylphenol polyethoxylates (NP10EO, NP20EO, and NP30EO) were provided by Huntsman (Salt Lake City, UT) as 100% active, having 10, 20, and 30 ethoxylate (EO) groups, respectively. Another nonylphenol ethoxylate with 40 EO's, NP40EO, was also provided by Huntsman and received as 70% active solution in water. A linear alcohol ethoxylate (LA41EO), with 40 EOs, was provided by Dow Chemical (Midland, MI) as 100% active. The structures for the surfactants are shown in Table A1 (Appendix A). Sodium chloride (NaCl) and calcium chloride dihydrate ($CaCl_2 \bullet 2H_2O$) were purchased from Sigma Aldrich.

iii. Porous media

For the sand pack tests, Ottawa sand and crushed Berea sandstone were used. Ottawa sand (F-95) was purchased from U.S. Silica. Ottawa sand size distribution is between 75 μm and 300 μm with d50 at 145 μm.[38] Crushed Berea was provided by Stim-Lab (Duncan, OK) with particle size ranging between 75 μm and 250 μm. The mean grain diameter of Berea sand is measured to be 147 μm. Both sands were used without any treatment.

2.2.2 Experimental Methods

i. Dispersion of MWNT

Stock solutions for each surfactant were prepared at 1 wt% in deionized water (DI) at room temperature. After diluting stock solutions to the target concentration, MWNTs

were added into each samples, followed by 1 hour sonication with a horn sonicator (9-12W, 20 kHz). The dispersion was then diluted with DI water or/and 20 wt% API brine to bring the MWNT concentration of 100 mg/L at the target electrolyte concentration levels (the ratio between NaCl and $CaCl_2$ was kept constant at 4:1). A stirring bar was subsequently added into the vials and the sample was placed on a stirrer for 1 hour to mix it homogeneously, followed by centrifugation at 2000 rpm for 1 hour, to allow any remaining non-dispersed nanotube aggregates to be separated from the stable, suspended nanotubes. Finally, the dispersion was filtered through a one micron glass fiber filter to remove aggregates that were not removed by the centrifugation process. The concentration of nanotubes in the dispersion was measured using an ultraviolet−visible (UV−Vis) spectrophotometer (Thermoscientific, Genesys10s) at 800 nm[29] and compared to calibration standards of known concentrations.

ii. Surfactant adsorption on MWNT

MWNT were added at a concentration of 10 mg/L into surfactant solutions of varying concentration in API brine. The suspension was then sonicated and poured into a glass beaker. The surface tension was measured by a dynamic contact angle analyzer DCA-322 (Cahn Instruments, USA) utilizing a technique based on the Wilhelmy plate principle. Details of the procedure have been mentioned elsewhere.[6]

iii. Sand pack test

Crushed Berea sandstone or Ottawa sand were dry packed into glass chromatography columns purchased from Kimble Chase®. Most experiments were run in a 1 in. (L) × 1 in. (D) sand pack at room temperature, unless otherwise stated. Porosity and permeability

of Berea sand columns were determined in our laboratory as 35% and 2.0 Darcy respectively. For the Ottawa sand packs the porosity and permeability were measured as 37.5% and 4.0 Darcy respectively.

After dry packing the columns, DI water or saline solution was injected using a Masterflex® peristaltic pump purchased from Cole Parmer®; at least 10 pore volumes (PVs) were injected through the columns from the bottom to ensure the homogeneous compaction of the sand pack. Thereafter, various surfactants suspended nanotube dispersions was injected into the column for a fixed number of PVs, followed by post-water flush at the same ionic strength, which was continued until no MWNT were detected in the effluent. Usually in these experiments an undetectable concentration of nanotube is achieved following 3 PV of water flooding. As described earlier, the injected dispersion was pre-filtered through 1 micron size glass fiber filter to eliminate any residual aggregates which may cause filter cake to form at the sand face in the column test. The experimental fluids were injected into the sand packs at a flow rate of 0.3 mL/min (pore velocity 2.8×10^{-3} cm/s). Effluent samples from the column were collected by a fraction collector at specific time intervals. They were then analyzed by a UV-Vis spectrophotometer at 800 nm wavelength. The normalized MWNT concentrations in the effluent and cumulative recovery of carbon nanotubes were plotted versus pore volumes injected.

2.3 Results and discussions

2.3.1 Dispersion of MWNT

We investigated the effectiveness of various surfactants to stabilize dispersions of MWNT under saline conditions without the presence of a water soluble polymer. Dispersants are categorized as anionic surfactant, nonionic surfactant, and anionic-nonionic binary surfactant mixtures.

i. Anionic surfactant

Preliminary screening shows that SDBS exhibited good performance to create stable, homogeneous MWNT dispersions in DI water. Eighty percent of nanotubes remain stably dispersed in the filtrate after the centrifugation and filtration steps described above, when the nanotube feed concentration was 100 mg/L. This indicates a dodecyl chain is sufficient to coat MWNTs surfaces and stabilize the dispersion properly; however, a 0.1 wt% API brine solution destabilized the SDBS nanotube dispersion.

(a) Effect of functionalized head group

Properly functionalized surfactant head groups can improve waters solubility and salinity tolerance to drastically enhance the performance of nanotube dispersions at elevated ionic strength. Four surfactants, a disulfonate, SDDPDS, a propoxysulfate, $C_{12,13}(PO)_4SO_4Na$, an ethoxysulfate, $C_{12}EOSO_4Na$, and an ethoxysulfate with a longer EO moiety, $C_{12}(EO)_3SO_4Na$, clearly illustrate the positive effects of the more electrolyte tolerant head groups on the stable dispersion of nanotubes in brine. They not only show better aqueous solubility in electrolyte than the SDBS -- up to 5 wt % electrolyte concentration -- these surfactants also possess the same dodecyl chains as the SDBS, so that the distinction in

dispersion stability at elevated ionic strength lies in the more electrolyte tolerant head groups.

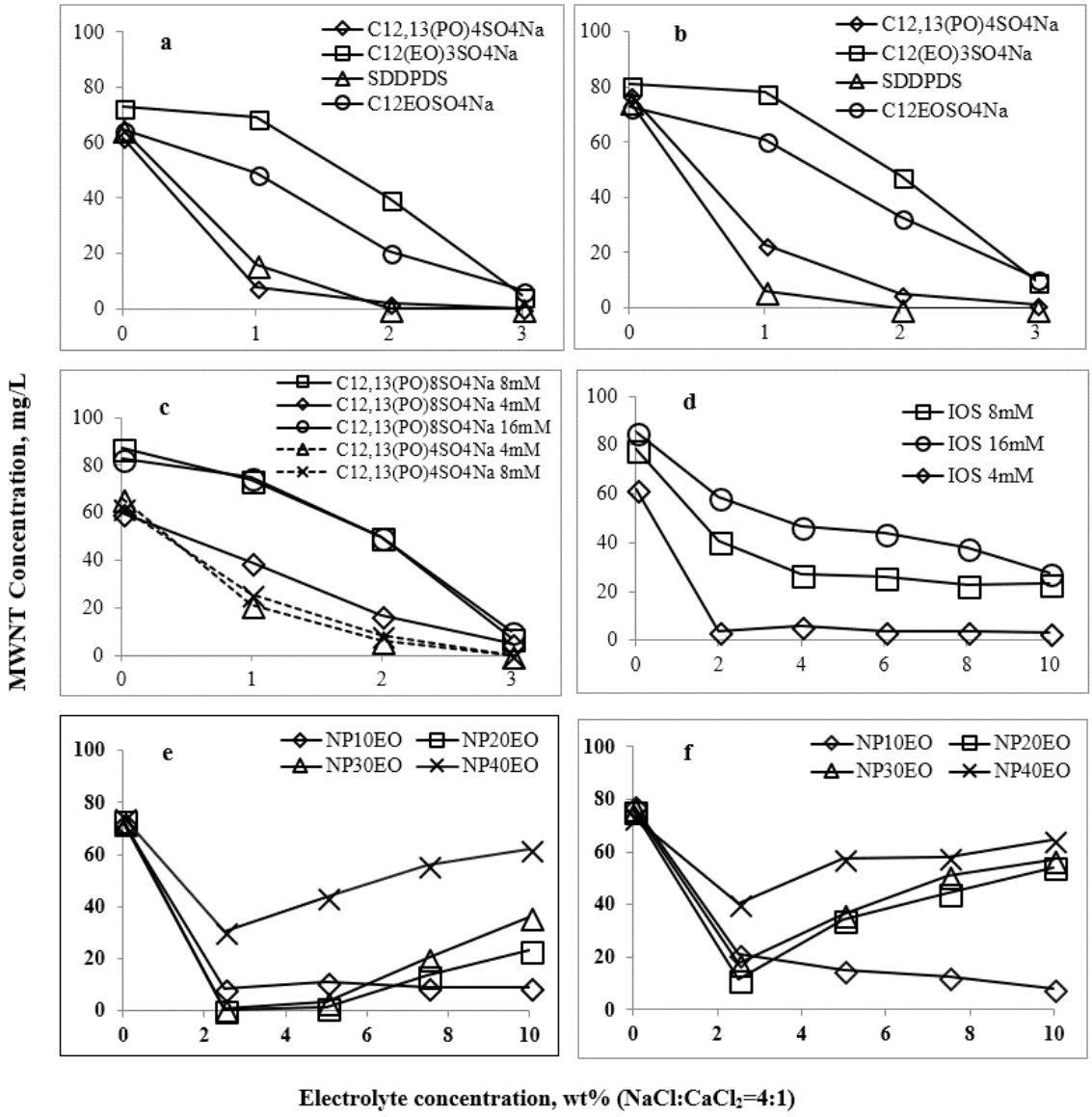

Figure 2.1. Stability of MWNT dispersions at different electrolyte concentration (NaCl : $CaCl_2$ = 4:1) a. with 4 mM anionic surfactants SDDPDS, $C_{12,13}(PO)_4SO_4Na$, $C_{12}EOSO_4Na$, and $C_{12}(EO)_3SO_4Na$; b. 8 mM anionic surfactant SDDPDS, $C_{12,13}(PO)_4SO_4Na$, $C_{12}EOSO_4Na$, and $C_{12}(EO)_3SO_4Na$; c. $C_{12,13}(PO)_8SO_4Na$ and $C_{12}(EO)_3SO_4Na$ at ratio of 3:1, with total surfactant concentration 4 mM, 8 mM, and 16 mM (solid lines); $C_{12,13}(PO)_4SO_4Na$ and $C_{12}(EO)_3SO_4Na$ at ratio of 3:1, with total concentration 4 mM and 8 mM (dashed lines); d. IOS and $C_{12}(EO)_3SO_4Na$ at ratio of 3:1; e. 1 mM NPE surfactants; f. 2 mM NPE surfactants

Figure 2.1a shows dispersed MWNTs concentrations in the filtrate with a 4 mM surfactant concentration at different ionic strength. All of these surfactants created stable dispersions in DI water. At 1 wt % brine, the concentration of MWNTs in $C_{12}(EO)_3SO_4Na$ solution dropped slightly, with a remarkable reduction in $C_{12}EOSO_4Na$ from 65mg/L to 49mg/L, while in $C_{12,13}(PO)_4SO_4Na$ and SDDPDS solutions, MWNTs concentrations were both drastically reduced to below 20 mg/L. The dispersed nanotubes with $C_{12}(EO)_3SO_4Na$ decreased linearly beyond 1 wt% electrolyte concentration, whereas in $C_{12,13}(PO)_4SO_4Na$ and SDDPDS solution, nearly all MWNTs sedimented at 2 wt % API brine.

Figure 2.2 shows the appearance of dispersed MWNTs in 4 mM $C_{12,13}(PO)_4SO_4Na$ at increasing electrolyte concentrations after filtration. The filtered samples turn from dark black, to light black, to translucent, and then to transparent at increasing ionic strength.

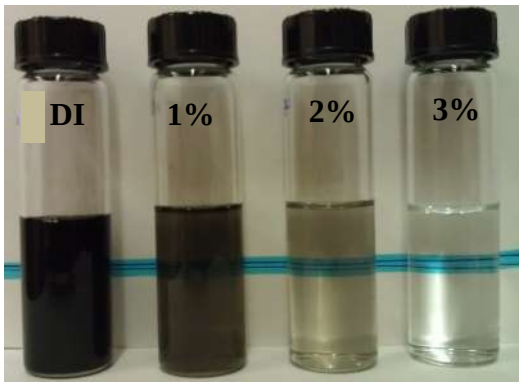

Figure 2.2. MWNT dispersion with 4 mM $C_{12,13}(PO)_4SO_4Na$ at electrolyte concentration from 0-3%.

In DI water, surfactant tails adsorb onto nanotube surfaces due to hydrophobic attraction, with hydrophilic heads directed toward aqueous solution.[3, 6, 7] The ionic head creates charged layers on the nanotubes, which exert repulsive force to prevent similarly charged nanotubes from moving close enough to each other to become flocculated by van der

Waals attraction.[8-10] The addition of electrolyte, however, compresses the electrical double layer around the nanotubes, allowing the nanotubes to approach closely enough to aggregate.

Compared to the other anionic surfactants ($C_{12,13}(PO)_4SO_4Na$ and SDDPDS), the ionic head group (SO_4^-) of sodium laureth sulfates (SLES EO_1 and EO_3) is attached to hydrophilic EO groups separating the head group from the alkyl chain; this is known to improve the hardness and salinity tolerance of anionic surfactants. Improved dispersion stability with the laureth sulfates was observed with SLES's at 1 wt % and 2 wt % electrolyte concentration. It is obvious that the 3 EO groups in $C_{12}(EO)_3SO_4Na$ are more effective to enhance dispersion stability than the single EO in $C_{12}EOSO_4Na$. It is suggested that under low electrolyte concentration conditions, although the electrostatic repulsive force between nanotubes due to the adsorbed sulfate groups is reduced as a result of compression of the electrical double layer, the EO groups with less salt sensitivity could still extend sufficiently into the aqueous phase to produce a steric barrier to prevent the close approach of nanotubes. However, at higher electrolyte concentrations, the steric contribution becomes inadequate to stop close approach of the surfactant coated nanotubes, due to further reduction in repulsive forces, which results in the attractive van der Waals force becoming dominant, as predicted by DLVO theory.

Dispersion stability in increased surfactant concentrations (8 mM) is shown in Figure 2.1b. It is clear that doubling the concentration of surfactants used did not improve stability of MWNT dispersion significantly. This is consistent with the distribution of surfactant between a monomer phase in solution, micellar pseudophase that does not contribute to additional adsorption of surfactant on the nanotubes, and an adsorbed

surfactant layer on surface of the nanotubes: surfactant micelles do not increase the surfactant adsorption density on the nanotubes and do not contribute to the repulsive forces between the surfactant-coated nanotubes.

(b) Effect of hydrophobic tail

Surfactant is believed to adsorb onto the nanotube surface because of strong hydrophobic interactions; therefore, an increase in the hydrophobe size of the surfactant should increase the magnitude of adsorption[39] and is expected to improve nanotube dispersion stability. $C_{12,13}(PO)_8SO_4Na$ and IOS were selected to study the effects of hydrophobe size on dispersion stability. Since the solubility of surfactant monomers decreases with increase in length of the hydrophobic tail, $C_{12}(EO)_3SO_4Na$ is used as solubilizer at a molar ratio of 1:3 to the main surfactant. The total surfactant concentrations were varied at 4 mM, 8 mM, and 16 mM. $C_{12,13}(PO)_4SO_4Na$ and $C_{12}(EO)_3SO_4Na$-only solution was used as a base case with the same molar ratio.

At 4 mM total surfactant concentration, $C_{12,13}(PO)_8SO_4Na$ exhibited a steady decrease in the concentration of suspended MWNTs from 0 to 3 wt% electrolyte. At 8 mM surfactant concentration, more MWNTs were dispersed due to increasing surfactants available in the solution. However, further increase of surfactant concentration up to 16 mM did not show obvious benefit compared to the 8 mM concentration. It is possible that the larger PO moiety present in $C_{12,13}(PO)_8SO_4Na$ creates better hydrophobic bonding with nanotube surfaces, consequently, better stability is observed compared to $C_{12,13}(PO)_4SO_4Na$, as displayed by the dashed lines in Figure 2.1c.

Figure 2.1d illustrates the stability of IOS dispersed MWNTs over a wider electrolyte concentration range up to 10 wt%. Better performance with IOS in brine conditions is

possibly due to a twin-tail structure of IOS which maybe have higher hydrophobic interaction with nanotube surfaces than a single alkyl chain surfactant does. The plateau region appearing at high electrolyte concentration is likely due to a balance achieved between electrostatic repulsive and van der Waals attractive interaction among the dispersed nanotubes. The addition of counterions (Na^+, Ca^{2+}) can compress the electrical double layer surrounding the ionic heads of adsorbed surfactants; as a result, there will be a reduction in repulsion between the surfactants, which allows more surfactants to be adsorbed. Higher adsorbed surfactant density has two effects: a. increasing the van der Waals attractive force between individual dispersed nanotubes; b. enhancing the electrostatic repulsive force due to increased electrical charge on the nanotube. If the increase of repulsive force is greater than that of the attractive force, the net repulsion will prevent aggregation of the nanotubes. Better stability was observed at 16 mM surfactant concentration, which also implied higher adsorption occurred.

ii. Nonionic surfactant

SLESs exhibited better suspendability of MWNT compared to other anionic surfactants in low electrolyte concentration. It is believed that the hydrated EO groups in SLES extend into the aqueous phase and thus present a steric barrier to inhibit the close approach of individually dispersed nanotubes to each other. To further analyze the effect of EO groups on the stability of nanotubes dispersions, a series of nonionic nonylphenol ethoxylates (NPE) surfactants with EOs between 10 to 40, NP10EO, NP20EO, NP30EO, and NP40EO, were studied.

(a) Effect of EO groups

Figure 2.1e and Figure 2.1f display results for stability tests with 1 mM, and 2 mM concentrations of various NPE's, respectively. As can be seen, all the surfactants tested created stable dispersion in DI water. It is interesting to note that the concentration of suspended MWNTs decreased significantly at an electrolyte concentration of 2.5 wt% for all four surfactants but recovered at higher ionic strength. While we have not tried to verify the mechanism for this phenomenon, one possible explanation is the presence of impurities in these highly ethoxylated surfactants. At electrolyte concentration of 10 wt%, NP40EO suspended more than 60 mg/L of MWNTs in the filtrate. It is believed that strong steric barriers were created when 40 ethoxylates groups in NP40EO extend into the aqueous phase, which inhibited the dispersed nanotubes from flocculating. Doubling the surfactant concentration gave similar stability performance for NP40EO, but significant enhancement for NP20EO and NP30EO was observed by increasing the surfactant concentration. The levels of dispersed nanotubes concentrations improved from 23 mg/L to 54 mg/L for NP20EO, and 36 mg/L to 57 mg/L for NP30EO, respectively, when surfactant concentration increased from 1 mM to 2 mM at 10 wt% brine.

A stock solution with 1 mM NP40EO and 100 mg/L MWNT was prepared in 10 wt% API brine and split into two vials. One was left in room temperature, the other one was kept in a 50 ^{o}C oven. Their stabilities were monitored over a one month period. As seen in Figure 2.3, the stability for both samples are well maintained during the observation period, which demonstrates the longevity of NP40EO stabilized MWNT dispersions.

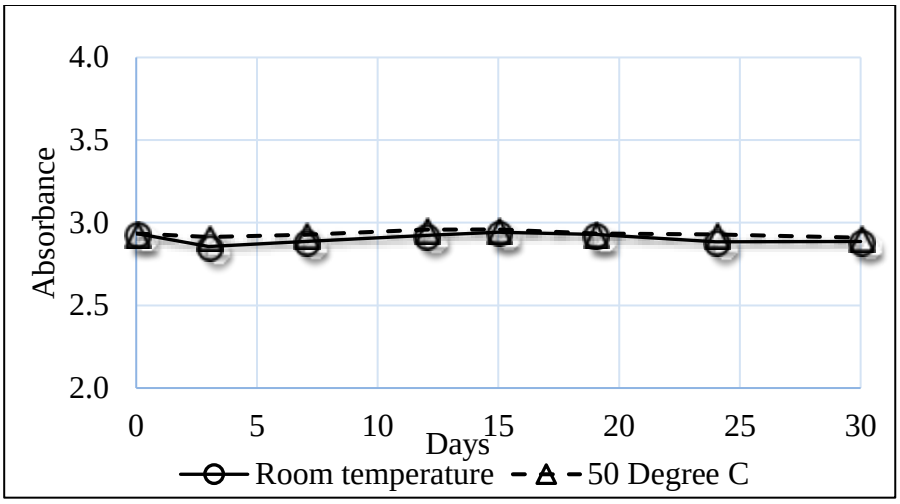

Figure 2.3. 30 days' stability of NP40EO-MWNT dispersion at room temperature and 50 ºC

(b) Suspendability MWNT at varying NP40EO concentrations

It is obvious that NP40EO has excellent performance to stabilize MWNTs dispersion at high ionic strength conditions. As a dispersant, the lower concentration of NP40EO required to stabilize nanotubes means better suspendability, and also means more economically viable in field application. Hence, how much NP40EO is necessary to suspend carbon nanotubes in API brine is important.

Table 2.1. Suspendability of NP40EO with MWNT dispersion in API brine

NP40EO, mM	0.1	0.25	0.5	1.0	1.25
MWNT, mg/L	1.7	47.0	56.6	68.4	73.4

Five scenarios were designed; in each of them, 100 mg/L MWNTs were prepared with different amount of NP40EO, varying at 0.1, 0.25, 0.5, 1.0, and 1.25 mM. Concentration of MWNTs in the filtrate were measured after high speed centrifuge to assess their suspendability. As shown in Table 2.1, at the lowest concentration of 0.1 mM NP40EO, hardly any nanotubes survived at 10% API brine. While with only 0.25 mM NP40EO, nearly half of MWNTs remained in stable dispersion. More nanotubes were detected in

the filtrate by increasing the amount of NP40EO used. A total of 1.25 mM is adequate to suspend more than 70% of MWNTs introduced.

iii. Binary anionic-nonionic surfactant formulations

Ionic surfactants stabilize the dispersed tubes mainly by electrostatic repulsion, whereas the stabilization mechanism of nonionic surfactant-coated tubes is mainly achieved by steric repulsion.[3, 7-9] Unfortunately, the ionic surfactants can hardly suspend nanotubes at ionic strength greater than 3 wt% API brine due to compression of electrical double layer. With nonionic surfactant, steric repulsion is not as susceptible to ionic strength change as electrical repulsion, therefore carbon nanotubes are highly stabilized even at high electrolyte solution. It is expected, however, that the adsorption density of the highly ethoxylated nonionic surfactants on the nanotube surfaces is likely much lower than that of ionic surfactants due to steric repulsion between the large headgroups of the nonionics. This suggests that a combination of ionic and nonionic surfactants might produce a superior dispersion of nanotubes in brines.

Stability of binary nonionic-ionic surfactant mixture were investigated with two binary systems. Both samples consisted of 1 mM NP40EO, while one contained 6 mM IOS, and the other included 6 mM $C_{12,13}(PO)_8SO_4Na$. 75% of the original charge of MWNTs was suspended in the sample with IOS/NP40EO, while 80% remain suspended in $C_{12,13}(PO)_8SO_4Na$ /NP40EO after filtration. By introducing small amounts of nonionic surfactant NP40EO, anionic surfactant could also achieve stable nanotube dispersions in 10 wt% API brine.

In a separate test, two more samples were made to observe synergistic effects in binary systems of anionic and nonionic surfactants. Both samples contained 0.25 mM NP40EO,

but differed in $C_{12,13}(PO)_8SO_4Na$ concentration, one having 0.67 mM and the other one with 1.33 mM. The base case was a dispersion stabilized by only 0.25 mM NP40EO in API brine, which gave 47 mg/L MWNT suspended in the filtrate as shown in Table 2.1. With 0.67 mM $C_{12,13}(PO)_8SO_4Na$, 19% more (56 mg/L) nanotubes were suspended, which indicated the improvement by mixing anionic surfactant with nonionic surfactant to form the MWNT dispersion. When the $C_{12,13}(PO)_8SO_4Na$ concentration was increased to 1.33 mM, only 7.7% more nanotubes (60.3 mg/L) were suspended as compared to 0.67 mM $C_{12,13}(PO)_8SO_4Na$. In this nonionic-anionic surfactant stabilized MWNT dispersion, nanotubes are believed to be coated by both anionic and nonionic surfactants, but the steric repulsion is considered as the dominant force to prevent coagulation of dispersed nanotubes in brine condition, the anionic surfactants serving primarily to increase the adsorption density on the surface of the nanotubes.

iv. Surfactant adsorption density onto MWNTs

The CMC of a binary surfactant mixture, alkyl propoxy sulfate $C_{12,13}(PO)_4SO_4Na$ and linear alcohol ethoxylates LA41EO, was measured at constant molar ratio of 1:4 in API brine in the absence and the presence of MWNT (10 mg/L). This was the maximum concentration of MWNT that could be suspended at concentrations of surfactant near the CMC of the surfactant mixture. The result is depicted in Figure 2.4. It is obvious that the 10 mg/L concentration of MWNT affects an apparent increase of the CMC of the mixed surfactant by approximately 46 mg/L, which is a 77% increase of the CMC without MWNT added.

The surfactant adsorption density onto MWNT surface is calculated by:

$$A_D = \frac{\frac{(CMC_2 - CMC_1)}{MW_{avg}} * N_A}{10^{18} * C_{MWNT} * SA} \quad (2.1)$$

Where A_D is surfactant adsorption density in molecules/nm^2, CMC_2, CMC_1 are critical micelle concentration in mg/L of surfactants with and without nanotubes respectively, C_{MWNT} is the concentration of nanotube in mg/L, $MW_{avg}$is average molecular weight of surfactant mixture in g/mol, N_A is Avogadro's number, SA is specific surface area of MWNT in m^2/g.

The calculated adsorption density of surfactant on CNT surface is 9 molecules/nm^2. As a comparison, a typical head area of an anionic surfactant residing at the gas/liquid interface is about 0.5/ nm^2,[11] in other words, a unit surface area of 1 nm^2 is occupied by 2 surfactant molecules at monolayer saturation. For nonionic surfactants the typic adsorption density at the air/water interface is approximately 1 molecule per square nanometer. Obviously, adsorption density of surfactant on CNT surface is much higher than that which occurs at the gas/liquid interface. The approximate cross sectional area of a methylene chain is about 0.2 nm^2.[11] For 1 nm^2 area on nanotube surface, a maximum packing number in a monolayer is 5 molecules, allowing for the alkyl chains to be packed perpendicular to the MWNT surface. Thus, for an adsorption density of 9 molecules/nm^2, it is anticipated that multilayer adsorption would have to occur on the nanotube surface. A physical mechanism by which this could occur is not obvious, though perhaps there is some affect from the curvature of the nanotube surface.

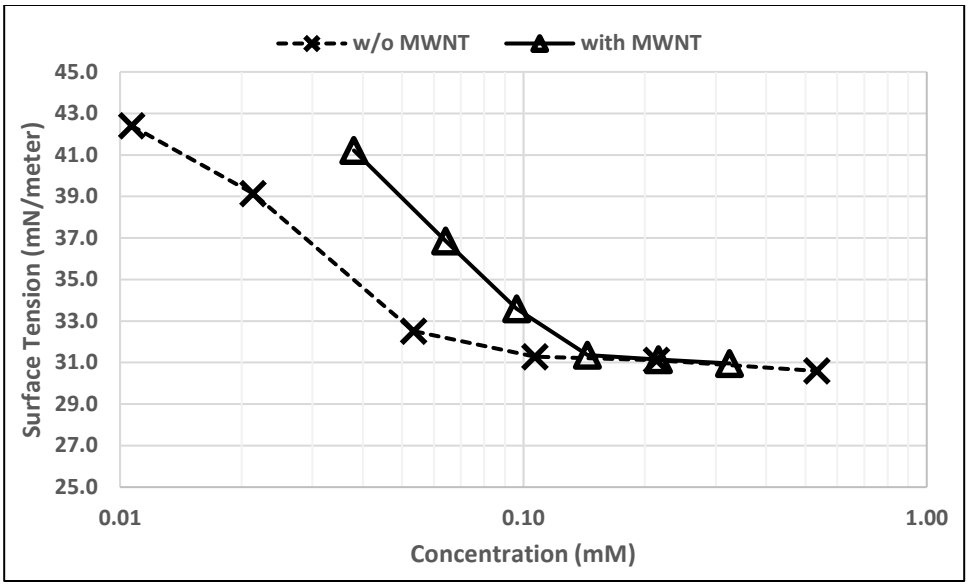

Figure 2.4. Surface tension measurement, CMC $_{\text{w/o MWNT}}$ = 0.0654 mM (60 mg/L), and CMC $_{\text{with MWNT}}$ =0.1103 mM (106 mg/L)

2.3.2 Sand pack tests – nanotube propagation

Previously, in the use of a non-covalent methodology for stabilizing nanotubes dispersions in brine, various polymers have been reported to disperse carbon nanotubes and propagate the dispersion through porous media.[35, 40, 41] The adsorption of nanotubes onto pore walls has been revealed as the primary barrier for effective tube propagation, once a stable dispersion has been achieved and all aggregates capable of blocking pore throats have been removed. In the non-covalent approach, MWNTs are covered by polymers or surfactants; hence, the retention and adsorption of MWNT in reservoir rock mainly depends on the effectiveness of dispersant used to stabilize them, as long as the dispersants themselves are not strongly adsorbed by the mineral surfaces.

i. Column test with anionic surfactant stabilized carbon nanotubes

Anionic surfactant IOS showed excellent suspendability for carbon nanotubes in DI water in the forementioned tests. Thus, transport of IOS suspended MWNTs in porous media

was firstly investigated under both DI water and saline solution conditions. The base run was Test 101, where the dispersion was made with 6 mM IOS and 2.4 mM $C_{12}(EO)_3SO_4Na$ in DI water. A 2'' dry-packed Ottawa sand was flushed by DI water for 10 PVs, then 5 pore volumes (PVs) of MWNT dispersion were injected, which is represented by the shaded area in Figure 2.5. Finally, water flooding was conducted to propagate the MWNT dispersions through the sand pack. In Test 102, the dispersion was made in a 5 wt% API brine, and the surfactant concentration was doubled in order to improve stability as illustrated in the previous section's stability test.

Figure 2.5a presents results for two column runs by showing plots of normalized carbon nanotubes concentration in the effluent against the pore volumes injected. The breakthrough of MWNT for both tests occurred at 1.3 PV. In the DI condition, effluent concentration quickly reached a plateau of 95% of the injected concentration at second PV. In the 5 wt% brine, the normalized concentration continued to increase from 1.3 PV to 2.0 PV, followed by a slight increase until 1 PV after water flooding. A similar breakthrough curve in quartz sand has been observed for functionalized MWNT at 10 mM ionic strength as well as for SDBS coated MWNT at 0.5 mM $CaCl_2$.[20, 29] The lower effluent concentration in Test 102 plus absence of a concentration plateau demonstrated that MWNT retention occurred at a much higher level in the brine, indicating deposition in porous media had not reached equilibrium,[20] despite the stability of the suspension in brine. The cumulative recovery for DI system and 5 wt% brine case were shown in Figure A1 (Appendix A) as 97% and 65%, respectively. The sand pack was carefully evacuated from the column after the test. Clean sand face in Test 101 also confirmed that barely any nanotubes were retained in the sand pack by mechanical trapping, indicating that

surfactant dispersed MWNTs in DI were highly mobile in the porous media. However, at 5 wt% brine, the sand face appeared dark due to nanotube adsorption losses, and correspondingly, the cumulative recovery of MWNT was much less than that in DI. The results for the tests are summarized in Table 2.2.

ii. Column test with nonionic surfactants stabilized carbon nanotubes

Nonionic surfactant NP40EO exhibited excellent suspendability for carbon nanotubes in aqueous solution at high electrolyte concentration conditions, due to the large polyethoxylate groups (EO = 40) in its hydrophilic head providing steric repulsion in aqueous solution. Test 201 was conducted with stable MWNT dispersion with 1.25 mM NP40EO in API brine.

As seen in Figure 2.5b, the nanotubes breakthrough occurred at the 2nd PV of dispersion injected, and normalized concentration displayed an upward trend until 1 PV post-water flood was initiated, revealing that equilibrium adsorption was not achieved in this run. The maximum effluent normalized concentration and cumulative recovery were 0.51 and 35%, respectively. Visual observation verified that the sand face as well as a cross section at 0.5'' behind sand face turned dark during the run, indicating adsorption occurred evenly in the porous media, thus eliminating trapping and filtration as mechanisms. The high adsorption of MWNT is believed to be on account of strong hydrophilic interaction between EO groups of NP40EO with the hydrophilic adsorbent,[39] such as the silica that is the principal component of the Ottawa sand. Polyethoxylated nonionic surfactants are known to exhibit high adsorption densities on silica surfaces.

iii. Column test with binary anionic-nonionic surfactant-stabilized carbon nanotubes

A stable binary surfactant dispersion of MWNT's was prepared with 6 mM IOS and 1.25 mM NP40EO in API brine. Test 301 was conducted in 1'' Ottawa sand pack, while Test 302 was in a 1'' crushed Berea sand pack.

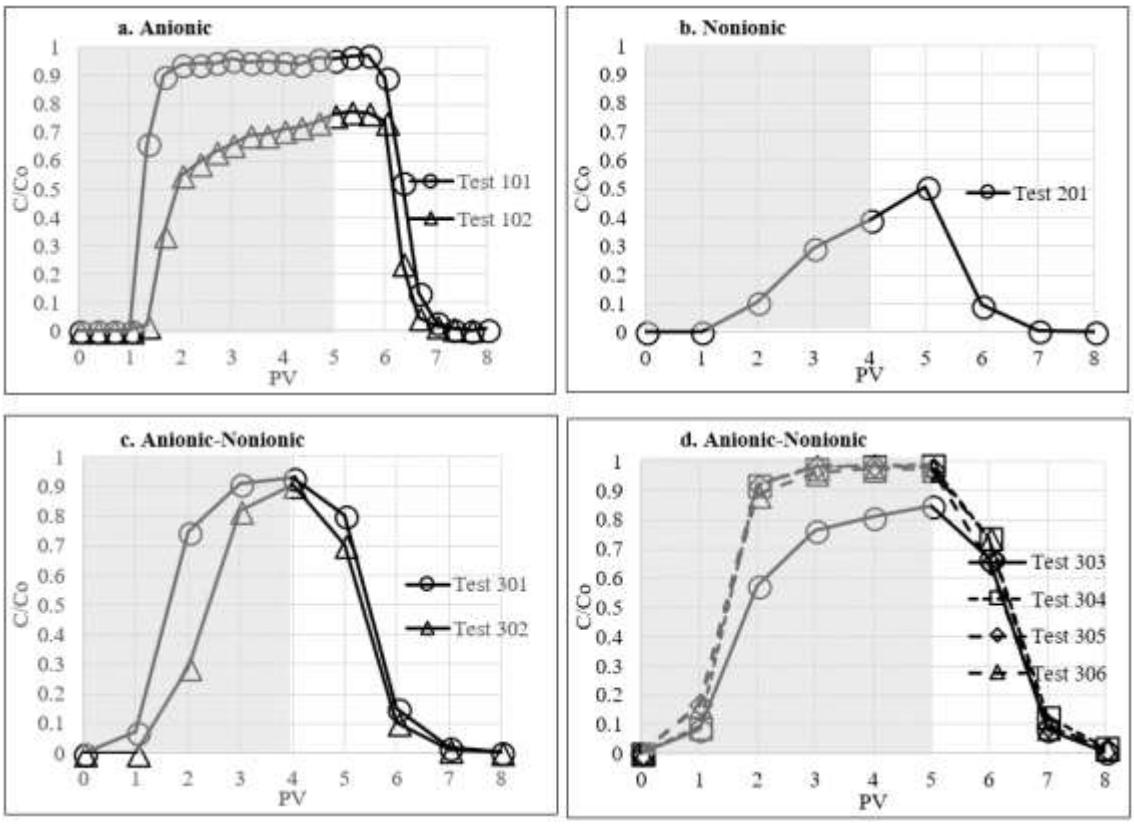

Figure 2.5. Normalized concentration vs. pore volumes (shaded area is dispersion injection period) a. Test 101 (95 mg/L MWNT with 6 mM IOS, 2.4 mM C12(EO)3SO4Na in DI) and Test 102 (37 mg/L MWNT with 12 mM IOS, 4.8 mM C12(EO)3SO4Na in 5 wt% brine) in 2'' Ottawa sand packs; b. Test 201 (75 mg/L MWNT with 1.25 mM NP40EO in API brine) in 1'' Ottawa sand pack; c. Test 301 in 1'' Ottawa sand pack and Test 302 in 1'' Berea sand pack (77 mg/L MWNT with 6 mM IOS and 1.25 mM NP40EO in API brine); d. Test 303-306 in 1'' Ottawa sand packs (MWNT concentration was 72, 73, 73, and 75 mg/L respectively; surfactants were 1 mM NP40EO with 2, 4, 6, and 8 mM $C_{12,13}(PO)_8SO_4Na$ respectively in API brine)

Figure 2.5c shows the results for the two column tests. The breakthrough of MWNTs in Test 301 occurred at the 1st PV, whereas in test 302 during the 2nd PV. The delay in propagation through the crushed Berea sand might be due to its complex composition (e.g., Berea contains significant amounts of clay minerals) causing stronger tube-sand interactions. The lower height of the concentration plateau observed in crushed Berea Sand implies higher nanotube retention due to heterogeneity of the media. It has been demonstrated that the mobility of MWNTs in porous media is positively correlated to porous media sand content while inversely correlated to clay content, e.g., 20% (v/v) of clay in the sand pack could retained 50-90 % of MWNTs.[42] The cumulative recoveries for Test 301 and Test 302 were 91% and 71% respectively.

Table 2.2. Summary of sand pack column tests. All tests were conducted at 25°C, with flow rate of 0.3 mL/min (pore velocity 2.8×10^{-3} cm/s)

Test	Electrolytes, wt%	Surfactant formulation	Total surfactant concentration, wt%	Injected MWNT, mg/L	MWNT recovery, %	Porous media
101	DI	6 mM IOS, 2.4 mM $C_{12}(EO)_3SO_4Na$	0.35	95	97	2'' Ottawa
102	5	12mM IOS, 4.8 mM $C_{12}(EO)_3SO_4Na$	0.7	37	65	2'' Ottawa
201	10	1.25 mM NP40EO	0.25	75	35	1'' Ottawa
301	10	1.25 mM NP40EO, 6mM IOS	0.5	77	91	1'' Ottawa
302	10	1.25 mM NP40EO, 6mM IOS	0.5	77	71	1'' Berea
303	10	1mM NP40EO, 2mM $C_{12,13}(PO)_8SO_4Na$	0.35	72	76.7	1'' Ottawa
304	10	1mM NP40EO, 4mM $C_{12,13}(PO)_8SO_4Na$	0.5	73	97.1	1'' Ottawa
305	10	1mM NP40EO, 6mM $C_{12,13}(PO)_8SO_4Na$	0.65	73	96.3	1'' Ottawa
306	10	1mM NP40EO, 8mM $C_{12,13}(PO)_8SO_4Na$	0.8	75	96.1	1'' Ottawa

In the binary nonionic-anionic surfactant mixture, nanotubes are coated by both nonionic and anionic surfactants. The nonionic offers steric repulsion to prevent coagulation of dispersed nanotubes in saline conditions, while the anionic one, with negatively charged head group, exhibits tube-tube, and tube-sand surface electrical repulsion, and allows greater adsorption densities than with the nonionic surfactant alone, and hence facilitates the MWNT transport in porous media. Since both electrical repulsive force and steric repulsion are crucial for stable nanotubes dispersion, it is anticipated that a combination of any anionic surfactant and nonionic surfactant with high of EO numbers, in proper proportion, should achieve stable dispersions in salinity conditions and exhibit successful propagation through porous media.

To confirm this hypothesis, the anionic surfactant $C_{12,13}(PO)_8SO_4Na$ was selected to create a MWNT dispersion with nonionic surfactant NP40EO in Tests 303-306. In each test, NP40EO was used at a concentration of 1 mM, while the concentration for $C_{12,13}(PO)_8SO_4Na$ was varied at 2 mM, 4 mM, 6 mM, and 8 mM, respectively.

Figure 2.5d illustrates the results for these column tests. As clearly seen, apart from Test 303, all other tests achieve improved propagation, with cumulative recovery greater than 96%. In Test 303, the recovery of MWNT in effluent reached 76.7%, however, no plateau was seen in the effluent concentration, which means the carbon nanotube adsorption onto the sand surface did not reach equilibrium. In tests 304-306 a plateau attained at the 3rd PV lasted until water flooding, with normalized concentrations as high as 98% of the injected concentration. The high adsorption loss in Test 303 caused the sand face to become darkened while in the remaining cases the sand faces are relatively cleaner. In Figure 2.5d, the normalized concentration curves are overlapped with each other for Test

304-306, which indicates surfactant ratios at 1:4, 1:6, 1:8 are viable for propagating carbon nanotubes dispersion in porous media.

2.4 Conclusions

This study explored the performance of various surfactant systems, in terms of their ability to stabilize MWNT dispersions and propagate them through porous media. Anionic surfactants are able to stabilize MWNTs and propagate them through a sand pack in DI water, but in brine solutions, stability and propagation are highly impaired because of the compression of the electrical double layer around the adsorbed anionic surfactants. Nonionic nonylphenol polyethoxyalte surfactants exhibit excellent performance to stabilize MWNT dispersions in API brine; however, high adsorption losses onto Ottawa sand are observed as a result of the strong interaction between NP40EO and the sand surface. Mixtures of anionic surfactant and polyethoxylated nonionic surfactant in the proper proportion can obtain stability under high electrolyte concentration conditions and also achieve successful propagation through porous media. Anionic-nonionic surfactant stabilized MWNT dispersions have both steric and electrostatic repulsion between nanotubes and the negatively charged sand surface, even in 10% API brine; as a result, this enables the nanotube dispersion to propagate through the porous media. In an anionic/nonionic mixture surfactant-based MWNT dispersion, the surfactant adsorption density on the MWNT surface is on the order of 9 molecules/nm^2. This number implies that multilayer adsorption would likely occur on the nanotube surface; however, there is no obvious physical mechanism that would lead to the development of a multilayer of surfactant on the hydrophobic surface of the nanotubes. The authors are unaware of any similar situation on hydrophobic surfaces.

To our knowledge, this is the first time that stable surfactant-only nanotube dispersions have been propagated through porous media under conditions of high electrolyte concentration (10 wt% API brine). Nonionic surfactant NP40EO shows excellent performance as a dispersant for nanotubes in API brine. One potential application is proposed, in which a stable nanotube dispersion can be utilized to deliver surfactants to subsurface reservoir to enhance crude oil recovery.

Acknowledgments

This work was supported by the Advanced Energy Consortium (http://www.beg.utexas.edu/aec/). Member companies include Repsol, Statoil, Shell, and Total.

Reference

1. Baughman, R. H.; Zakhidov, A. A.; De Heer, W. A., Carbon nanotubes--the route toward applications. *science* **2002,** 297, (5582), 787-792.

2. Ham, H. T.; Choi, Y. S.; Chung, I. J., An explanation of dispersion states of single-walled carbon nanotubes in solvents and aqueous surfactant solutions using solubility parameters. *Journal of Colloid and Interface Science* **2005,** 286, (1), 216-223.

3. Vaisman, L.; Wagner, H. D.; Marom, G., The role of surfactants in dispersion of carbon nanotubes. *Advances in colloid and interface science* **2006,** 128, 37-46.

4. Islam, M.; Rojas, E.; Bergey, D.; Johnson, A.; Yodh, A., High weight fraction surfactant solubilization of single-wall carbon nanotubes in water. *Nano letters* **2003,** 3, (2), 269-273.

5. Moore, V. C.; Strano, M. S.; Haroz, E. H.; Hauge, R. H.; Smalley, R. E.; Schmidt, J.; Talmon, Y., Individually suspended single-walled carbon nanotubes in various surfactants. *Nano letters* **2003,** 3, (10), 1379-1382.

6. Matarredona, O.; Rhoads, H.; Li, Z.; Harwell, J. H.; Balzano, L.; Resasco, D. E., Dispersion of single-walled carbon nanotubes in aqueous solutions of the anionic surfactant NaDDBS. *The Journal of Physical Chemistry B* **2003,** 107, (48), 13357-13367.

7. Bai, Y.; Lin, D.; Wu, F.; Wang, Z.; Xing, B., Adsorption of Triton X-series surfactants and its role in stabilizing multi-walled carbon nanotube suspensions. *Chemosphere* **2010,** 79, (4), 362-367.

8. Huang, Y. Y.; Terentjev, E. M., Dispersion of carbon nanotubes: mixing, sonication, stabilization, and composite properties. *Polymers* **2012,** 4, (1), 275-295.

9. White, B.; Banerjee, S.; O'Brien, S.; Turro, N. J.; Herman, I. P., Zeta-potential measurements of surfactant-wrapped individual single-walled carbon nanotubes. *The Journal of Physical Chemistry C* **2007,** 111, (37), 13684-13690.

10. Sun, Z.; Nicolosi, V.; Rickard, D.; Bergin, S. D.; Aherne, D.; Coleman, J. N., Quantitative evaluation of surfactant-stabilized single-walled carbon nanotubes: dispersion quality and its correlation with zeta potential. *The Journal of Physical Chemistry C* **2008,** 112, (29), 10692-10699.

11. Rosen, M. J.; Kunjappu, J. T., *Surfactants and interfacial phenomena*. John Wiley & Sons: 2012.

12. Bradford, S. A.; Simunek, J.; Bettahar, M.; Tadassa, Y. F.; van Genuchten, M. T.; Yates, S. R., Straining of colloids at textural interfaces. *Water Resources Research* **2005,** 41, (10).

13. Johnson, W. P.; Pazmino, E.; Ma, H., Direct observations of colloid retention in granular media in the presence of energy barriers, and implications for inferred mechanisms from indirect observations. *water research* **2010,** 44, (4), 1158-1169.

14. Wang, Y.; Kim, J.-H.; Baek, J.-B.; Miller, G. W.; Pennell, K. D., Transport behavior of functionalized multi-wall carbon nanotubes in water-saturated quartz sand as a function of tube length. *water research* **2012,** 46, (14), 4521-4531.

15. Jaisi, D. P.; Elimelech, M., Single-walled carbon nanotubes exhibit limited transport in soil columns. *Environmental science & technology* **2009,** 43, (24), 9161-9166.

16. Tian, Y.; Gao, B.; Morales, V. L.; Wang, Y.; Wu, L., Effect of surface modification on single-walled carbon nanotube retention and transport in saturated and unsaturated porous media. *Journal of hazardous materials* **2012,** 239, 333-339.

17. Tian, Y.; Gao, B.; Silvera-Batista, C.; Ziegler, K. J., Transport of engineered nanoparticles in saturated porous media. *Journal of Nanoparticle Research* **2010,** 12, (7), 2371-2380.

18. Jaisi, D. P.; Saleh, N. B.; Blake, R. E.; Elimelech, M., Transport of single-walled carbon nanotubes in porous media: filtration mechanisms and reversibility. *Environmental science & technology* **2008,** 42, (22), 8317-8323.

19. Lecoanet, H. F.; Wiesner, M. R., Velocity effects on fullerene and oxide nanoparticle deposition in porous media. *Environmental Science & Technology* **2004,** 38, (16), 4377-4382.

20. Liu, X.; O'Carroll, D. M.; Petersen, E. J.; Huang, Q.; Anderson, C. L., Mobility of multiwalled carbon nanotubes in porous media. *Environmental science & technology* **2009,** 43, (21), 8153-8158.

21. Kasel, D.; Bradford, S. A.; Šimůnek, J.; Heggen, M.; Vereecken, H.; Klumpp, E., Transport and retention of multi-walled carbon nanotubes in saturated porous media: Effects of input concentration and grain size. *water research* **2013,** 47, (2), 933-944.

22. Mattison, N. T.; O'Carroll, D. M.; Kerry Rowe, R.; Petersen, E. J., Impact of porous media grain size on the transport of multi-walled carbon nanotubes. *Environmental science & technology* **2011,** 45, (22), 9765-9775.

23. Shen, C.; Li, B.; Wang, C.; Huang, Y.; Jin, Y., Surface roughness effect on deposition of nano-and micro-sized colloids in saturated columns at different solution ionic strengths. *Vadose Zone Journal* **2011,** 10, (3), 1071-1081.

24. Tian, Y.; Gao, B.; Wu, L.; Muñoz-Carpena, R.; Huang, Q., Effect of solution chemistry on multi-walled carbon nanotube deposition and mobilization in clean porous media. *Journal of hazardous materials* **2012,** 231, 79-87.

25. O'Carroll, D.; Liu, X.; Mattison, N.; Petersen, E., Impact of diameter on carbon nanotube transport in sand. *Journal of colloid and interface science* **2013,** 390, (1), 96-104.

26. Elimelech, M.; O'Melia, C. R., Kinetics of deposition of colloidal particles in porous media. *Environmental science & technology* **1990,** 24, (10), 1528-1536.

27. Gao, B.; Saiers, J. E.; Ryan, J. N., Deposition and mobilization of clay colloids in unsaturated porous media. *Water Resources Research* **2004,** 40, (8).

28. Compère, F.; Porel, G.; Delay, F., Transport and retention of clay particles in saturated porous media. Influence of ionic strength and pore velocity. *Journal of Contaminant Hydrology* **2001,** 49, (1-2), 1-21.

29. Lu, Y.; Xu, X.; Yang, K.; Lin, D., The effects of surfactants and solution chemistry on the transport of multiwalled carbon nanotubes in quartz sand-packed columns. *Environmental pollution* **2013,** 182, 269-277.

30. Wang, P.; Shi, Q.; Liang, H.; Steuerman, D. W.; Stucky, G. D.; Keller, A. A., Enhanced environmental mobility of carbon nanotubes in the presence of humic acid and their removal from aqueous solution. *small* **2008,** 4, (12), 2166-2170.

31. Sharma, P.; Bao, D.; Fagerlund, F., Deposition and mobilization of functionalized multiwall carbon nanotubes in saturated porous media: effect of grain size, flow velocity and solution chemistry. *Environmental Earth Sciences* **2014,** 72, (8), 3025-3035.

32. Tian, Y.; Gao, B.; Ziegler, K. J., High mobility of SDBS-dispersed single-walled carbon nanotubes in saturated and unsaturated porous media. *Journal of hazardous materials* **2011,** 186, (2-3), 1766-1772.

33. Lecoanet, H. F.; Bottero, J.-Y.; Wiesner, M. R., Laboratory assessment of the mobility of nanomaterials in porous media. *Environmental science & technology* **2004,** 38, (19), 5164-5169.

34. Liang, L.; Ju, L.; Hu, J.; Zhang, W.; Wang, X., Transport of sodium dodecylbenzene sulfonate (SDBS)-dispersed carbon nanotubes and enhanced mobility of tetrabromobisphenol A (TBBPA) in saturated porous media. *Colloids and Surfaces A: Physicochemical and Engineering Aspects* **2016,** 497, 205-213.

35. Kadhum, M. J.; Swatske, D. P.; Harwell, J. H.; Shiau, B.; Resasco, D. E., Propagation of interfacially active carbon nanohybrids in porous media. *Energy & Fuels* **2013,** 27, (11), 6518-6527.

36. Guo, J.; Liu, Y.; Prada‐Silvy, R.; Tan, Y.; Azad, S.; Krause, B.; Pötschke, P.; Grady, B. P., Aspect ratio effects of multi‐walled carbon nanotubes on electrical, mechanical, and thermal properties of polycarbonate/MWCNT composites. *Journal of Polymer Science Part B: Polymer Physics* **2014,** 52, (1), 73-83.

37. Barnes, J. R.; Smit, J.; Smit, J.; Shpakoff, G.; Raney, K. H.; Puerto, M. In *Development of surfactants for chemical flooding at difficult reservoir conditions*, SPE Symposium on Improved Oil Recovery, 2008; Society of Petroleum Engineers: 2008.

38. Geiger, S. L.; Durnford, D. S., Infiltration in homogeneous sands and a mechanistic model of unstable flow. *Soil Science Society of America Journal* **2000,** 64, (2), 460-469.

39. Paria, S.; Khilar, K. C., A review on experimental studies of surfactant adsorption at the hydrophilic solid–water interface. *Advances in colloid and interface science* **2004,** 110, (3), 75-95.

40. Villamizar, L. C.; Lohateeraparp, P.; Harwell, J. H.; Resasco, D. E.; Shiau, B. J. B. In *Interfacially active SWNT/silica nanohybrid used in enhanced oil recovery*, SPE Improved Oil Recovery Symposium, 2010; Society of Petroleum Engineers: 2010.

41. Baez, J.; Ruiz, M. P.; Faria, J.; Harwell, J. H.; Shiau, B.; Resasco, D. E. In *Stabilization of interfacially-active-nanohybrids/polymer suspensions and transport through porous media*, SPE Improved Oil Recovery Symposium, 2012; Society of Petroleum Engineers: 2012.

42. Fang, J.; Shan, X.-q.; Wen, B.; Huang, R.-x., Mobility of TX100 suspended multiwalled carbon nanotubes (MWCNTs) and the facilitated transport of phenanthrene in real soil columns. *Geoderma* **2013,** 207, 1-7.

Chapter 3 Using Carbonaceous Nanoparticles as Surfactant Carrier in Enhanced Oil Recovery: A Laboratory Study

Graphical abstract

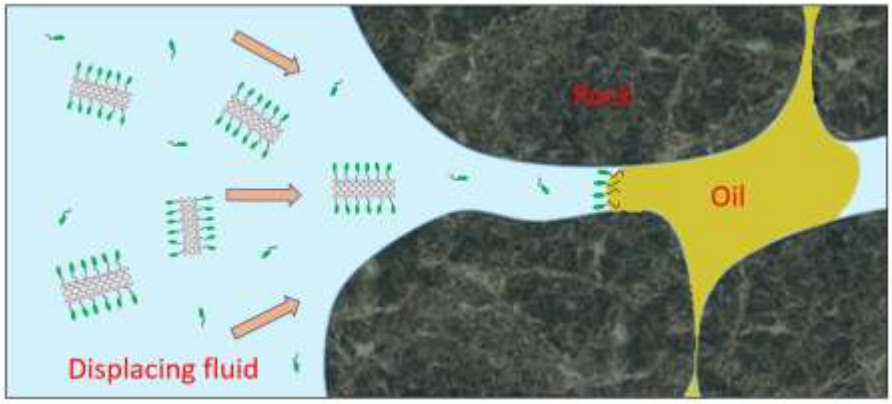

Abstract

Carbonaceous nanoparticles multi-walled carbon nanotubes (MWNTs) and carbon blacks (CBs) exhibit promising properties for potential applications in crude oil production. The combination of large specific surface area and the strong affinity toward surfactants of nanoparticles mark their candidacy for delivering surfactant deep inside the reservoir. This study is aimed to assess the feasibility of surfactant carriers in tertiary oil recovery. Stable dispersions of aqueous-phase MWNTs or CBs that are formulated and able to propagate through the reservoir medium (3 wt% brine and 60 ^{o}C) were first examined as a prerequisite for reservoir application. Competitive adsorption of surfactant on nanoparticles was beneficial to decrease adsorptive loss on Ottawa sand at equilibrium concentration below critical micelle concentration (CMC). As a proof of concept, phase behavior of a ternary surfactant microemulsion system confirmed that the chosen nanoparticles (100 mg/L) successfully delivered surfactants and spontaneously released

them to the O/W interface. The observed phenomenon is in accordance with calculation of the Gibbs free energy associated with oil/water/surfactant system. Besides, surfactants carried by nanoparticles achieved equilibrium ultralow interfacial tension between excess oil and aqueous phase similar to the value of surfactant-only formulation (0.007-0.009 mN/m). In one-dimensional sand pack tests, injection of MWNT-surfactant blend achieved faster and higher tertiary recovery than surfactant-only formulation, with cumulative tertiary oil recovery of 42.7% versus 38.1%. It has been noticed that once surfactant been released, destabilization of nanoparticle dispersion occurred and thus increased their retention in porous medium. In case of tight formations, further improvements may be addressed by applying functionalized carbonaceous nanoparticles to assure their transport in porous media after release of surfactant.

3.1 Introduction

Surfactant flooding is an enhanced oil recovery (EOR) technique, which mobilizes trapped oil by injecting finite slug of surfactant-only or mixture of surfactant/polymer solution into reservoir mainly to dramatically reduce the residual oil/water interfacial tension (IFT) [1-3]. Surfactant flooding was proven for decades a technically viable method from extensive laboratory efforts and numerous pilot tests, however, large field scale implementations have yet been realized due to the complexity of chemical flooding design and in many instances excessive adsorption of surfactant on formation rocks which adversely challenges economic viability of the projects [2, 4].

The controlling mechanisms of adsorptive losses onto rock surfaces are complex phenomena depending on various parameters, including surfactant characteristics, e.g. type of surfactant, functional group, alkyl chain length, molecular weight;

physicochemical properties of solution, such as solution pH, electrolytes concentration, divalent ions level, reservoir temperature; as well as formation mineral composition and clay content [1, 5-9]. Among these, the dominant mechanisms governing surfactants adsorption onto formation rocks from aqueous solution include ion exchange, ion pairing, hydrophobic bonding, adsorption by polarization of π electrons, and adsorption by dispersion forces [10, 11]. Thus, a proper control of surfactant adsorption over the course of chemical flooding is of great essence of successful recovery operations.

Normally surfactants with same charge as formation rocks are preferred owing to the electrostatic repulsion between surfactant head and rock surface which would mitigate the surfactant adsorption, for instance, anionic surfactants are preferably used in negatively charged sandstones formations at neutral pH [5, 12]. In reality, however, it is impossible to completely eliminate surfactant adsorptive loss by changing the type or electrical property of surfactants [13], simply due to the inherent heterogeneity of formation rocks. The complex mineral compositions and their organic contents allow their surface properties to be altered along with sudden changes in dissolved constituents, pH of the solution, as well as advance or recession of wetting phase, therefore leave behind patchy surfactant adsorption.

Addition of polyelectrolytes, e.g. sodium polyacrylate, polystyrene sulfonate, have been considered serving as sacrificial agents for their capability to reduce adsorption of surfactants in reservoirs rocks [12-14]. These high-molecular weight sacrificial agents are believed to irreversibly occupy adsorptive sites on the substrate thus render a competition against surfactant molecules. Nevertheless, a typical preflush pattern of sacrificial agent may require similar injected volume as a chemical slug, which not only offset potential

cost savings on surfactants but also drag field operations up to months, leading to less viability in a full-scale field project.

Recently, nanotechnology have gained increasing attention in the petroleum industry. Successful applications of nanotechnology have been reported in reservoir characterization, drilling and completion, hydraulic fracturing, and acid diversion [15-20]. Oil and gas researchers are also exploring use of nanotechnology for solving some EOR challenges more effectively. Nyankson et al. [21] studied halloysite clay nanotubes loading with different surfactants for remediation of crude oil spill. It was stated that controlled release of surfactant from the lumen of the halloysite nanomaterial could reduce the amount of chemical wastes and cost associated with the cleanup efforts. Neves Libório De Avila et al. [22] used crosslinked polystyrene nanoparticles as surfactant carriers by trapping surfactant molecules in the nanoparticles' microstructure. Once in contact with oil phase, swelling of these nanoparticles occurred, as a result, surfactants were released into the medium before partitioning at oil/water interface. Romero-Zerón and Kittisrisawai [23] developed a sugar-based complexation formulation with surfactant/β-cyclodextrin to prevent surfactant adsorption onto porous media. A total of 61% reduction of surfactant dynamic adsorption onto sand/kaolin blend media was evidenced for an equimolar surfactant/β-cyclodextrin inclusion complex.

Carbonaceous nanoparticles e.g. carbon nanotubes (CNTs), fullerene, carbon blacks (CBs) are potential candidates for various applications in petroleum industry. For instance, Berlin et al. [24] explored the application of engineered CBs as carriers of hydrophobic compound (2,2',5,5'-tetrachlorobiphenyl) in detecting presence of hydrocarbons in oil reservoirs. Drexler et al. [25] reported that amphiphilic nanohybrids

of CNT/silica and CNT/alumina can simultaneously act as emulsion stabilizers as well as carriers for catalysts. The superior characteristics of carbonaceous nanoparticle involve that other hydrophobic compounds or the hydrophobic moiety of an amphiphilic molecule, e.g. long surfactant tail, will strongly attract to these nanoparticle surfaces because of the entropy-driven hydrophobic interactions. Besides, enormous specific surface area of these nanoparticles (close to 250 m^2/g for nanotubes in this study) could afford substantial amount of hydrophobic molecules to be loaded onto their surfaces. Previously, Matarredona et al. [26] documented the net adsorption of sodium dodecyl benzene sulfonate (SDBS) on single-walled nanotube (SWNT) surface reaching as high as 11.6 molecules per nm^2.

Based on our prior studies [27], we focused on two carbonaceous nanomaterials, multi-walled nanotubes (MWNTs) and CBs to investigate their potential serving as surfactant carriers, in particular covering three aspects in dealing with the feasibility in EOR applications. First, the influence of MWNT in surfactant adsorption was quantified through the batch adsorption tests of anionic surfactant alpha olefin sulfonate (AOS) on Ottawa sand. Second, example of ultralow-IFT microemulsions phase behavior as well as Gibbs free energy change associated with oil/water/surfactant system were examined to affirm whether the loaded surfactants could be released from the treated MWNTs surfaces to oil/water interface once met the oil phase. Third, sand pack column tests were carried out to compare the extent of oil recovery for an optimum surfactant formulation between cases of presence and absence of nanoparticles added. Moreover, stability of nanoparticle dispersion under mimic reservoir conditions (3 wt% brine and 60 ^oC) as well

as transport and fate of these stable nano-fluids in porous medium were first examined as a prerequisite for any field applications.

3.2 Experimental

3.2.1 Materials

i. Nanomaterials

The MWNTs samples used in this study were purchased from US Research Nanomaterials, Inc (Houston, TX). The nanotube length is approximately 0.5-2 micron (μm) with an average outer diameter (OD) of approximately 5-15 nanometers (nm). The selected CBs nanoparticles were provided by Cabot Corporation (Billerica, MA) with primary particle size around 24 nm, and specific surface area (SSA) around 110 m^2/g. Examples of electron microscopy images of these MWNTs as well as CBs have been reported previously by others [28, 29].

ii. Surfactants

Three anionic EOR surfactants were used in this study. Alpha olefin sulfonate ($C_{14-16}SO_3Na$, AOS) was manufactured and provided by Stepan Company (Northfield, IL) as 39 wt% active aqueous solution. Internal olefin sulfonate (IOS) with an average alkyl chain length of 19-23 carbons, was received from Shell Chemicals (Houston, TX) as 26.8 wt% active solution. Dioctyl sodium sulfosuccinate (AOT) was supplied by Fisher Scientific (Hampton, NH) as 99 wt% active wax. Among nonionic surfactant dispersants used, nonylphenol polyethoxylates with 30, and 40 ethylene oxide (EO) groups (NP30EO, and NP40EO, respectively) were both provided by Huntsman (Salt Lake City, UT) as 100% active. Linear alcohol ethoxylates with 40 ethoxylate groups (LA40EO)

was provided by Dow Chemical Company (Midland, MI) as 100% active. All surfactants were used as received without further purification. Sodium chloride (NaCl) and calcium chloride dihydrate ($CaCl_2 \cdot 2H_2O$) were purchased from Sigma Aldrich.

iii. Porous medium

Ottawa sand (F-95) was purchased from U.S. Silica. The size distribution of Ottawa sand is between 75 μm and 300 μm with d50 at 145 μm [30]. For sand pack tests, Ottawa sand were used without any treatment. For surfactant adsorption analysis, Ottawa sand were thoroughly washed and rinsed in deionized water (DI) to remove any soluble impurities which may affect conductivity measurement, then completely air-dried overnight in oven of 80 °C. The resulted supernatant separated from the washed Ottawa sand (served as sample blank in adsorption tests) exhibited the conductivity readings mostly < 4 μS/cm, which was negligible compared to conductivities of surfactant solutions.

3.2.2 Methods

i. Preparation of nanoparticle dispersion

Stock solutions for individual surfactant were prepared at 1wt% in DI at room temperature (22 ± 1 °C). After diluting stock solutions to the target concentration at electrolytes level of either DI or 3 wt% brine (2.4 wt% NaCl and 0.6 wt% $CaCl_2$), MWNTs or CBs were added to each sample, followed by 30 minutes of sonication with a horn sonicator (20 W, 20 kHz). The resulting nano dispersions were centrifuged at 2000 rpm for 1 hour, to allow any remaining non-dispersed nanoparticles/aggregates to be easily separated from the stable, suspended nanoparticles. The supernatant was then carefully decanted and collected for further tests. Concentration of MWNTs or CBs in

the stable dispersion was measured using an ultraviolet−visible (UV−Vis) spectrophotometer (Thermoscientific, Genesys10s) at 800 nm as described previously [27] and compared to a group of calibration standards of known concentrations.

ii. Surfactant adsorption on nanoparticles

MWNTs and CBs were added at concentration of 370 mg/L and 450 mg/L, respectively, into AOS solutions of varying concentration prepared in DI. The suspension was then sonicated and poured into a glass beaker. The surface tension of surfactant nano mixed solution was measured by a dynamic contact angle analyzer DCA-322 (Cahn Instruments, USA) utilizing a technique based on the Wilhelmy plate principle. Details of the procedure have been mentioned elsewhere.[26] The critical micelle concentration (CMC) values were determined from the break point in the curve of surface tension versus the logarithm of surfactant concentration. And the amount of surfactant adsorbed on nanoparticles could be interpreted from the increment of CMC values.

iii. Surfactant adsorption on sand

A total of 4 grams of washed Ottawa sands were introduced with 12 mL of surfactant-only in DI or MWNTs amended surfactant solution in 40 mL glass reactors. A horizontal movement shaker was used to carry out the tests by steadily shaking the reactors at 300 rpm for 24 hours at 22^{o}C, which is normally sufficient to reach the adsorption equilibrium [12]. After equilibration, samples were centrifuged at 2000 rpm, and supernatants were carefully extracted for conductivity measurements using a Mettler Toledo S230 SevenCompact Conductivity Meter (Columbus, OH). The detecting cell used is Cond probe InLab 731-ISM-2m with cell constant of 0.57 cm^{-}. Errors of the measured

conductivity values were within ± 0.5%. It has been observed that applying this method for surfactant adsorption measurement offer advantage of the solution conductivity readings being rather independent of MWNT concentrations used. The measured conductivity and the surfactant levels were quantified against the calibrated standards of known concentration.

iv. Phase behavior of microemulsions

Phase behavior test was performed in flat-bottom glass vials with Teflon-lined screw caps. A synthetic isoparaffinic hydrocarbon solvent, Isopar^{TM} -L (>98% C_{11}-C_{13}) was used as representative oil phase. In control group, after preheated surfactant solution (0.68 wt% surfactants in 3 wt% brine) and oil at 50 ^{o}C, equal volume of surfactant solution and oil (5 mL each) were added into the vial. In experimental groups, 100 mg/L of MWNTs or CBs dispersion prepared with same surfactant formulation used in the control group were studied for their influence on microemulsion phase behaviors. All test tubes were first gently hand-shaken for 20 seconds, and subsequently kept in an oven setting at 50 ^{o}C to allow equilibration and visual observations. After the systems reached equilibrium, the resulted interfacial tension (IFT) between the excess water and excess oil phases of microemulsions was measured at 50 ^{o}C with a M6500 Spinning Drop Tensiometer (Grace Instrument, Houston, TX). The detailed method has been documented by Witthayapanyanon et al [31].

v. One-dimensional sand pack test

The Ottawa sand medium was dry packed into a chromatographic glass column purchased from Kimble Chase. Experiments were run in a 6 in. (L) × 1 in. (D) sand pack dimension

with water circulating inside the column glass jacket to maintain operating temperature at 50 ^{o}C. Average porosity and permeability of the sand packs were measured as 37.5% and 4.0 Darcy, respectively.

In general, after dry packing the column, a house build vacuum was first applied to remove air trapped in the sand pack, followed by steady injection of 3 wt% brine in an up-flow mode using a Masterflex peristaltic pump (Cole Parmer, IL); at least 10 pore volumes (PVs) of brine were injected through the columns to ensure the homogeneous compaction of the sand pack without residual air pockets. A conservative tracer test using 5 PVs 10 wt% brine (8 wt% NaCl and 2 wt% $CaCl_2$) was carried out immediately after completed saturation of the sand pack. The details of the tracer test has been reported before [32]. Prior to injection of nanoparticles/surfactant mixture, the flushing fluid was switched back to original 3 wt% brine for another 10 PVs.

Surfactants loaded MWNT or CB dispersions were injected into the column for 5 PVs, followed by post-brine flush (3 wt%), which was last until no nanoparticles were detected in the effluents. Typically, over the course of these experiments an undetectable concentration of nanoparticle is realized shortly following 3 PV of post-brine flooding. The flushing fluids were delivered into the sand packs at a constant flow rate of 0.3 mL/min (corresponding to a pore water velocity of 2.6×10^{-3} cm/s). All column effluents were collected by a fraction collector at pre-set time intervals. The nanoparticle concentrations in the collected samples were analyzed by the UV-Vis spectrophotometer (800 nm wavelength) as described previously. The normalized nanoparticle concentrations (based on the injected concentration) in the effluent were plotted against total PVs injected.

vi. Oil recovery test

After vacuumed down dry sand pack columns, 2 PVs (ca. 57 mL) of Isopar^{TM} -L oil were introduced into the column in similar up-flow mode at a flow rate of 0.3 mL/min. The displacing fluid was subsequently switched to 3 wt% brine kept at same flow rate to displace most mobile oil until the oil-cut in effluent approached < 1%, typically after 5 PVs of water flooding is delivered. The slug of chemical flooding was then initiated via injecting 3 PVs either surfactant-only formulation or MWNT-amended surfactant solution (the developed 0.1wt% ultralow IFT formulation), and was immediately followed by 5 PVs post-brine flush. Effluent samples were collected in graduated burettes to estimate the cumulative tertiary oil recovery.

3.3 Results

3.3.1 Thermal stability of nanoparticle dispersion

Previously in this group, we have developed surfactant stabilized MWNT dispersion formulations under harsh saline conditions (10 wt% brine containing 8 wt% NaCl and 2 wt% $CaCl_2$) [27]. The binary surfactant system, which consists of one nonionic surfactant with certain high EO numbers (> 30) and another salt-tolerant anionic surfactant, offered exceptional performance of propagating MWNT dispersions through the porous medium. It is believed that, surfactant tails are anchored on the nanotubes hydrophobic surface due to non-covalent hydrophobic interactions, while surfactant hydrophilic head groups are oriented toward the aqueous solution, enabling nanotubes to be well dispersed in the solution owing to dominant electrostatic repulsion or steric repulsion among the head groups of surfactant [33, 34]. However, the EO groups of nonionic surfactant are well

known dehydrated as temperature approaching cloud point of nonionic surfactant. Shikata et al. [35] revealed that EO units bear dual groups of hydrated water molecules, where the primary ones directly hydrated the oxygen atom of the EO unit, while secondary hydrated water molecules hydrated to the primary water molecules. At elevated temperatures, the group of secondary hydrated water molecules would dehydrate more readily than the group of primary ones, hence weakening the steric repulsive forces between bulky ethylene oxides. With the presence of electrolytes, the salting out effects could further deteriorate the extent of dehydration, leading to sudden agglomeration of dispersed nanoparticles, e.g. clouds points of NP30EO and NP40EO are 114 and 114.5 ^{o}C, respectively in DI [36]; 91 and 93 ^{o}C, respectively in 3 wt% brine. Thus, the thermal stability of nanoparticle dispersion is carefully scrutinized at elevated temperatures as a prerequisite for its field applications.

Table 3.1. Thermal stability (UV-Vis absorbance data) of 100 mg/L MWNT or CB with different surfactant formulation in DI and brine. Formulation 1. 1000 mg/L NP30EO, 2. 1000 mg/L NP30EO with 1000 mg/L AOS, 3. 1000 mg/L NP40EO, 4. 1000 mg/L NP40EO with 1000 mg/L AOS.

Batch	Day	0	3	7	15	30	0	3	7	15	30
MWNT	Formulation	DI (80 ^{o}C)					3 wt% brine (50 ^{o}C)				
	1	1.561	1.559	1.553	1.564	1.549	1.521	1.492	1.441	1.392	1.361
	2	1.507	1.511	1.504	1.499	1.51	1.469	0.201	-	-	-
	3	1.574	1.571	1.569	1.579	1.577	1.587	1.591	1.576	1.545	1.529
	4	1.639	1.641	1.639	1.636	1.629	1.572	1.526	1.489	1.321	1.065
CB	Formulation	DI (80 ^{o}C)					3 wt% brine (60 ^{o}C)				
	1	5.532	5.509	5.524	5.551	5.546	5.375	5.076	4.931	4.804	4.607
	2	5.654	5.646	5.671	5.633	5.639	5.363	4.894	4.653	4.214	3.889
	3	5.631	5.643	5.647	5.657	5.651	5.617	5.609	5.595	5.577	5.545
	4	5.466	5.452	5.469	5.435	5.447	5.264	5.245	5.207	5.192	5.171

MWNTs and CBs exhibited excellent thermal stability (80 ^{o}C) in DI with all formulations tested because of strong electrostatic repulsion and/or steric repulsion. Addition of 3 wt% brine, electrostatic repulsion was largely shielded due to compression of electrical double

layer; on the other hand, steric repulsion was independent of the electrolytes concentration. Good stability has been maintained through a 30-day period for both MWNT and CB with pure nonionic surfactants system (formulation 1 and 3 in Table 3.1). Ionic surfactant AOS in formulation 2 and 4 occupied some portions of nanoparticle surface which would otherwise be taken by ethoxylated alcohol, therefore decreased the steric repulsive force exerted by nonionic surfactant. This was manifested by weakening stability of MWNT dispersion after adding 1000 mg/L AOS along NP30EO at 50 ^{o}C. With a longer EO chain, NP40EO, better dispersion stability was observed as a result of enhancement of steric repulsion between the bulkier head groups as compared to NP30EO. Overall, CB exhibited superior stability than MWNT using similar dispersants. This may result from smaller particle size of CB than MWNT (average hydrodynamic diameter of 124 nm vs. 164 nm by dynamic light scattering, details in Table B1 in Appendix B).

3.3.2 Propagation of nanoparticles

Mobility of stable dispersion of MWNTs as well as CBs through porous media were examined in Ottawa sand pack with aforementioned formulation 4. 6'' Ottawa sand was packed in a jacked chromatography glass column with heated water circulation to maintain constant temperature of 50 ^{o}C.

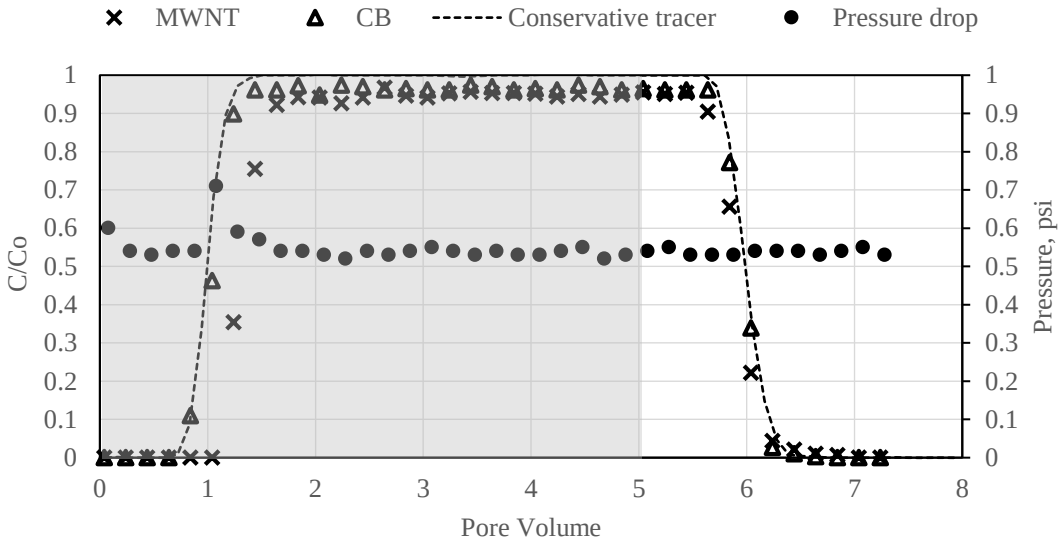

Figure 3.1. Breakthrough curves for MWNTs and CBs with formulation 4 (1000 mg/L NP40EO with 1000 mg/L AOS) in 6'' Ottawa sand pack at 50 ºC. Nanoparticle input concentration = 100 mg/L in 3 wt% brine. Pressure drop is differential pressure across the sand pack during injection of MWNT. Shaded area is the dispersion injection period. Peclet number P_e for tracer is 195 ($P_e = vL/D_H$, v is pore velocity, L is column height, and D_H is hydrodynamic dispersion coefficient, data obtained from Ref 32 as $2.15 \times 10^{-4} cm^2/s$).

The breakthrough of CB occurred coincidentally with the migration of conservative tracer, while MWNT breakthrough was observed shortly after 1 PV of fluid injection. In the case of CB, the eluted concentration quickly reached plateau of 97% of the injected concentration at 1.5 PV, and MWNT scenario achieved effluent plateau slightly later approximate at 2 PV with normalized concentrations close to 95% of the injected concentration. The differences in transport behavior between CB and MWNT may be related to their distinct morphologies and characters. It is suspected that cylindrical MWNT (aspect ratio as high as 200) was more involved with physical straining in the porous media [37, 38], and in this study visual inspection of the dismantled sand column after the test revealed most retention of MWNT mainly occurred at the inlet sand face. Nevertheless, pressure drop across the sand pack was stable during the whole flow test,

indicating negligible change on permeability resulting from deposition of MWNTs. While transport of CBs, associated with their smaller sizes and predominant sphere shape, was likely controlled by mostly advection in sand pack, consequently the resulting breakthrough curve largely overlapped with that of conservative tracer. A 3 wt% brine solution was injected as the chasing fluid after 5 PVs of dispersed fluid. Cumulative particle recovered in the effluent were 88% versus 95% for MWNT and CB, respectively. The particle retention of MWNT and CB onto Ottawa sand were 0.011 mg/g and 0.004 mg/g, respectively. Such adsorption value is amazingly low as compared to typical surfactant adsorption loss in the sands, 0.5 mg/g to 1.0 mg/g [8].

3.3.3 Decrease of surfactant adsorption in sand

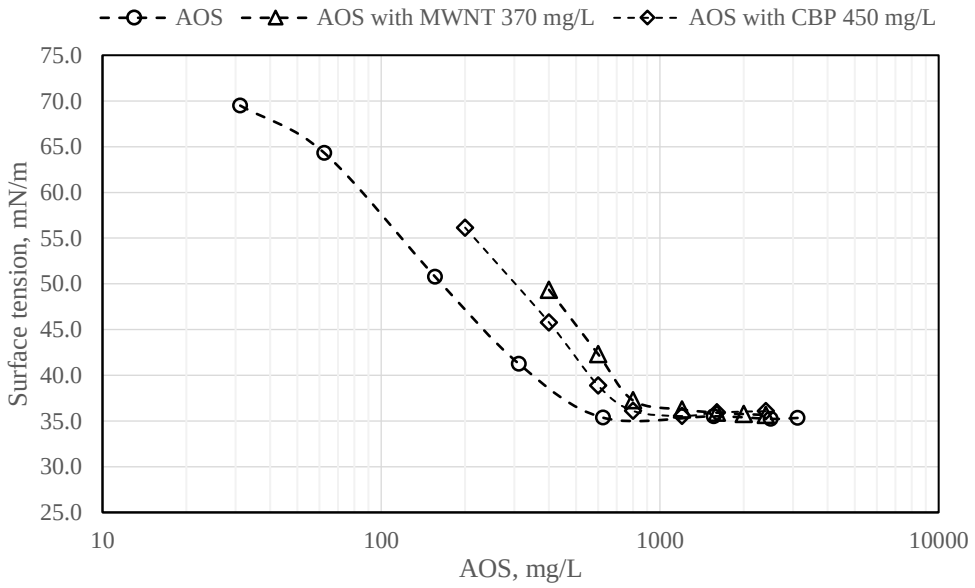

Figure 3.2. Surface tension measurement. CMC of AOS = 500 mg/L, with 370 mg/L MWNT CMC = 820 mg/L, with 450 mg/L CB CMC = 720 mg/L.

As shown in Figure 3.2, the CMC of neat surfactant is lower than CMC with presence of nanoparticles, due to uptake of surfactant monomers by the dispersed nanoparticles [26, 39]. For instance, with presence of 370 mg/L MWNT, CMC of AOS increased by

approximately 320 mg/L, that is the amount adsorbed on the nanotube surface. And CMC shifted by 220 mg/L for the case with 450 mg/L CB. The mass ratio between loaded surfactant and carrier were 0.86 and 0.49 for MWNT and CB, respectively. In contrast, in the study of Romero-Zerón and Kittisrisawai [23], surfactant carrier β-cyclodextrin demonstrated an equimolar stoichiometric ratio to the loaded surfactant, yielding a mass ratio of 0.28 assuming AOS being used. Obviously, MWNT exhibited highest efficiency in carrying same amount of surfactants among these candidates. Given specific surface area values of MWNT and CB are approximately 250 m^2/g and 110 m^2/g, respectively, the adsorption density of AOS was calculated as 6.2 molecules/nm^2 on MWNT and 7.8 molecules/nm^2 on CB. The slight difference is possibly related to the curvature of the nanoparticle surfaces [27]. In contrast, AOS adsorption density at gas/water interface estimated by Gibbs adsorption isotherm was only 1.5 molecules/ nm^2. Clearly, surfactant adsorption at MWNT or CB surface is around 4 - 5 times denser than that occurred at gas/water interface.

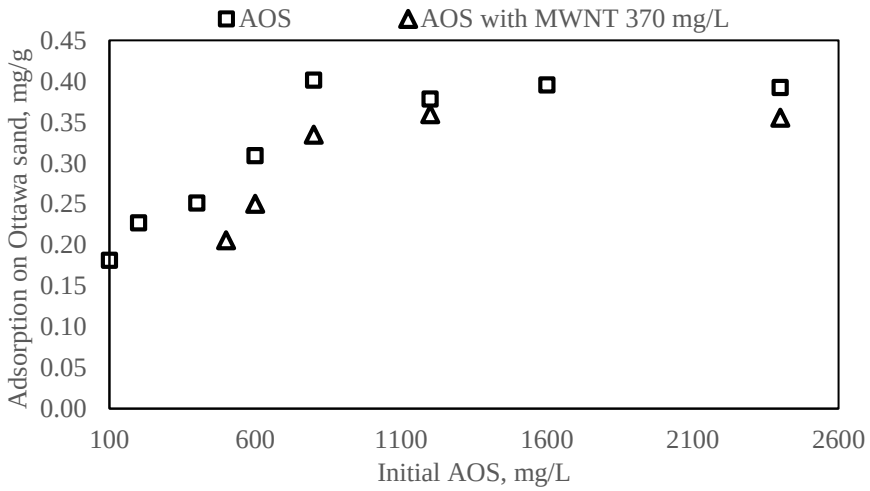

Figure 3.3. Adsorption isotherm of AOS on washed Ottawa sand.

Surfactant adsorption on formation rocks typically attained the maximum level once equilibrium concentration of surfactant reaches CMC in the solution. With presence of nanoparticle carriers, competitive adsorption of surfactant on particle surface will bring down available surfactant molecules in the solution. If the newly established equilibrium concentration is below CMC, a net reduction of surfactant adsorption on reservoir rocks can be anticipated. This has been confirmed by the adsorption of AOS on Ottawa sand. As depicted in Figure 3.3, below the CMC of AOS (820 mg/L with MWNT), the competitive adsorption of AOS on the nanotubes led to less available monomers in the solution, thus decrease of AOS adsorption onto sand was observed, e.g. adsorption was reduced from 0.4 mg/g to 0.33 mg/g at initial AOS of 800 mg/L. While above the CMC, as nanotube surfaces being saturated by surfactants, surfactant adsorption on sands was no longer influenced by nanotubes, therefore adsorption leveled off at plateau region with a similar level as that in the absence of MWNTs.

The principle behind this modified delivery system is to apply nanoparticle carrying surfactant at concentration under CMC, which would be close to or above CMC in the absence of nanoparticle, such that the surfactant adsorption on reservoir rocks can be reduced substantially. By adjusting surface properties of nanoparticle, EOR surfactants can be controlled to preferentially adsorb onto nanoparticles instead of rock surfaces, therefore alleviate large amount of surfactant adsorption loss in reservoir.

3.3.4 Release surfactant to oil/water interface

Carbonaceous nanoparticles have exhibited exceptional ability to load surfactants on their surface. Serving as surfactant carriers, nanoparticles are required to release surfactants once reach the targeted zone (presence of residual oil) so that the released surfactants can

partition at the oil/water interface to lower the IFT and mobilize the residual oil. In order to better understand the feasibility of surfactant carriers, we take the next step on considering the Gibbs free energy associated with the change of surfactants' states in a MWNT-water-oil system.

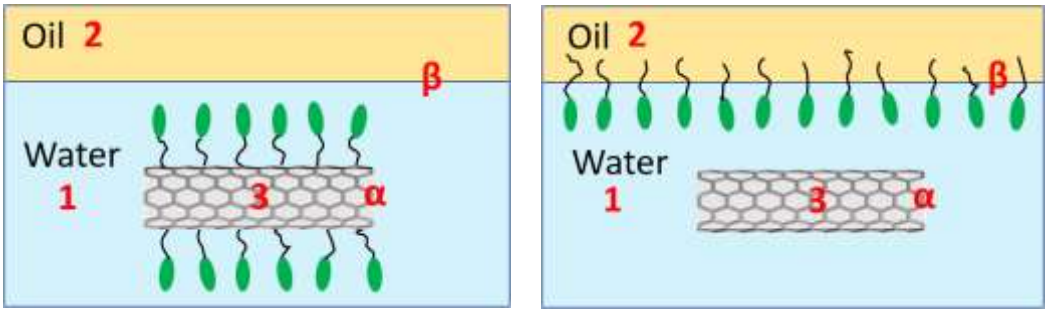

Figure 3.4. Sketch of surfactant released from MWNT surface to oil/water interface. Left. surfactants adsorb at MWNT surface; Right. Surfactants partition at oil/water interface.

Given a system as illustrated in Figure 3.4, comprised of three phases, water phase 1, residual oil phase 2, and solid MWNT phase 3; and two interfaces, MWNT/water interface α and oil/water interface β. The total Gibbs energy of this system is:

$$G = G^1 + G^2 + G^3 + G^\alpha + G^\beta \tag{3.1}$$

For the bulk phases, the Gibbs energy can be expressed as:

$$G^{1,2,3} = U + PV - TS + \sum u_i n_i \tag{3.2}$$

Then,

$$dG^{1,2,3} = Vdp - SdT + \sum u_i dn_i \tag{3.3}$$

Where U is the internal energy, P is pressure, V is volume, T is temperature, S is the entropy, u_i is the chemical potential of the ith component, and n_i is the number of the particles composing ith chemical component.

And for the MWNT/W and O/W interfaces, we have,

$$G^{\alpha,\beta} = U + PV - TS + \sum u_i n_i + \delta A \tag{3.4}$$

then,

$$dG^{\alpha,\beta} = Vdp - SdT + \sum u_i dn_i + \delta dA + Ad\delta \tag{3.5}$$

Where δ is the interfacial tension, and A is the interface area.

Assuming constant temperature and pressure encountered in reservoir, the fisrt two terms in equation 3.3, and 3.5 can be eliminated. At adsorption equilibrium, the chemical potential of component, u_i, is equal in phases 1, 2, 3 and at interfaces α, and β; also considering mass conservation of each component, thus,

$$\sum_{1,2,3,\alpha,\beta} u_i dn_i = 0 \tag{3.6}$$

We can also assume the interface areas A_α , A_β are constants. This is true for MWNT/water interface. While for oil droplets trapped in pore throats, surfactants would organize themselves at oil/water interface to lower IFT, hence trapped oil can easily deform to pass thorough pore throats. During which process, interface areas will increase. Nevertheless, we can still safely assume a constant area of oil/water interface at the very moment surfactants are just desorbed from MWNT surfaces to partition at O/W interface. Hence, derivative term $\delta dA = 0$, and change of Gibbs free energy for the system is reduced to,

$$dG = A_\alpha d\delta_\alpha + A_\beta d\delta_\beta \tag{3.7}$$

Consider a complete release of surfactants from MWNT surface as depicted inFigure 3.4, then Equation 3.7 can be integrated,

$$\Delta G = A_\alpha * \left(\delta_\alpha - \delta_{\alpha\_surf}\right) + A_\beta * \left(\delta_{\beta\_surf} - \delta_\beta\right) \quad (3.8)$$

IFTs in the second bracket are easily detected from experiments. In the first bracket, δ_α can be estimated from Young's equation if contact angle and surface tensions are known. While the value of δ_{α_surf} is hardly known because it depends on the type and quantity of adsorbed surfactants on MWNT surface.

Pristine carbonaceous particles like MWNT are extremely hydrophobic materials. A typical contact angle, θ is reported around 155° - 165° [40, 41], and surface energy of MWNT, δ_{SG} is about 40-45 mJ/m^2 [42]. With Young's equation [11],

$$cos\,\theta = \frac{\delta_{SG} - \delta_{SL}}{\delta_{LG}} \quad (3.9)$$

δ_{SL} between MWNT and water is determined as 113 mN/m. A typical value of crude oil/water IFT, $\delta_{o/w}$ is about 30 mN/m, and with surfactant, it is typically less than 1 mN/m, which could be ignored in the calculation. With obtained values,

$$\Delta G = A_\alpha * \left(113 - \delta_{\alpha_{surf}}\right) - A_\beta * 30 \quad (3.10)$$

Assume surfactant at oil/water interface bear a monolayer adsorption, with same adsorption density as that at gas/water interface. Also consider a monolayer surfactant structure on MWNT surface. Thus, we have mass balance of surfactants,

$$A_\alpha \rho_\alpha = A_\beta \rho_\beta \quad (3.11)$$

Where ρ_α, ρ_β are surfactant density at interfaces α, and β, respectively. A_β is governed by the density of surfactant adsorbed at oil/water and MWNT/water interfaces. In previous section, surfactant adsorption at MWNT surface is determined about 4 times

higher than that at gas/water interface, in turn, A_β is 4 times larger than A_α, then Equation 3.10 reduce to,

$$\Delta G = A_\alpha * \left(113 - 120 - \delta_{\alpha_{surf}}\right) < 0 \qquad (3.12)$$

This indicates that surfactant desorbing from MWNT surface to partition at oil/water interface should be a spontaneous process.

The assumption that surfactants completely released from MWNT surface is imprecise. In reality, we should have incomplete desorption of surfactant from MWNT surface, otherwise super hydrophobic pristine MWNT surface would be surrounded by a highly structured "ice-cage" water molecules [43]. The formation of "ice-cage" would decrease entropy of water molecules substantially, thus not favored by the MWNT-water-oil system. With incomplete release of surfactants, thermodynamic consideration could be more complicated. Instead, the observed phase behavior phenomena could give a quick hint.

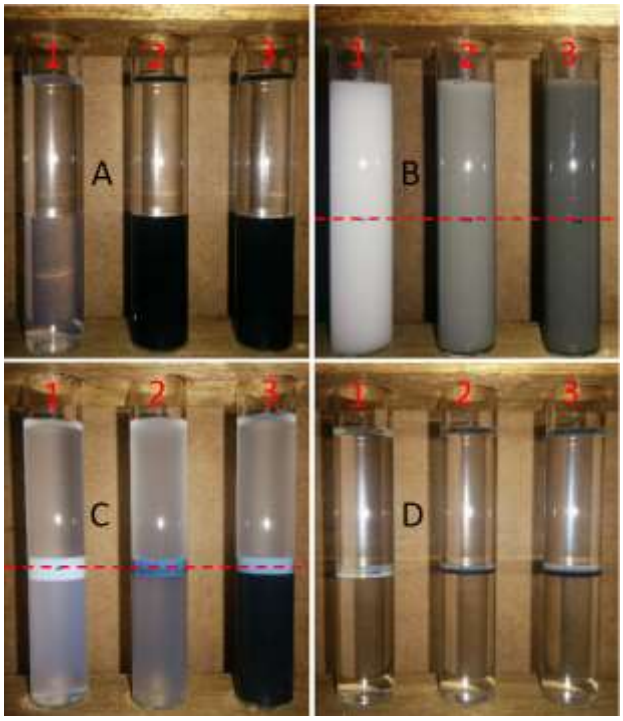

Figure 3.5. Phase behavior of synthetic oil Isopar^{TM} -L and ternary surfactant formulation (0.2 wt% LA40EO, 0.31 wt% AOT, and 0.17 wt% IOS) in 3 wt% brine at 50 ^{o}C. Sample 1. Surfactant only system; 2. Surfactant with 100 mg/L MWNT; 3. Surfactant with 100 mg/L CB. Panel A. 5 mL of oil and 5 mL of aqueous solution before shake; B. Right after shake; C. 5 minutes after shake; D. Equilibrium reached 2 hours after shake. Dashed line indicates initial oil/water interface.

Figure 3.5 shows phase behavior of a ternary surfactant system LAE-AOT-IOS with synthetic oil Isopar^{TM} -L at 50 ^{o}C. Control group adopted surfactant-only solution as the aqueous phase, while in experimental groups 100 mg/L MWNT or CB was introduced. Coalescence rates were fast for all tested samples. In Figure 3.5c, opaque middle phase appeared between the excess oil and aqueous phases just 5 minutes after shake. In the MWNT sample, distinct black aqueous phase, the original appearance of nanoparticle dispersion as shown in Figure 3.5a, faded away meanwhile MWNT quickly enriched in middle phase. Equilibrium was reached as seen in Figure 3.5d after 2 hours, translucent middle phase existed with clear transparent excess oil and aqueous phases in all samples. For samples with MWNT and CB, nanoparticles were seen enriched in the lower portion of middle phase and formed a thin black layer. Equilibrium IFTs between excess oil and excess aqueous phase of microemulsions were measured as 0.007, 0.009, 0.008 mN/m for surfactant-only, MWNT, and CB samples, respectively. Zargartalebi et al. [44] studied the effect of silica nanoparticle on IFT of kerosene and sodium dodecyl sulfate (SDS) solution, and they observed that nanoparticle-amended surfactant solution could achieve even lower IFT in comparison to surfactant-only solution. Note that the range of IFT values observed in Zargartalebi study were higher than the ultra-low values of this work. While for MWNTs and CBs, which were not surface active, the authors believe that the ultralow IFTs attained were only attributed to surfactants partitioning at oil/water interface and nanoparticles had hardly any effects on the IFTs. Phase behavior and IFT

were in accordance with the calculation of Gibbs free energy, thus further confirmed that surfactants were spontaneously released from nanoparticles surface to oil/water interface once dispersed particles contact oil.

3.3.5 Impact of oil recovery

Ternary surfactants LAE-AOT-IOS exhibited ultralow IFT with oil Isopar^{TM} -L, which was considered as a good candidate in chemical EOR. As a proof of concept, this formulation was adopted here to illustrate the effect of addition of MWNTs in surfactant chemical flooding. In the base case, 3PV optimum surfactant slug at 0.1wt% (maintaining same ratio as in 0.68 wt% solution, CMC = 0.03 wt%) was injected in chemical flooding, while in experimental nano carrier case, injected formulation also contained 100 mg/L MWNT with identical surfactants of 0.1 wt%. The viscosities of both formula were 1.2 cP, slightly higher than that of water. Oil breakthrough occurred simultaneously in both tests. Result of MWNT case was characterized by a sharp rise in oil cut right after oil breakthrough, with a maximum of 10.4% reached at 1.3 PV, while the oil cut in surfactant-only case slowly increased until a maximum of 5.2% attained at 2.7 PV. Cumulative oil recovery was 42.7% in the MWNT case versus 38.1% in base case. Apart from the higher tertiary oil recovery achieved with addition of MWNTs, a speedy oil recovery pattern further manifested surfactant carrier's superiority. For instance, oil recovery was 35% versus 14% after 2 PV chemical slug injection; and was 42% versus 30% after 3 PV chemical slug injection. The addition of MWNTs has essentially no effect on the solution viscosity (Figure B1 in Appendix B). Thus, the faster oil recovery is likely an important benefit of managing surfactant supply for any field project, as a result of the competitive adsorption on MWNTs has alleviated the surfactant loss in the sand pack.

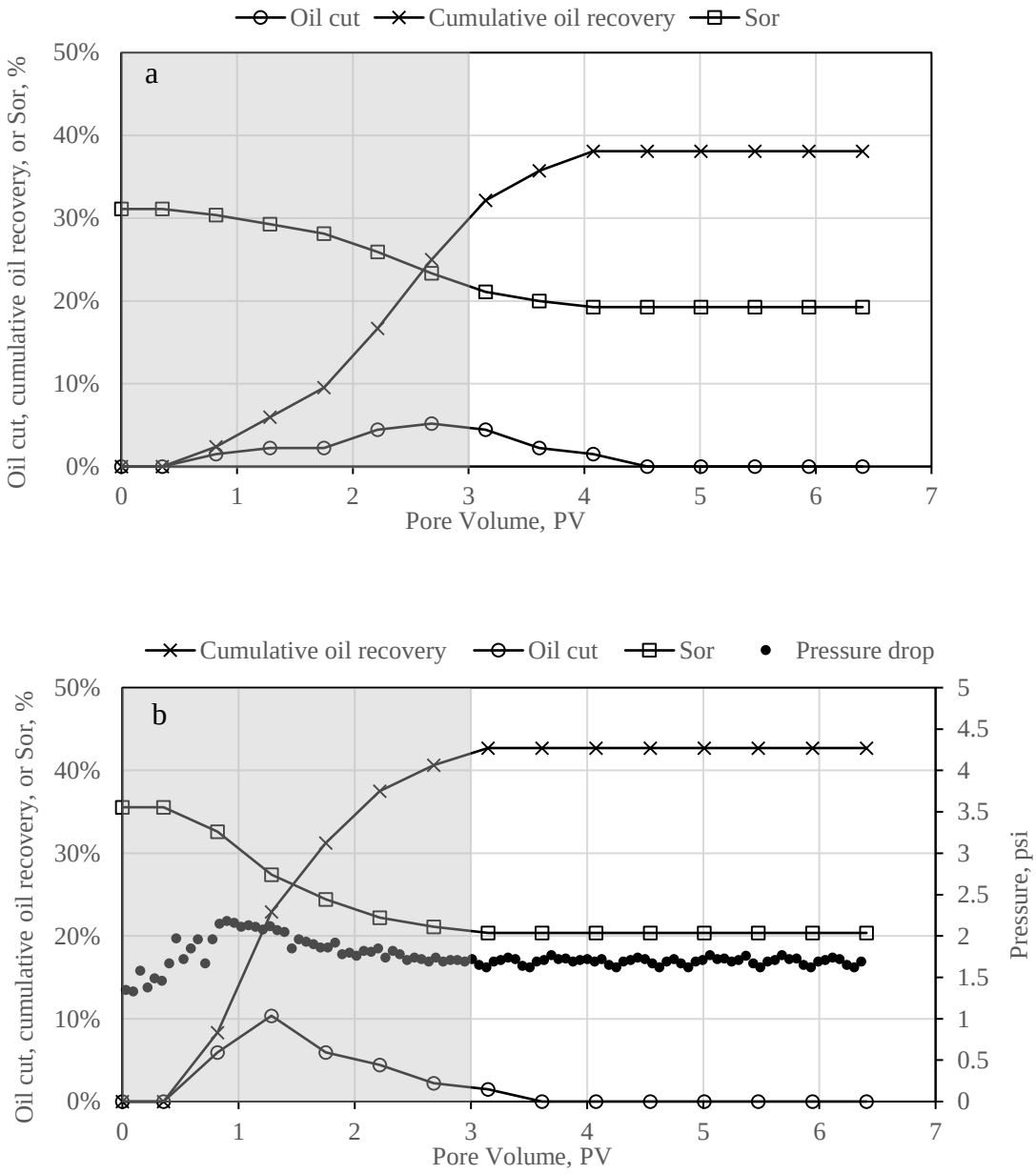

Figure 3.6. Tertiary oil recovery after injection of 3 PVs chemical slug (shaded area) in 3 wt% brine at 50 ºC. a, Surfactant-only slug at concentration of 0.1 wt%, initial Sor was 31.1%, and cumulative oil recovery was 38.1%; b, 0.1 wt% surfactant slug with 100 mg/L MWNT, initial Sor was 35.6%, and cumulative oil recovery was 42.7%

3.4 Discussion

Previously, SDBS adsorption density on SWNTs surface was determined by Matarredona et al. [26] as 11.6 molecules/nm^2, around twofold higher than AOS adsorption on MWNT calculated in this study (6.2 molecules/nm^2). Such distinction possibly resulted from dissimilar packing of surfactants on nanotubes surface due to dissimilar curvatures and specific surface areas of these two types of nanotubes, e.g. SWNT has a OD of 0.8 nm, and SSA 500 m^2/g, versus MWNT with OD 5-15 nm, SSA 250 m^2/g. Besides, high concentration of MWNT (370 mg/L) may cause agglomeration of nanotubes into small bundles in the solution, while at lower concentration (170 mg/L) in the study of Matarredona et al., SWNT were more likely to be individually dispersed. The impact of bundling could reduce the available surface area of nanotubes considerably thus led to a less efficiency on carrying surfactants. This has been confirmed by Sa and Kornev [39] in an extensive study on the adsorption of SDS on dispersed SWNTs at various levels of nanotube loading. Considering a hexagonal packing geometry of nanotube aggregates, Sa and Kornev determined the surface area of the aggregates was only 43% of that possessed by same amount of individually dispersed nanotubes. The growth of nanotube aggregates was also revealed by a disproportional relationship between the quantity of dispersed nanotubes and the uptake of surfactants. For instance, 750 mg/L SWNT was able to load 0.75 mM SDS, while double concentration of SWNT to 1500 mg/L only adsorbed 1 mM SDS.

In the oil recovery test, the retention of MWNT on Ottawa sand was 0.05 mg/g, approximately five folds higher than that occurred in absence of oil (0.011mg/g). Release of surfactants from MWNTs surface facilitated agglomeration of the dispersed nanotubes,

like MWNTs aggregated at the interface shown in Figure 3.5d, thus impeded transport of MWNT in the sand pack. Although significant pressure rise was not observed in Figure 3.6b for sand pack with high permeability of 4.0 Darcy, retention of nanoparticles may block pore throats in low permeable rocks and cause injectivity issue. On the other hand, working fluid would prefer to flow through the larger pores due to lower flow resistance. Once the nanotubes deposit on the large pore throat surface after detachment of surfactant, it is possible that fluid is diverted to the smaller pores therefore to increase the sweep efficiency. Similar high retention has also been observed in oil recovery test with CBs (Figure B2 in Appendix B).

Using pristine MWNTs or CB as surfactant carriers may be not practically feasible for various reservoir conditions. Further improvements can be made by tailoring the surface of nanoparticle with functional groups, such as hydroxyl groups, which should be able to provide stability for dispersed nanoparticles after surfactants are released from their surface, thus to ensure the transport of nanoparticles, especially in tight rock matrix. Recovered functionalized nanoparticles could be recycled to re-load surfactants before re-injection. Besides, surface functionalized groups have been reported to improve colloidal stability of nanotubes in aqueous media by dispersing them in individual form [45, 46], as a result, higher surface utilization and efficiency is also expected.

3.5 Conclusions

This study explored the feasibility of using carbonaceous nanoparticles MWNTs and CBs as surfactants carriers in enhanced crude oil recovery. Stability of the well-dispersed nanoparticles and their transport in porous media were examined in mimic reservoir condition. Particles retention was found as low as 0.004-0.011 mg/g in Ottawa sand. The

strong affinity to surfactant hydrophobic tails plus substantial surface area, enable MWNTs and CBs to load high density of surfactants. Competitive adsorption of AOS on MWNT surface against Ottawa sand was beneficial to reduce AOS adsorption loss on Ottawa sand at equilibrium concentration below CMC. Results of microemulsion phase behavior confirmed that nanoparticles successfully delivered surfactants and spontaneously released them to the oil/water interfaces once contacted oil. Presence of nanoparticles did not influence the ultralow IFT values between excess oil and aqueous phase, as measured around 0.007-0.009 mN/m. Nanoparticles-amended surfactant formulations achieved faster and higher tertiary oil recovery than surfactant-only formulation, however, release of surfactant led to nanoparticle instability thus retained in the reservoir medium. Further research effort is required to inspect occurrence of potential formation damages caused by severe retention of nanoparticles and offer any modifications on using functionalized carbonaceous nanoparticles to guarantee their fate and transport in porous medium after release of surfactant.

Acknowledgement

The authors would like to thank Advanced Energy Consortium for their partial financial support for this work.

Reference

[1] Green DW, Willhite GP. Enhanced oil recovery. Society of Petroleum Engineers; 1998.

[2] Salager J-L, Forgiarini AM, Bullón J. How to Attain Ultralow Interfacial Tension and Three-Phase Behavior with Surfactant Formulation for Enhanced Oil Recovery: A Review. Part 1. Optimum Formulation for Simple Surfactant–Oil–Water Ternary Systems. Journal of Surfactants and Detergents 2013;16(4):449-72.

[3] Hirasaki G, Miller CA, Puerto M. Recent Advances in Surfactant EOR. SPE Journal 2011;16(04):889-907.

[4] Wesson LL, Harwell JH. Surfactant adsorption in porous media. Surfactants: Fundamentals and Applications in the Petroleum Industry 2000;121:158.

[5] Scamehorn J, Schechter R, Wade W. Adsorption of surfactants on mineral oxide surfaces from aqueous solutions: I: Isomerically pure anionic surfactants. Journal of Colloid and Interface Science 1982;85(2):463-78.

[6] Somasundaran P, Zhang L. Adsorption of surfactants on minerals for wettability control in improved oil recovery processes. Journal of Petroleum Science and Engineering 2006;52(1-4):198-212.

[7] Zhang R, Somasundaran P. Advances in adsorption of surfactants and their mixtures at solid/solution interfaces. Advances in colloid and interface science 2006;123:213-29.

[8] Bera A, Kumar T, Ojha K, Mandal A. Adsorption of surfactants on sand surface in enhanced oil recovery: Isotherms, kinetics and thermodynamic studies. Applied Surface Science 2013;284:87-99.

[9] Amirianshoja T, Junin R, Idris AK, Rahmani O. A comparative study of surfactant adsorption by clay minerals. Journal of Petroleum Science and Engineering 2013;101:21-7.

[10] Paria S, Khilar KC. A review on experimental studies of surfactant adsorption at the hydrophilic solid-water interface. Adv Colloid Interface Sci 2004;110(3):75-95.

[11] Rosen MJ, Kunjappu JT. Surfactants and interfacial phenomena. John Wiley & Sons; 2012.

[12] Budhathoki M, Barnee SHR, Shiau B-J, Harwell JH. Improved oil recovery by reducing surfactant adsorption with polyelectrolyte in high saline brine. Colloids and Surfaces A: Physicochemical and Engineering Aspects 2016;498:66-73.

[13] Weston JS, Harwell JH, Shiau BJ, Kabir M. Disrupting admicelle formation and preventing surfactant adsorption on metal oxide surfaces using sacrificial polyelectrolytes. Langmuir 2014;30(22):6384-8.

[14] ShamsiJazeyi H, Verduzco R, Hirasaki GJ. Reducing adsorption of anionic surfactant for enhanced oil recovery: Part I. Competitive adsorption mechanism. Colloids and Surfaces A: Physicochemical and Engineering Aspects 2014;453:162-7.

[15] Rahmani AR, Bryant S, Huh C, Athey A, Ahmadian M, Chen J, et al. Crosswell magnetic sensing of superparamagnetic nanoparticles for subsurface applications. SPE Journal 2015;20(05):1,067-1,82.

[16] Mahmoud O, Nasr-El-Din HA, Vryzas Z, Kelessidis VC. Nanoparticle-based drilling fluids for minimizing formation damage in HP/HT applications. *SPE International Conference and Exhibition on Formation Damage Control.* Society of Petroleum Engineers; 2016.

[17] Zakaria M, Husein MM, Harland G. Novel nanoparticle-based drilling fluid with improved characteristics. *SPE International Oilfield Nanotechnology Conference and Exhibition.* Society of Petroleum Engineers; 2012.

[18] Barati R. Application of nanoparticles as fluid loss control additives for hydraulic fracturing of tight and ultra-tight hydrocarbon-bearing formations. Journal of Natural Gas Science and Engineering 2015;27:1321-7.

[19] Fakoya M, Shah S. Enhancement of Filtration Properties in Surfactant-Based and Polymeric Fluids by Nanoparticles. *SPE Eastern Regional Meeting.* Society of Petroleum Engineers; 2014.

[20] Abdelfatah E, Bang S, Pournik M, Shiau BJ, Harwell J, Haroun M, et al. Acid Diversion in Carbonates with Nanoparticles-Based in Situ Gelled Acid. *SPE Abu Dhabi International Petroleum Exhibition & Conference.* Society of Petroleum Engineers; 2017.

[21] Nyankson E, Olasehinde O, John VT, Gupta RB. Surfactant-Loaded Halloysite Clay Nanotube Dispersants for Crude Oil Spill Remediation. Industrial & Engineering Chemistry Research 2015;54(38):9328-41.

[22] Neves Libório De Avila J, Louise Grecco Cavalcanti De Araujo L, Drexler S, de Almeida Rodrigues J, Sandra Veiga Nascimento R. Polystyrene nanoparticles as surfactant carriers for enhanced oil recovery. Journal of Applied Polymer Science 2016;133(32).

[23] Romero-Zerón LB, Kittisrisawai S. Evaluation of a surfactant carrier for the effective propagation and target release of surfactants within porous media during enhanced oil recovery. Part I: Dynamic adsorption study. Fuel 2015;148:238-45.

[24] Berlin JM, Yu J, Lu W, Walsh EE, Zhang L, Zhang P, et al. Engineered Nanoparticles for Hydrocarbon Dectection in Oil-Field Rocks. *SPE International Symposium on Oilfield Chemistry.* Society of Petroleum Engineers; 2011.

[25] Drexler S, Faria J, Ruiz MP, Harwell JH, Resasco DE. Amphiphilic Nanohybrid Catalysts for Reactions at the Water/Oil Interface in Subsurface Reservoirs. Energy & Fuels 2012;26(4):2231-41.

[26] Matarredona O, Rhoads H, Li Z, Harwell JH, Balzano L, Resasco DE. Dispersion of single-walled carbon nanotubes in aqueous solutions of the anionic surfactant NaDDBS. The Journal of Physical Chemistry B 2003;107(48):13357-67.

[27] Chen C, Kadhum MJ, Mercado MC, Shiau B, Harwell JH. Surfactant-Only Stabilized Dispersions of Multiwalled Carbon Nanotubes in High-Electrolyte-Concentration Brines. Energy & Fuels 2016;30(11):8952-61.

[28] Sarafraz MM, Hormozi F, Silakhori M, Peyghambarzadeh SM. On the fouling formation of functionalized and non-functionalized carbon nanotube nano-fluids under pool boiling condition. Applied Thermal Engineering 2016;95:433-44.

[29] Ferraro G, Fratini E, Rausa R, Fiaschi P, Baglioni P. Multiscale Characterization of Some Commercial Carbon Blacks and Diesel Engine Soot. Energy & Fuels 2016;30(11):9859-66.

[30] Geiger SL, Durnford DS. Infiltration in homogeneous sands and a mechanistic model of unstable flow. Soil Sci Soc Am J 2000;64(2):460-9.

[31] Witthayapanyanon A, Harwell JH, Sabatini DA. Hydrophilic-lipophilic deviation (HLD) method for characterizing conventional and extended surfactants. J Colloid Interface Sci 2008;325(1):259-66.

[32] Pham NH, Harwell JH, Resasco DE, Papavassiliou DV, Chen C, Shiau B. Transport and deposition kinetics of polymer‐coated multiwalled carbon nanotubes in packed beds. AIChE Journal 2016;62(10):3774-83.

[33] Vaisman L, Wagner HD, Marom G. The role of surfactants in dispersion of carbon nanotubes. Adv Colloid Interface Sci 2006;128-130:37-46.

[34] Huang YY, Terentjev EM. Dispersion of Carbon Nanotubes: Mixing, Sonication, Stabilization, and Composite Properties. Polymers 2012;4(4):275-95.

[35] Shikata T, Okuzono M, Sugimoto N. Temperature-Dependent Hydration/Dehydration Behavior of Poly(ethylene oxide)s in Aqueous Solution. Macromolecules 2013;46(5):1956-61.

[36] Chen C, Wang S, Tian W, Wang S, Shiau B-J, Harwell JH. Micellar interaction of binary mixtures of alpha olefin sulfonate and nonylphenol polyethylene glycol

ethers: Length effects of ethylene oxide. Colloids and Surfaces A: Physicochemical and Engineering Aspects 2018;542:31-41.

[37] Wang Y, Kim JH, Baek JB, Miller GW, Pennell KD. Transport behavior of functionalized multi-wall carbon nanotubes in water-saturated quartz sand as a function of tube length. Water Res 2012;46(14):4521-31.

[38] Jaisi DP, Elimelech M. Single-walled carbon nanotubes exhibit limited transport in soil columns. Environmental science & technology 2009;43(24):9161-6.

[39] Sa V, Kornev KG. Analysis of stability of nanotube dispersions using surface tension isotherms. Langmuir 2011;27(22):13451-60.

[40] Journet C, Moulinet S, Ybert C, Purcell ST, Bocquet L. Contact angle measurements on superhydrophobic carbon nanotube forests: effect of fluid pressure. EPL (Europhysics Letters) 2005;71(1):104.

[41] De Nicola F, Castrucci P, Scarselli M, Nanni F, Cacciotti I, De Crescenzi M. Super-hydrophobic multi-walled carbon nanotube coatings for stainless steel. Nanotechnology 2015;26(14):145701.

[42] Nuriel S, Liu L, Barber A, Wagner H. Direct measurement of multiwall nanotube surface tension. Chemical Physics Letters 2005;404(4):263-6.

[43] Berg JC. An introduction to interfaces & colloids: the bridge to nanoscience. World Scientific; 2010.

[44] Zargartalebi M, Barati N, Kharrat R. Influences of hydrophilic and hydrophobic silica nanoparticles on anionic surfactant properties: Interfacial and adsorption behaviors. Journal of Petroleum Science and Engineering 2014;119:36-43.

[45] Smith B, Wepasnick K, Schrote KE, Cho HH, Ball WP, Fairbrother DH. Influence of surface oxides on the colloidal stability of multi-walled carbon nanotubes: a structure-property relationship. Langmuir 2009;25(17):9767-76.

[46] Osorio AG, Silveira ICL, Bueno VL, Bergmann CP. H2SO4/HNO3/HCl—Functionalization and its effect on dispersion of carbon nanotubes in aqueous media. Applied Surface Science 2008;255(5):2485-9.

Chapter 4 Micellar Interaction of Binary Mixtures of Alpha Olefin Sulfonate and Nonylphenol Polyethylene Glycol Ethers: Length Effects of Ethylene Oxide

Graphical abstract

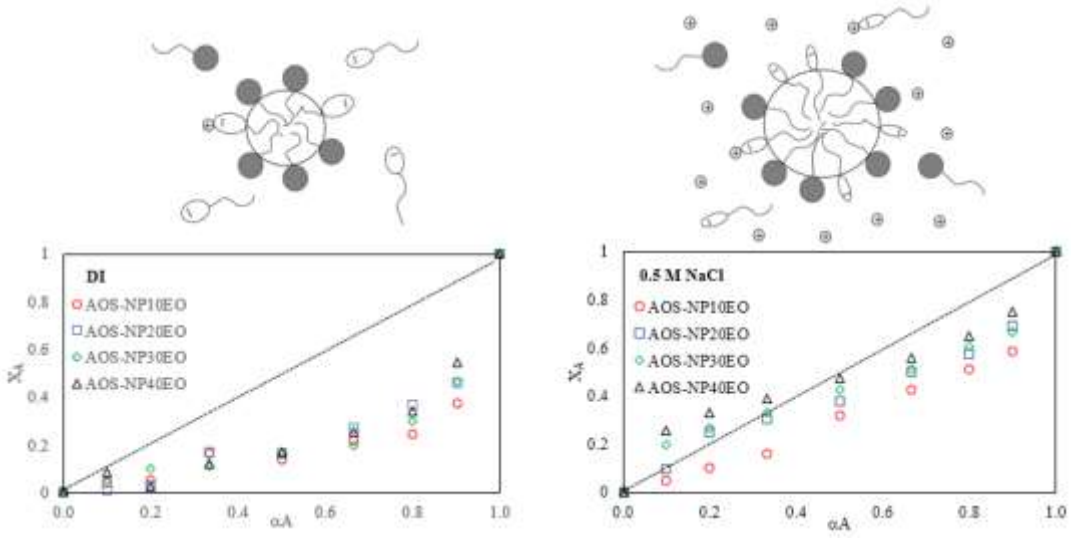

Abstract

The micellization behavior of binary surfactant mixtures constituted by an anionic surfactant, alpha olefin sulfonate (AOS), and a nonionic surfactant nonylphenol polyethylene glycol ether (NPE) with different numbers of ethylene oxide (EO), namely, NP10EO, NP20EO, NP30EO, and NP40EO was comprehensively investigated by surface tensiometer, conductometer, cloud point measurement, and dynamic light scattering. Theoretical treatments were carried out to explain molecular interaction in the mixed micelles based on regular solution theory of Rubingh, micellization thermodynamics of Molyneux et al. and Maeda, and molecular thermodynamic theory of

Pavvada and Blankschtein. Results indicate non-ideal mixing behavior in all AOS-NPE mixtures, where nonionic surfactant EO chain length was found to play critical roles. In the absence of additional electrolytes, NPEs exhibited substantially higher activity in micelles than bulk solution; with growth of EO groups, shrinkage on the scale of synergistic interaction was evidenced. In contrary, with swamping amount of electrolytes, synergistic interactions enlarged with the rise of EO groups, and AOS activity in mixed micelles was found depending on both EO length and bulk mole fraction (α_A). These findings are of great significance in mixed surfactant formulation design/optimization to maximize the synergistic efficiency of the system thus to minimize the chemical consumption and cost.

Keywords

Micellar interaction, anionic-nonionic mixture, alpha olefin sulfonate, ethylene oxide, electrolytes, synergism

4.1 Introduction

Surfactant mixtures are of great interest in a variety of practical applications because their mixed micellar aggregates exhibiting excellent properties compared to individual surfactant component, viz. synergism. Synergistic interactions in mixed surfactant system are highly favorable since they are associated with stronger surface/interfacial activity, lower critical micelle concentration (CMC), higher solubilizing power, better dispersion stability, and most importantly for routine industrial applications, less chemical consumptions and project costs [1-7]. Binary surfactant systems of anionic-nonionic mixtures are important from both fundamental and application point of views as addition of nonionic surfactant to ionic surfactant micelle can reduce the electrostatic repulsion

between the charged surfactant heads therefore greatly facilitate mixed micelle formation [2, 8-10]. In recent years, considerable investigations on the interfacial and bulk properties of mixtures containing anionic and nonionic surfactants have been carried out in fields such as detergency, cosmetic products, drug delivery, soil remediation, and enhanced oil recovery [11-15]. A thorough understanding of the physicochemical properties of non-ideal mixing behaviors of mixed micellar solution, such as surface excess, counterion binding and thermodynamics of micelle formation, has great importance for practical formulation design/optimization to control the behavior of mixed surfactants with desired properties [16].

Among anionic-nonionic surfactant mixtures, ionic surfactant, sodium dodecyl sulfate (SDS) or sodium dodecyl benzenesulfonate (SDBS), associated with nonionic, either alkyl polyethylene glycol ether (C_mE_n) or alkylphenol polyethylene glycol ether are the most extensively studied system, because they are widely applied in chemical, pharmaceutical, and industrial fields [4, 5, 8, 17, 18]. Varying the ethylene oxide (EO) number (i.e., hydrophilic lipophilic balance) of nonionic surfactant leads to substantial change in molecular interaction as well as mixture properties. Chen et al. [19] showed that anionic-nonionic surfactant mixtures containing nonionic surfactant with 40 EO groups exhibited outstanding dispersion stability of multi walled carbon nanotubes at harsh salinity conditions (10 wt% brine) than those with low EO numbers of 10-20. Zhou and Rosen examined the interactions between the mixtures of sodium dodecyl sulfonate ($C_{12}SO_3Na$) and $C_{12}E_n$ with n = 4 to 8 EO groups, and observed slightly more negative values of interaction parameter (β) with larger EO number [3]. Stronger synergistic interactions (i.e., larger net β) with longer EO chain was confirmed by Joshi et al. [4] in

mixtures of SDS and $C_{12}E_n$ (12, and 15 EOs). However, studies by Sahu et al. [18] on the mixture of SDBS with $C_{13\text{-}15}E_n$ (7, 9, and 12 EOs) and by Ren et al. [17] on interaction between amphoteric surfactant (alkyl amino sulfonate, $C_{12}AS$) with octylphenol polyethoxylates (4, 7, and 10 EOs) under the influence of 0.25 M different species of inorganic cations failed to show a distinct impact of EO length on those interaction or thermodynamic parameters involved. Despite widespread applications of anionic-nonionic mixed surfactant systems, their interactions had not been well understood at a fundamental molecular level [9, 20]. Thus, a systematic analysis on the effect of EO length on binary mixed micellar interactions is of great importance to pave the way of developing superior performance formulations.

This work deals with a detailed investigation on the physicochemical characterization of alpha olefin sulfonate (AOS) and nonylphenol polyethylene glycol ether, also known as nonylphenol ethoxylates (NPE), and their binary mixtures in aqueous solution. Due to its unique molecular structure, AOS is an effective emulsifier and outstanding detergent, which has high compatibility with hard water (superior than SDBS and SDS) as well as good wetting, foaming, and thermal stability properties [21, 22]. All these features combined with low adsorption on sandstone [22] enabling AOS to be an excellent candidate as foam booster in enhanced oil recovery. The counterpart nonionic, NPE is a popular surfactant which has been used in many fields, including detergency, textile and paper processing, paints and coatings, and oil and gas recovery. The values of CMC, counterion binding constant, cloud point, micellar hydrodynamic size, and adsorption properties of the individual and mixed surfactant systems have been determined at both DI and 0.5 M NaCl solution. In this work, a wide range of EO numbers (10-40) is used

to illustrate impact of EO length on the mixed micellar behaviors. The composition of the mixed micelles (X), activity coefficient (f_A, f_N), interaction parameter between two surfactants (β), Gibbs energy of micellization (ΔG_m), and excess energy of micellization (ΔG_{ex}) are evaluated from Rubingh's regular solution theory (RST) [23, 24] as well as Maeda's thermodynamic approach [25]. Molecular thermodynamic theory [26, 27] of Pavvada and Blankschtein (PB theory) is also applied to capture the evolution of electrostatic and steric free energy in micellization. Results of this study is instrumental in understanding aggregation behavior of ionic-nonionic surfactant mixtures, and therefore facilitating design/optimization of synergistically interacted surfactant formulations for soil remediation, foam booster, and enhanced oil recovery.

4.2 Experimental

4.2.1 Materials

Alpha olefin sulfonate ($C_{14\text{-}16}SO_3Na$, AOS) was manufactured and provided by Stepan Company (Northfield, IL) as 39 wt% active water solution. Nonylphenol polyethoxylates with 10, 20, 30, and 40 ethylene oxide (EO) groups (NP10EO, NP20EO, NP30EO, and NP40EO, respectively) were all provided by Huntsman (Salt Lake City, UT) as 100% active. All surfactants were used as received without further purification. Sodium chloride (NaCl) was purchased from Sigma Aldrich.

4.2.2 Surface Tension Measurements

Measurements were conducted at 25 ^oC by a dynamic contact angle analyzer DCA-322 (Cahn Instruments, USA) utilizing a technique based on the Wilhelmy plate principle. The equipment was calibrated by double distilled water at 25 ^oC (72.0±0.5 mN/m) each

day before experiments. Glass plate was thoroughly cleaned then flame-dried before each measurement. Measurements were duplicated and the mean value was recorded. The critical micelle concentration (CMC) values were determined from the break point in the curve of surface tension versus the logarithm of surfactant concentration.

4.2.3 Conductivity Measurements

Conductivity measurements were carried out for AOS and AOS-NPE mixtures in deionized water (DI) at 25 ^{o}C using a Mettler Toledo S230 SevenCompact Conductivity Meter (Columbus, OH). The cell used is Cond probe InLab 731-ISM-2m with cell constant of 0.57 cm^{-1}. Errors of the measured conductivity values were within $\pm$ 0.5%.

4.2.4 Cloud Point Measurements

Cloud point was determined by controlled heating in a constant temperature oven DKN402C (Yamato Scientific, Japan). Fixed concentration of NPE (1 wt%) adjusted with different concentrations of AOS in DI or 0.5 M NaCl solution was taken in a sealed 10 mL Pyrex pressure vessel to maintain the vapor pressure developed inside the reactors. The heating rate for the samples was controlled at 1^{o}C/min. The first appearance of turbidity (and verified by the cooling cycle and disappearance of cloudiness) was taken as the cloud point and reproducibility of the measurement was found to be within $\pm$ 0.5^{o}C.

4.2.5 Dynamic Light Scattering

Micellar size distribution for various surfactant samples were determined by dynamic light scattering (DLS) using ZetaPALS (Brookhaven Instruments, Holtsville, NY) with a

wavelength of 659 nm. The scattering angle was fixed at 90°. All correlation spectra were recorded at 25 ^{o}C and analyzed with the installed particle solution software provided by Brookhaven. Results were reported as the average from triplicates of DLS measurements of individual sample.

4.3 Results and Discussion

4.3.1 Surface Tension

Representative surface tension versus surfactant molar concentration plots for individual surfactants and their binary mixtures are shown in Figure C1 (Appendix C). The break point where the surface tension begins to level off implies the forming of micelles. The measured CMC of AOS in DI is 1.602 mM. In comparison, all nonionic NPEs tested exhibit much lower CMC values (0.066-0.180 mM in DI), reflecting less repulsion between their head groups opposing micellization, and among NPEs an evident rise in their surface tensions at CMC, γ_{CMC}, was observed with increase of EO groups. Based on surface tension isotherms, surface excess concentration, Γ, in mol/m^2 and minimum area per surfactant molecule, A_{min}, in nm^2 at the air/liquid interface can be estimated graphically using the Gibbs adsorption equation [1],

$$\Gamma = -\frac{1}{2.303nRT}\left(\frac{\partial\gamma}{\partial log C}\right)_T \tag{4.1}$$

$$A_{min} = \frac{10^{21}}{N_A\Gamma} \tag{4.2}$$

where n is the number of species of ions that arise from dissociation of surfactant, and its value largely depends on electrolytes, e.g. n is 1 for nonionic surfactant or monomeric surfactant in the presence of a swamping (elevated) amount of electrolytes. n is taken as

2 represents for monomeric surfactant without extra electrolytes. R is the universal gas constant, T is absolute temperature, γ is surface tension, C is surfactant concentration, and N_A is Avogardo's number. Data of CMC, γ_{CMC}, Γ, and A_{min} are summarized in Table 4.1.

Table 4.1. Interfacial parameters for individual surfactant

NaCl, M	Surfactant	CMC, mM	γ_{CMC}, mN/m	10^6 Γ, mol/m^2	A_{min}, nm^2/molecule
0	AOS	1.602 (3.1[a])	34.5	2.65	0.627
	NP10EO	0.066 (0.075[b])	32.0 (31[b])	3.56	0.467
	NP20EO	0.133 (0.14[b])	39.5 (38[b])	2.08	0.797
	NP30EO	0.162 (0.185[b])	42.0 (41[b])	2.06	0.804
	NP40EO	0.180	44.2	1.66	0.998
0.5	AOS	0.201	28.4	5.81	0.286
	NP10EO	0.057	32.7	4.02	0.413
	NP20EO	0.101	39.5	2.66	0.625
	NP30EO	0.106	43.6	1.86	0.894
	NP40EO	0.162	46.4	1.66	0.999

[a] Reference [22]. [b] Reference [28]

It has been observed that, the values of A_{min}, CMC as well as γ_{CMC} increased with increase in ethoxylation of nonionic surfactants (larger EO numbers). As the EO chain grows bigger, much larger steric repulsive interactions among hydrophilic head groups lead to greater energy barrier for nonylphenol tails to accumulate at surface, thus high EO surfactants molecules exhibited less surface activity [3, 6]. Besides, addition of 0.5 M NaCl resulted in a drastic reduction on the CMC of AOS to 0.201 mM vs. 1.602 mM in DI, accompanied with a decrease on γ_{CMC} from 34.5 mN/m to 28.4 mN/m. The electrostatic repulsion between negatively charged AOS head groups are largely shielded by a swamping amount of counterions, so that monomers can easily form micelles in elevated salt condition and accumulate (adsorb) densely at interface. In contrast, adding salt has less significant influence on micelle formation of NPEs. The resulted CMC values

of various binary systems (discussed later in section 3.6, Table 4.3 and Table 4.4) in DI condition likely fell between those of individual surfactants, while mixed CMC in 0.5 M NaCl could achieve even lower values compared to that of single surfactant.

4.3.2 Counterion Binding

Conductivity measurements allow associated counterions to be evaluated in ionic surfactant-only micelle as well as in ionic-nonionic mixed micelles in the solution. The degree of counterion dissociation is interpreted from the ratio of supra-cmc and sub-cmc slopes corresponding to the linear approximation plots of solution conductivity [9], as depicted in Figure C2 (Appendix C). The degree of counterion binding, B, is simply calculated by subtracting the counterion dissociation from unity. Results for counterion binding is presented in Table 4.3 and discussed in details later. For the AOS-NPE mixtures, two apparent trends were noticed: first, with the rise in (mole) fraction of nonionic surfactant in the mixture, the ion binding, B, gradually decreased due to a dilution of surface charge in mixed micelles; second, for a fixed fraction of AOS in different binary mixtures, the B values increased with growing EO numbers of nonionic surfactant, e.g. for same AOS mole fraction of 0.8, the B values are 0.060, 0.074, 0.098, and 0.169 for mixture with NP-10, 20, 30, and 40 EOs, respectively. The rise in B may be a result of much stronger ion-dipole interactions associated with larger EO numbers in turn dissociation of counterion is brought down.

4.3.3 Cloud Point

The cloud point is an important property for nonionic surfactants above which homogeneous solution appears to separate into an almost micelle-free dilute phase of

surfactant and a surfactant-rich micellar phase [1]. Upon heating the nonionic surfactant solution, ethoxylated group in hydrophilic head starts to dehydrate, resulting in an increase in the aggregation number and decrease in inter-micellar repulsion [29, 30]. Eventually, it leads to distinct phase separation of solution. Results of cloud points for different NPEs and nonionic-anionic mixtures depending on the AOS concentrations are depicted in Figure 4.1. The value of cloud point largely depends on the EO numbers as well as introducing such additives as electrolytes in these mixed micellar systems. In DI, NP10EO has cloud point at 66 ºC. With additional 10 EO groups, the cloud point for NP20EO soared to 112 ºC. In general, with identical hydrophobic group, the larger the oxyethylene length exist in the head group, the higher the cloud point is [1]. Beyond 20 EOs in the surfactant molecule, however, further increase in EO numbers did not generate much difference on cloud points. With presence of 0.5 M NaCl, The values of cloud point for NP10EO and NP20EO dropped to 55 ºC and 96 ºC, respectively, attributed mainly to the salting out effects of the hydrophobic groups by the addition of electrolytes [31, 32].

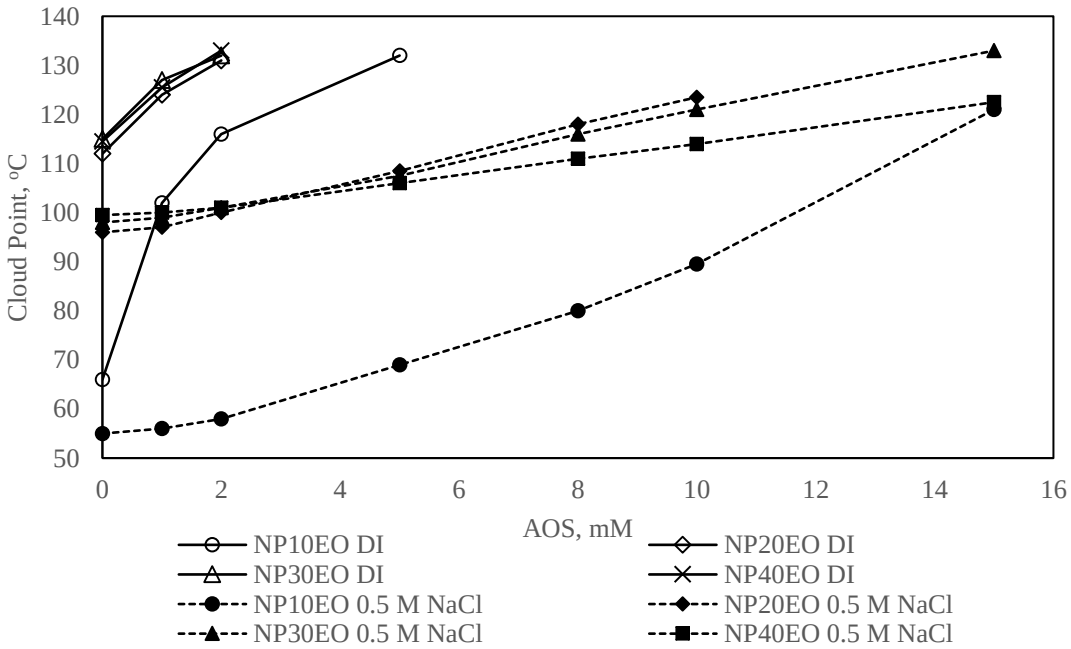

Figure 4.1. Cloud point of 1 wt% NPE with 10-40 EOs in DI (opened symbols) or 0.5 M NaCl solution (filled symbols) as a function of AOS concentration.

It is notable that adding anionic AOS improves cloud points (to higher temperatures) for all NPE-AOS mixtures tested. For instance, cloud point for NP10EO in DI drastically increased from 66 ^{o}C to 102 ^{o}C with merely 1 mM AOS added. Addition of extra 5 mM AOS could further enhance cloud point to temperature greater than 130 ^{o}C. It is anticipated that incorporation of ionic surfactants into the nonionics would build up electrical charges on mixed micelles surface. Increasing electrostatic repulsion presented between mixed micelles thus effectively hinder their aggregation and other phase separation behaviors, like coacervation, consequently cloud point is raised. In Figure 4.1, solid curves represent cloud points in DI, charaterized by a much steeper slope compared to that of dashed curves for presence of NaCl cases. Presence of swamping electrolytes causes significant compression of the electrical double layer of mixed micelles and, thus, largely reduces electrostatic repulsion betweeen micelles. On the other hand, incorporation of anionic surfactants in mixed micelles could decrease the fraction of nonionic surfactant in micelle, which in turn alleviates the extent of dehydration of EO groups. Therefore, increasing mole fraction of AOS shows positive effects on raising the cloud points of NPEs in the 0.5 M NaCl cases, but not as significant as what has been observed in DI. For NPE-20EOs or greater, with modest AOS added (< 2mM), cloud points in 0.5 M NaCl are in the sequence NP20EO < NP30EO < NP40EO, while with greater amount of AOS (> 2mM), eventually, a reverse sequence of cloud points is noticed that NP20EO > NP30EO > NP40EO. The reason for such inversion is unclear, and further investigation of the detailed mechanisms involved is beyond the scope of this work.

4.3.4 Micelle Aggregation

Micelle size distributions were examined by DLS in both DI and 0.5 M salt solution. Hydrodynamic diameter of micelle is given by Stokes-Einstein equation, $d_H = kT/3\pi\eta D$. Where k is the Boltzmann constant, η is the viscosity of solvent, and D is diffusion coefficient. Molecular weight of micelle is estimated by MHS relation, $D = K_{MHS} * MW^{a_{MHS}}$. Where K_{MHS}, and a_{MHS} are a pair of constants corresponding to the solvent properties analyzed, taking as 7.89×10^{-5} and -0.43, respectively. The aggregation number of surfactant micelle can be determined with molecular weight of aggregate and surfactants, $N_{Agg} = MW_{agg}/MW_{avg}$. Once aggregation number is known, the area per surfactant at micelle core/water interface can be easily computed by $a = \pi d_H^2/N_{Agg}$.

Table 4.2. Mean hydrodynamic diameter and micelle aggregation number for surfactants in DI and 0.5 M NaCl solution.

NaCl, M	Surfactant	d_H, nm	Polydispersity	Agg MW	Agg Number	a, nm^2
0	AOS	3.64	0.097	1.24E+04	40	1.05
	NP10EO	10.81	0.073	1.60E+05	242 (276[a])	1.51
	NP20EO	8.35	0.132	8.80E+04	80 (62[a])	2.74
	NP30EO	9.06	0.108	9.60E+04	62 (44[a])	4.14
	NP40EO	8.91	0.096	1.03E+05	52	4.79
0.5	AOS	7.17	0.054	6.20E+04	199	0.81
	NP10EO	10.07	0.098	1.38E+05	209	1.52
	NP20EO	8.04	0.148	8.40E+04	76	2.66
	NP30EO	8.90	0.088	1.03E+05	67	3.72
	NP40EO	9.97	0.138	1.34E+05	68	4.61

[a] Reference [33]

Example of unimodal distribution plot for AOS and NP10EO is shown in Figure C3 (Appendix C). In the DI water, AOS possesses a mean hydrodynamic diameter of 3.64 nm, which agrees well with the literature value of 3.8 nm [21]. With presence of 0.5 M

salt, size distribution curve shifts toward the right side, leading to a larger d_H of 7.17 nm. AOS micelles swell due to the shielding electrostatic repulsion between head groups resulted in a larger aggregate. For NP10EO a hydrodynamic diamter of 10.81 nm was recorded in DI, versus a slightly smaller d_H of 10.07 nm for 0.5 M salt scenario. Results of mean hydrodynamic diameters with micelle aggregation number data are summarized in Table 4.2 for individual surfactants.

The variations in aggregation behavior of different AOS-NPE mixtures were further analyzed at various mole fractions of the AOS, α_A, and different solution conditions (DI and 0.5M NaCl). Since the surfactant concentration used at measuring the d_H of the AOS-NPE mixed micelles (10 mM) was much higher than the CMC's of these surfactant mixtures, therefore, we can safely assumed that the micelle composition, X_A is the same as the solution composition, such that $X_A = \alpha_A$ [34, 35]. Figure 4.2 displays 3 representative curves for variation of hydrodynamic diameter against the composition change in mixture system. For AOS-NP10EO system in DI, a sharp drop on d_H from 10.81 nm to 3.16 nm was noticed with as little as 0.1 mole fraction of AOS added in the mixture. This reflects a strong head-head repulsion once anionic molecule penetrated in the nonionic surfactant micelles. Further addition of AOS did not generate significant change on micelle size. A relatively stable diameter distribution around 3.25 nm (standard deviation = 0.36 nm) was recorded for α_A from 0.1 to 1.0. For AOS-NP10EO system in 0.5 M NaCl, along with rise in the AOS fraction in the mixture, a growth on mielle size was seen when $\alpha_A \leq 0.2$; at $\alpha_A = 0.2$, d_H reached a peak value of 12.03 nm; when $\alpha_A > 0.2$, a steady reduction occurred as micelle size gradually gets close to the diameter of pure AOS micelle in 0.5 M salt, 7.17 nm. Similar variation on micelle size has also been

reported previously for tetradecyltrimethylammonium bromide with $C_{12}E_{23}$ mixtures, and the peak size was believed to coincide with the least headgroup-headgroup repulsion in the mixed micelles [36]. For AOS-NP30EO system in 0.5 M NaCl, increase in α_A causes a steadily monotonic decrease in mixture micelle size from 8.9 to 7.17 nm. It is in agreement with smooth change of activity coefficients for both AOS and NP30EO, implying relatively stable interaction between them [4].

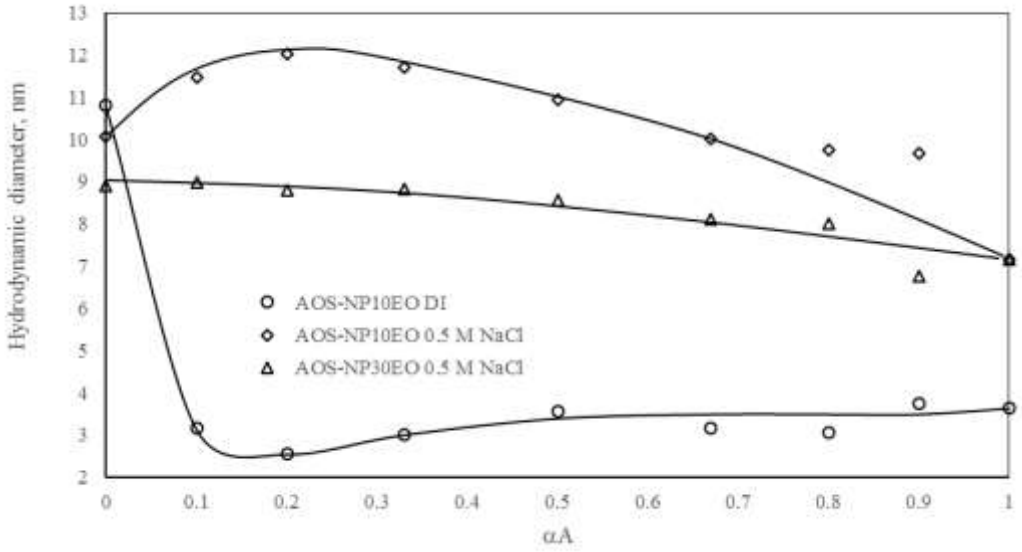

Figure 4.2. Variation of hydrodynamic diameter of mixture systems with mole fraction of AOS for AOS-NP10EO, in DI, and AOS-NP10EO, AOS-NP30EO in 0.5 M NaCl solution.

4.3.5 Mixed Micelles Theory

Rubingh (1979) proposed the well-known regular solution theory (RST) to conveniently predict the CMC of any mixtures of dual surfactants based on the CMC values of the individual surfactants and one or more mixtures of them [23, 24]. RST has been proven as a robust basis for evaluating the non-ideality of binary mixed systems, primarily because it offered a rather simple but effective quantitative tool-interaction parameter (β)

to describe common surfactant synergistic and antagonistic phenomena. According to RST, the mixed CMC of anionic and nonionic surfactants can be evaluated by [23]:

$$\frac{1}{\mathrm{CMC_M}} = \frac{\alpha_\mathrm{A}}{\mathrm{f_A CMC_A}} + \frac{1-\alpha_\mathrm{A}}{\mathrm{f_N CMC_N}} \tag{4.3}$$

where α_A is the mole fraction of anionic surfactant in the total mixed solution; $\mathrm{f_A}$, $\mathrm{f_N}$ are the activity coefficients of anionic and nonionic surfactant in mixed micelles; $\mathrm{CMC_A}$, $\mathrm{CMC_N}$, $\mathrm{CMC_M}$ are the CMC of anionic, nonionic, and mixture surfactant, respectively.

As for ideal mixing behavior, $\mathrm{f_A} = \mathrm{f_N} = 1$, hence above equation can be reduced to the form of Clint equation [37]:

$$\frac{1}{\mathrm{CMC_M}} = \frac{\alpha_\mathrm{A}}{\mathrm{CMC_A}} + \frac{1-\alpha_\mathrm{A}}{\mathrm{CMC_N}} \tag{4.4}$$

Interaction parameter, β is a quantitative indicator for the nature and strength of the interactions between the two components (A, N) in the mixed surfactants system [23]. A negative value of β implies the synergistic interactions, while a positive value suggests antagonistic interactions. A zero value of β indicates ideal mixing. Following relationship is suggested by Rubingh [23] to estimate the micellar composition for non-ideal mixing systems:

$$\frac{(\mathrm{X_A})^2 \ln[(\alpha_\mathrm{A}\mathrm{CMC_M}/\mathrm{X_A CMC_A})]}{(1-\mathrm{X_A})^2 \ln[(1-\alpha_\mathrm{A})\mathrm{CMC_M}/(1-\mathrm{X_A})\mathrm{CMC_N}]} = 1 \tag{4.5}$$

where X_A is the mole fraction of anionic surfactant in the mixed micelle. This equation needs to be solved by iteration, then interaction parameter and activity coefficients can be obtained conveniently with:

$$\beta = \frac{\ln[(\alpha_\mathrm{A}\mathrm{CMC_M}/\mathrm{X_A CMC_A})]}{(1-\mathrm{X_A})^2} \tag{4.6}$$

$$\mathrm{f_A} = \exp[\beta(1-\mathrm{X_A})^2] \tag{4.7}$$

$$f_N = \exp(\beta X_A^{\,2}) \tag{4.8}$$

Data obtained for mixture systems in DI are reported in Table 4.3. Apart from $\alpha_A = 0.9$ in AOS-NP30EO and AOS-NP40EO mixtures, β values for all the systems are negative, which manifested synergism prevailing in mixed AOS-NPE surfactants. In the DI water, anionic surfactant needs to overcome the electrostatic repulsion between ionic head groups to form micelle. With addition of nonionic surfactants, ethylene oxide chain of the nonionic surfactant mostly coils around the charged head group of the anionic surfactant. This helps dramatically reduce electrostatic repulsion between anionic-anionic head groups, and generate an ion-dipole attraction between two different hydrophilic head groups [3, 6].

Moreover, with greater ethoxylation of nonionic surfactant, average interaction parameter, β_{avg} became less negative, from -1.99, -1.37, -0.80, to -0.49 for 10, 20, 30, and 40 EOs, respectively, which signifies a weakened synergistic interaction between A/N surfactants with longer EO chain. This is possibly associated with a bulkier NPE head group with higher steric repulsion found itself harder to accommodate into a relatively small AOS micelle (d_H = 3.64 nm). Hu et al. [6] noticed similar variations in absolute value of β with increase in EO length in their investigation of $C_{12}E_n$ and cationic gemini surfactant mixtures. They evidenced that the polyethylene lauryl ether $C_{12}E_{42}$, which possesses longest 42 EO groups, resulted in the least CMC change among three binary surfactant systems tested. A series of curves of micelle mole fraction X_A against bulk mole fraction α_A are shown in Figure 4.3a for mixed micelles in DI, and Figure 4.3b in NaCl case. The dashed line represents the mixtures, which has equal X_A and α_A. The trends for all these anionic-nonionic mixtures are more or less the same. In DI, they all

exhibit lower mole fraction of AOS in the mixed micelle than that in bulk mixture solution, implying less transfer of AOS from the solution to the micellar phase while more nonionic surfactants dominant in the mixed micelles.

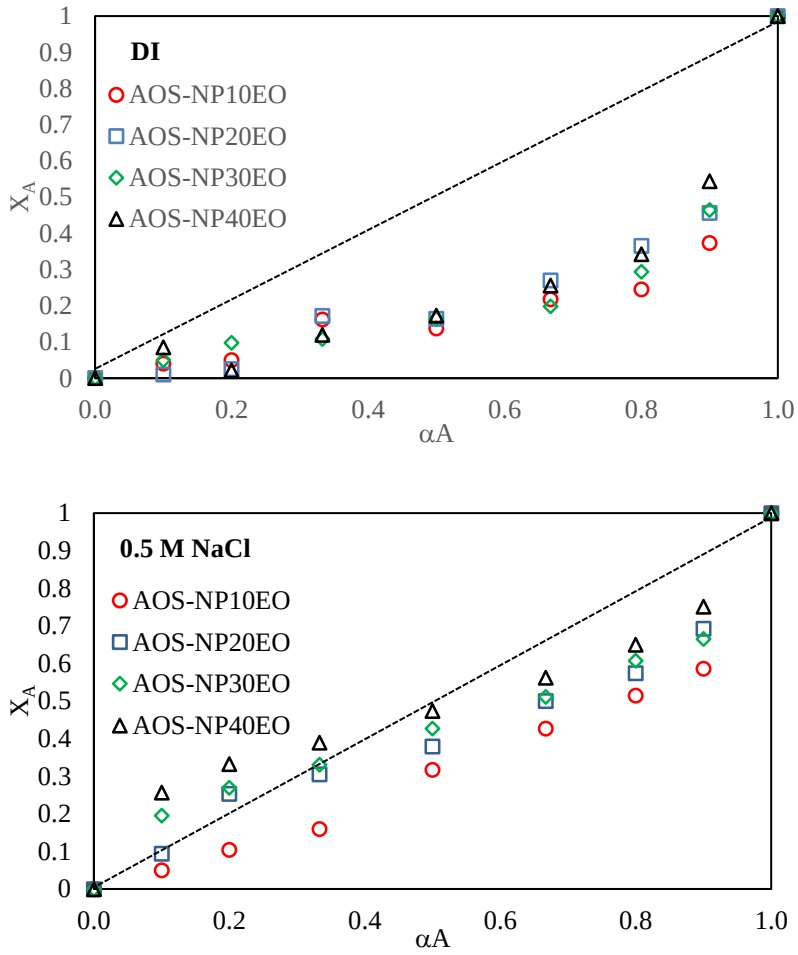

Figure 4.3. Mole fraction of AOS in mixed micelles (X_A) vs mole fraction in bulk solution (α_A). The dashed line represents similar composition in both bulk and mixed micelles ($X_A = \alpha_A$)

For AOS with NP10EO and NP30EO systems, low activity coefficient of the anionic surfactant, f_A, occurs along with low α_A. This reveals a very weak interaction between the anionic and nonionic surfactant in the micelle, which is in harmony with the small value of X_A (see Table 4.3). At higher α_A, a rise in both X_A and f_A indicates stronger interactions between two species of surfactants. In contrast, activity coefficient of the

nonionic surfactant, f_N is pretty stable and close to unity regardless of the change in bulk composition. Joshi and co-workers [4] have observed such behavior of activity coefficients in SDS-$C_{12}E_n$ mixtures, and they attributed the difference to that nonionic surfactant has reached its standard state while the anionic one has not yet.

Data obtained for mixture systems in 0.5 M NaCl solution are reported in Table 4.4. Synergistic interaction can be affirmed as β values for all systems are negative. Contrary to DI cases, β_{avg} in salt solution appears to be slightly more negative with increase in EO groups of NPEs, -1.51 ± 0.02 for 10/20 EOs, to -2.10 ± 0.08 for 30/40 EOs. A decreasing trend of β suggests greater synergistic interactions in AOS mixed with longer ethylene oxide chain. The geometry restriction on mixture micelles diminishes in 0.5 M salt solution since hydrodynamic diameters of AOS and NPEs micelles are about the similar size, 7-10 nm. A possible factor that dominates AOS-NPE interactions may rely on the attraction/repulsion between monomers during micellization. As suggested by Zhou and Rosen [3], polyethylene oxide chains could acquire some positive charges in the presence of anionic surfactant in mixed micelles, which the amount of positive charge obtained increases with growth of EO length. Therefore, a greater electrical attraction between AOS and NPE headgroups is expected when the length of EO groups is increased. This is consistent with the excess free energy of micellization (ΔG_{ex}) listed in Table 4.4, where NP40EO shows largest reduction on excess energy among four NPE surfactants in 0.5 M NaCl solution as further details discussed in later paragraph.

On the other hand, for AOS with NP30EO and NP40EO systems, f_A exhibits evident growing trend with increase α_A. In accordance with the growing value of X_A, an enhancement in the interaction between the anionic and nonionic surfactant is affirmed.

In contrast to DI cases (identical f_N), f_N in salt cases also grows with increase in nonionic bulk composition (1 - X_A). Figure 4.3**Error! Reference source not found.**b d epicts plot of X_A versus α_A in 0.5 M salt condition. In AOS-NP10EO system, X_A is consistently less than α_A across compositions, 0 – 1 of α_A, reflecting lower activity of AOS in micelles than in bulk solution. In the other 3 cases of NPEs, depending on length of EO group, mixed micelles composition is observed identical to bulk composition ($X_A = \alpha_A$) at different bulk ratio, e.g. α_A is around 0.25, 0.30, and 0.40 for NP20EO, NP30EO, and NP40EO, respectively. For α_A lower than reflection points, AOS molecules are highly enriched in mixture micelles rather than bulk solution. On the other hand, above these values, the micelles contain more share of nonionic surfactants than in bulk solution.

4.3.6 Thermodynamic Parameters

RST was criticized on some of the fundamental assumptions, for example, that entropy of mixing was approximated zero [20, 24], and β value only explained the head-head interactions, not encompassed the chain-chain interactions between the hydrophobic segments of the surfactant molecules, particularly when the chains were of dissimilar lengths [36].

Therefore, based on the pseudo-phase separation model, Maeda [25] developed a thermodynamic approach, which considered both (hydrophobic) chain-chain and headgroup-headgroup contributions to the stability and formation of mixed micelles, to describe free energy of micellization, (ΔG_{Ma}):

$$\Delta G_{Ma} = RT(B_0 + B_1 X_1 + B_2 X_1^2) \quad (4.9)$$

where B_0 is related to the CMC of nonionic surfactant,

$$B_0 = lnCMC_{\mathrm{N}} \tag{4.10}$$

B_1 represents for the chain-chain interaction, that contributes to the stability of micelle, and it can be obtained by:

$$B_1 + B_2 = ln\frac{CMC_{\mathrm{A}}}{CMC_{\mathrm{N}}} \tag{4.11}$$

And

$$B_2 = -\beta \tag{4.12}$$

Where β is interaction parameter as described previously.

For surfactants systems in DI, Gibbs energy change of micellization (ΔG_M) can be approximately calculated by the relationship proposed by Molyneux et al. [9, 38]:

$$\Delta G_M = (1 + B)RT(\ln CMC - \ln\omega) \tag{4.13}$$

where B is the degree of counterion binding, ω is the molar concentration of water (55.3 at 25 ^{o}C), and CMC represents CMC_M in the case of mixed micelle.

The calculated values of B_1, B_2, and Gibbs energy change of micellization, both ΔG_{Ma} and ΔG_M are listed in Table 4.3. It is evident that the free energy change values calculated from Molyneux's model matched with Maeda's approach reasonably well (within $\pm$5% difference). This suggests that the fraction of counterion bound to the mixed micelle is negligible, which agrees well with measured values of B, otherwise significant deviation would be seen between these two approaches [36]. It is worthy to note that for a certain fraction of anionic surfactant in the mixture, absolute value of ΔG_{Ma} decreases with growth of the EO groups. For instance, at $\alpha_A = 0.5$, the values of ΔG_{Ma} are -33.25, -31.54, -31.00, and -30.70 KJ/mol for systems with NP10EO, NP20EO, NP30EO, and NP40EO, respectively, clearly revealing that the interaction is strongest with shortest EO

length. The weakening of synergism with increase of EO groups is in accordance with the variation of β value observed from our experimental data.

Moreover, the excess energy of mixing (between monomeric and micellar state) can be calculated from the activity coefficients data [36, 39]:

$$\Delta G_{ex} = RT[X_1 \ln f_1 + (1 - X_1)\ln f_2)] \quad (4.14)$$

In this study, the calculated ΔG_{ex} values along with B_1, and ΔG_{Ma} are presented in Table 4.4 for 0.5 M NaCl cases. Apparently, all calculated ΔG_{ex} values are negative suggesting relatively more stable mixed micelles. It is notable that for a lower α_A in AOS-NP10EO, B_1 exhibits positive value. While at $\alpha_A > 0.33$, B_1 becomes negative. A positive value of B_1 indicates that head-head repulsions are dominant in the mixed micelle, which opposes formation of mixed micelles. On the other hand, a negative B_1 implies that the chain-chain hydrophobic interactions are favorable for stability of mixed micelles [36, 40]. This is coherent with a lower magnitude of ΔG_{ex} at $\alpha_A \leq 0.33$, while more negative ΔG_{ex} at $\alpha_A > 0.33$, implying that synergism between AOS and NP10EO becomes more evident with growth in AOS bulk fraction. For a particular α_A, the variation trend of B_1 value versus EO groups agrees well with the variation of β, e.g. at $\alpha_A = 0.5$, B_1 is -0.08, -0.14, -1.72, and -2.09 for binary mixture with NP10EO, NP20EO, NP30EO, and NP40EO, respectively. This observation again confirmed the enhancement of synergistic interaction by increasing EO numbers. On the contrary, Hu and co-workers reported that cationic-nonionic binary system containing longer PEO chains showed less negative ΔG_{ex} values than that with shorter PEO chains [6]. One plausible reason for such difference is that our samples contain a swamping amount of salt (0.5M NaCl) but Hu's study was conducted in DI.

Table 4.3. Interaction parameters and free energy of AOS-NPE mixture micellization in DI. Mixture CMC, mole fraction of AOS in bulk (α_A), and in mixed micelle (X_A), interaction parameter (β), activity coefficients (f_A , f_N), degree of counterion binding (B), Gibbs energy of micellization by Molyneux's (ΔGm) and Maeda's (ΔGma) approach.

Mixture	αA	CMC, mM	X_A	β ($-B_2$)	f_A	f_N	ΔGm, KJ mol^{-1}	B	B_0	B_1	ΔGma, KJ mol^{-1}
AOS-NP10EO	1.00	1.602	1.00				-33.87	0.308			
	0.90	0.320	0.37	-1.85	0.48	0.77	-31.76	0.063	-13.64	1.34	-31.92
	0.80	0.230	0.25	-1.33	0.47	0.92	-32.54	0.060	-13.64	1.86	-32.46
	0.67	0.140	0.22	-2.15	0.27	0.90	-33.40	0.046	-13.64	1.04	-32.98
	0.50	0.110	0.14	-1.86	0.25	0.97	-33.69	-	-13.64	1.33	-33.25
	0.33	0.076	0.16	-3.31	0.10	0.92	-34.24	-	-13.64	-0.13	-33.63
	0.20	0.094	0.05	-1.60	0.24	1.00	-33.38	-	-13.64	1.58	-33.58
	0.10	0.120	0.04	-1.82	0.19	1.00	-32.54	-	-13.64	1.37	-33.65
	0.00	0.066	0				-33.79	0			
	Avg			-1.99							
AOS-NP20EO	0.90	0.510	0.46	-1.57	0.63	0.72	-31.57	0.099	-12.96	0.94	-30.24
	0.80	0.310	0.37	-2.13	0.42	0.75	-32.17	0.074	-12.96	0.38	-31.06
	0.67	0.250	0.27	-1.79	0.39	0.88	-32.35	0.061	-12.96	0.72	-31.30
	0.50	0.210	0.16	-1.31	0.40	0.97	-32.44	0.049	-12.96	1.20	-31.54
	0.33	0.150	0.17	-2.49	0.18	0.93	-32.77	-	-12.96	0.02	-31.92
	0.20	0.160	0.03	-0.23	0.80	1.00	-32.18	-	-12.96	2.28	-31.97
	0.10	0.150	0.01	-0.07	0.94	1.00	-32.02	-	-12.96	2.44	-32.05
	0.00	0.133	0				-32.11	0			
	Avg			-1.37							
AOS-NP30EO	0.90	0.960	0.46	0.53	1.16	1.12	-30.72	0.131	-12.75	2.83	-28.62
	0.80	0.560	0.29	-0.10	0.95	0.99	-31.29	0.098	-12.75	2.20	-29.97
	0.67	0.380	0.20	-0.35	0.80	0.99	-31.49	0.069	-12.75	1.95	-30.60
	0.50	0.260	0.16	-1.01	0.49	0.97	-32.29	0.062	-12.75	1.29	-31.00
	0.33	0.240	0.11	-0.97	0.46	0.99	-31.81	-	-12.75	1.34	-31.21
	0.20	0.150	0.10	-2.03	0.19	0.98	-32.46	-	-12.75	0.27	-31.48
	0.10	0.180	0.05	-1.65	0.23	1.00	-31.58	-	-12.75	0.65	-31.51
	0.00	0.162	0				-31.60	0			
	Avg			-0.80							
AOS-NP40EO	0.90	1.450	0.54	1.92	1.49	1.76	-30.97	0.185	-12.64	4.11	-27.18
	0.80	0.560	0.34	-0.48	0.81	0.95	-33.31	0.169	-12.64	1.71	-29.71
	0.67	0.510	0.26	-0.35	0.83	0.98	-32.34	0.126	-12.64	1.84	-30.08
	0.50	0.290	0.17	-0.95	0.52	0.97	-33.17	0.101	-12.64	1.24	-30.70
	0.33	0.280	0.12	-0.94	0.48	0.99	-32.23	0.067	-12.64	1.25	-30.90
	0.20	0.220	0.02	-0.23	0.80	1.00	-32.02	-	-12.64	1.96	-31.20
	0.10	0.180	0.08	-2.42	0.13	0.98	-31.89	-	-12.64	-0.23	-31.31
	0.00	0.180	0				-31.30	0			
	Avg			-0.49							

Table 4.4. Interaction parameters and free energy of AOS-NPE mixture micellization in 0.5 M NaCl solution. Mixture CMC, mole fraction of AOS in bulk (α_A), in mixed micelle (X_A), interaction parameter (β), activity coefficients (f_A , f_N), excess free energy (ΔGex) and Gibbs energy of micellization by Maeda's (ΔGma) approach.

Mixture	αA	CMC, mM	X_A	β ($-B_2$)	f_A	f_N	ΔGex, KJ mol^{-1}	B_0	B_1	ΔGma, KJ mol^{-1}
AOS-NP10EO	1.00	0.201	1							
	0.90	0.072	0.59	-3.46	0.55	0.31	-2.08	-13.79	-2.20	-34.31
	0.80	0.073	0.51	-2.41	0.57	0.53	-1.49	-13.79	-1.15	-34.04
	0.67	0.070	0.43	-1.84	0.55	0.71	-1.12	-13.79	-0.59	-33.94
	0.50	0.068	0.32	-1.34	0.54	0.87	-0.72	-13.79	-0.08	-33.89
	0.33	0.071	0.16	-0.43	0.74	0.99	-0.14	-13.79	0.83	-33.80
	0.20	0.067	0.10	-0.55	0.64	0.99	-0.13	-13.79	0.71	-33.96
	0.10	0.054	0.05	-0.68	0.54	1.00	-0.08	-13.79	0.57	-34.08
	0.00	0.057	0							
	Avg			-1.53						
AOS-NP20EO	0.90	0.130	0.69	-1.79	0.84	0.42	-0.94	-13.22	-1.10	-32.52
	0.80	0.089	0.57	-2.64	0.62	0.42	-1.60	-13.22	-1.95	-33.37
	0.67	0.120	0.50	-0.89	0.80	0.80	-0.55	-13.22	-0.20	-32.46
	0.50	0.110	0.38	-0.84	0.72	0.89	-0.49	-13.22	-0.14	-32.60
	0.33	0.091	0.31	-1.45	0.50	0.87	-0.76	-13.22	-0.76	-33.00
	0.20	0.082	0.25	-2.02	0.32	0.88	-0.95	-13.22	-1.33	-33.27
	0.10	0.100	0.09	-0.77	0.53	0.99	-0.16	-13.22	-0.08	-32.76
	0.00	0.101	0							
	Avg			-1.49						
AOS-NP30EO	0.90	0.110	0.67	-2.64	0.74	0.31	-1.46	-13.16	-2.01	-33.03
	0.80	0.120	0.61	-1.53	0.79	0.57	-0.90	-13.16	-0.90	-32.57
	0.67	0.110	0.51	-1.39	0.72	0.70	-0.86	-13.16	-0.75	-32.67
	0.50	0.079	0.43	-2.35	0.46	0.65	-1.43	-13.16	-1.72	-33.37
	0.33	0.087	0.33	-1.84	0.44	0.82	-1.01	-13.16	-1.21	-33.11
	0.20	0.084	0.27	-2.18	0.31	0.85	-1.06	-13.16	-1.55	-33.26
	0.10	0.088	0.20	-2.31	0.22	0.92	-0.90	-13.16	-1.67	-33.21
	0.00	0.106	0							
	Avg			-2.03						
AOS-NP40EO	0.90	0.150	0.75	-1.72	0.90	0.38	-0.80	-12.75	-1.50	-31.98
	0.80	0.130	0.65	-1.82	0.80	0.46	-1.02	-12.75	-1.59	-32.26
	0.67	0.120	0.56	-1.77	0.71	0.57	-1.08	-12.75	-1.55	-32.37
	0.50	0.100	0.47	-2.31	0.53	0.59	-1.43	-12.75	-2.09	-32.76
	0.33	0.106	0.39	-2.13	0.45	0.72	-1.25	-12.75	-1.90	-32.63
	0.20	0.099	0.33	-2.71	0.30	0.74	-1.49	-12.75	-2.49	-32.90
	0.10	0.110	0.26	-2.79	0.21	0.83	-1.32	-12.75	-2.56	-32.77
	0.00	0.162	0							
	Avg			-2.18						

4.3.7 The PB theory

A great advancement in modeling the surfactant mixtures was brought by Puvvada and Blankschtein [26, 27] with their molecular thermodynamic theory (PB theory). The PB models accounted for micellar mixing nonidealities resulting from different molecular contributions, such as electrostatic and steric interactions between the surfactant hydrophilic head groups, and from the packing of surfactant hydrophobic tails of unequal length in the micellar core to predict properties for binary mixture surfactants [34, 35]. According to the PB theory, the total free energy of mixed micellization is the sum of free energy contribution of follows [26, 34, 35],

$$g_{mic} = g_{tr} + g_{int} + g_{pack} + g_{elec} + g_{st} \quad (4.15)$$

The first three terms on the right (g_{tr}, g_{int}, g_{pack}) are transferring free energy, interfacial free energy, and packing free energy, respectively. They involve free energy contributions only from the hydrophobic tails. And the last two terms (g_{elec}, g_{st}) are electrostatic free energy, and steric free energy, associated with free energy contributions only from surfactant heads [34]. In this study, we mainly focus on the effect of different hydrophilic head groups, thus, only g_{elec}, and g_{st} are analyzed. And steric free energy in micellization is given by [26],

$$g_{st} = -kT[X_A \ln\left(1 - \frac{a_{hA}}{a}\right) + (1 - X_A)\ln(1 - \frac{a_{hB}}{a})] \quad (4.16)$$

Where a_{hA} and a_{hB} are head cross-sectional area of surfactants A and B, respectively. They are obtained from Gibbs adsorption isotherm. And a is the area per surfactant molecule at the micellar core/water interface, which can be estimated from micelle aggregation number N_{agg} and hydrodynamic diameter d_H obtained from dynamic light scattering.

An approximate analytical solution of Poisson-Boltzmann equation is used to calculate g_{elec} of pure ionic surfactant [41, 42],

$$g_{elec} = 2kT\left[\ln\left(\frac{s}{2}+\left(1+\left(\frac{s}{2}\right)^2\right)^{\frac{1}{2}}\right)-\frac{\left(1+\left(\frac{s}{2}\right)^2\right)^{\frac{1}{2}}-1}{\frac{s}{2}}\right] - 2kT\left[\frac{4}{s\kappa R}\ln\left(\frac{1+\left(1+\left(\frac{s}{2}\right)^2\right)^{\frac{1}{2}}}{2}\right)\right] \quad (4.17)$$

where $s = \frac{4\pi Z e^2}{\epsilon a k T \kappa}$ and $\kappa = (\frac{8\pi C_o e^2 Z^2}{\epsilon k T})^{1/2}$.

k is the Boltzmann constant, T is the absolute temperature, s is a convenient dimensionless parameter, κ^{-1} is the Debye screening length, R is the radius of spherical surface, Z is the valence of ionic surfactant, e is the electronic charge, ϵ is the solvent dielectric constant, and C_o is the bulk ionic concentration.

A representative steric and electrostatic free energy result for AOS-NP30EO is illustrated in Figure 4.4. As we can see, electrostatic energy, g_{elec}, in DI was close to 0 when α_A < 0.5. This is because that AOS micellar composition, X_A, is basically negligible at low AOS bulk composition (α_A). At α_A > 0.5, more AOS molecules were present in the mixed micelles. Thus, larger electrostatic repulsion between charged head groups were expected from 0.06 kT at α_A = 0.5 to 1.07 kT at α_A = 0.9. A sharp increase of g_{elec} was observed at α_A = 1.0, resulted from strong electrostatic energy of a pure ionic AOS micelle. In contrast, g_{elec} increased constantly in 0.5 M NaCl solution with rise in α_A. This is consistent with the monotonic increase of AOS composition in the mixed micelle and

proved that AOS molecules are more active to participate in mixed micelles at salt condition than in DI.

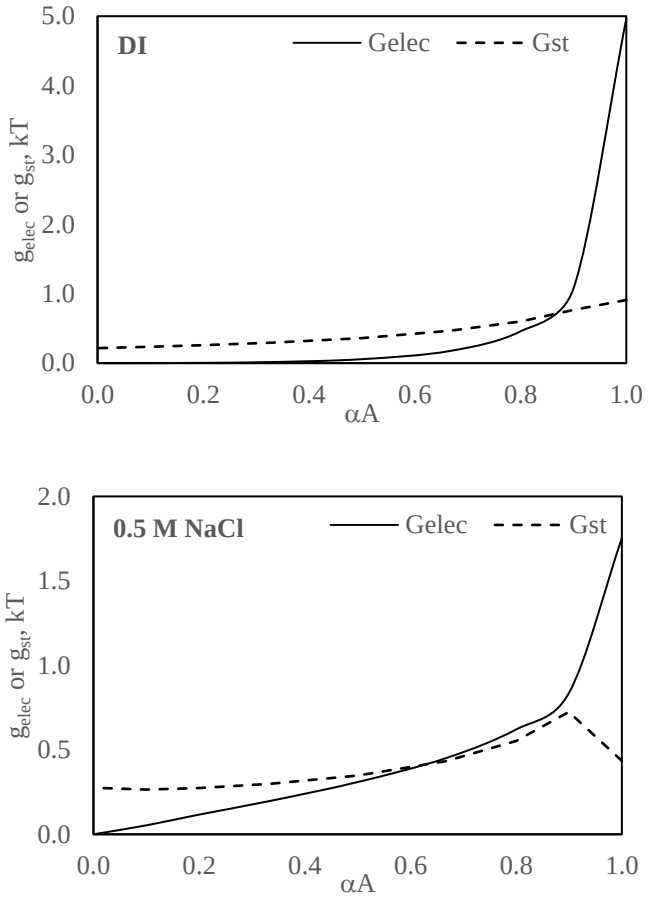

Figure 4.4. Calculated steric free energy, g_{st}, and electrostatic free energy, g_{elec}, as a function of AOS bulk composition for AOS-NP30EO micelle in DI as well as in 0.5 M NaCl solution at the mixture CMC.

The steric contribution, g_{st}, exhibited a slight rising trend with increase in α. Surprisingly, higher NP30EO composition in the micelle, which occupies a relatively larger head group compared to AOS, did not bring much greater steric contribution. The reason is that the area per surfactant molecule at the micellar core/water interface, a, increased drastically with rise in NP30EO micelle composition, as a result, the fraction of free area per surfactant at interface, $1-a_h/a$, approached to a constant value, thus little change of steric

free energy was seen at low AOS composition. While at higher α, more AOS were present in mixture micelle, and the contrast between two different head groups resulted in much stronger steric contribution.

For ideal surfactant mixture, the free energy of micellization is:

$$g_{mic}^{ideal} = X_A g_{mic}^{A} + (1 - X_A) g_{mic}^{B} + kT[X_A \ln X_A + (1 - X_A)\ln(1 - X_A)] \quad (4.18)$$

Which considers a linear interpolation between micellization energy of two species of surfactants (A & B) and an ideal entropy of mixing. According to the PB theory, nonideality of surfactant mixture originates from any deviations of g_{mic} from g_{mic}^{ideal}. And the difference between g_{mic} and g_{mic}^{ideal} is connected with Rugbingh's RST [27, 35],

$$\Delta G_{mic} = X_A(1 - X_A)\beta^{PB} \quad (4.19)$$

Where β^{PB} is the interaction parameter, unlike β in RST, the PB theory provides a direct tool to actually predict β instead of fitting it to experimental CMC data.

Sarmoria et al. [42] simplified PB models for ionic-nonionic surfactants mixtures by accounting only electrostatic contribution among mixture head groups. As suggested by Sarmoria et al., β^{PB} reflects mainly two free energy contributions in the mixture micellization,

$$\beta^{PB} \approx g_{core}^{AB} + g_{elec}^{AB} \quad (4.20)$$

Where, g_{core}^{AB} is associated with interaction between the hydrophobic moieties of surfactants A and B in the micellar core, and g_{elec}^{AB} is associated with electrostatic interactions between the charged hydrophilic moieties of surfactants A and B. g_{core}^{AB} is typically 0 for a mixture of two hydrocarbon-based surfactants, thus for monovalent-nonionic mixture, above equation is reduced to [7],

$$\beta^{PB} \approx g_{elec}^{AB} = -K_{elec} \tag{4.21}$$

Where K_{elec} is a numerical prefactor that can be evaluated from electrostatic theory,

$$g_{elec} = K_{elec}(\alpha^*)^2 \tag{4.22}$$

$\alpha^*$is the optimal micellar composition, where the free energy of micellization attains its minimum value. By equating the Equations 4.17 and 4.22 at $\alpha^* = 1$ for pure ionic surfactant, K_{elec} can be computed, and β^{PB} is also determined. Once β^{PB} is known, following relations could be used to predict the CMC of mixtures,

$$\frac{\beta^{PB}}{kT}(1-2\alpha^*) + \ln\left(\frac{\alpha^*}{1-\alpha^*}\right) = \ln(\frac{\alpha}{1-\alpha}\frac{CMC_N}{CMC_A}) \tag{4.23}$$

$$f_A = \exp\left[\frac{\beta^{PB}}{kT}(1-\alpha^*)^2\right] \tag{4.24}$$

$$f_N = \exp(\frac{\beta^{PB}}{kT}(\alpha^*)^2) \tag{4.25}$$

$$\frac{1}{CMC_M} = \frac{\alpha_A}{f_A CMC_A} + \frac{1-\alpha_A}{f_N CMC_N} \tag{4.26}$$

Similar as Rubingh's RST, with CMC_M known from experimental data, β^{PB} can also be determined from above equations with iteration. β^{opt} represents the optimal value of β^{PB} that best fits the experimental CMC_M versus α data in a least-squares fit sense,

$$F = \sum[\left(CMC_M^{exp}\right)_i - (\frac{\alpha}{f_A CMC_A} + \frac{1-\alpha}{f_N CMC_N})^{-1}]^2 \tag{4.27}$$

Here we compare the experimentally-deduced optimal β^{opt} with predicted value of β^{PB}, denoting as β^{pre}, for all AOS-NPE surfactant mixtures. Results are summarized in Table 4.5 with β^{avg} obtained from the RST model.

Table 4.5. Values of β^{opt}, β^{opt} calculated from PB theory, and β^{avg} from regular solution theory

NaCl, M	Mixture	β^{pre}	β^{opt}	β^{avg}
0	AOS-NP10EO	-4.97	-1.75	-1.99
	AOS-NP20EO		-1.72	-1.37
	AOS-NP30EO		-0.20	-0.80
	AOS-NP40EO		-0.18	-0.49
0.5	AOS-NP10EO	-1.75	-2.30	-1.53
	AOS-NP20EO		-1.58	-1.49
	AOS-NP30EO		-1.96	-2.03
	AOS-NP40EO		-2.11	-2.18

Obviously, with consideration of only electrostatic free energy in mixed micelles, predicted β^{pre} failed to capture any change resulted from the variation of ethylene oxides groups. In DI, β^{pre} also overestimated the synergistic interaction between AOS-NPE mixtures. In one example, Sarmoria et al. [42] analyzed the SDS-NPE mixtures based on simplified PB theory and the predicted interaction parameter was -4.1 with EO groups ranging from 5 to 20. Compared to their result, β^{pre} of -4.97 in this work appears a reasonable value for AOS-NPE mixtures considering only g_{elec}. Hence, it is safe to say that the overestimation of β^{pre} comes from the nonideality due to mixture steric free energy and maybe free energy associated with hydrophobic tails. The best fitted β^{opt} in DI decreased from -1.74$\pm$0.02 for mixture with NPE-10, 20 EO to -0.19$\pm$0.01 with NPE-30, 40 EO. Although an order magnitude drop of β^{opt} was seen at 20/30 EO rather than a stepwise reduction, the trend is coherent with what have been observed in RST, that synergism between AOS-NPE decrease with rise in ethylene oxide length. In the 0.5 M NaCl solution, predicted β^{pre} is in harmony with the range of β^{opt}, -1.99$\pm$0.31, as well as the range of β^{avg}, -1.99$\pm$0.35. The validity of these results is also convinced by exceptional agreement between the predicted mixed CMC_M from PB theory and those

from surface tension measurements. The variations of β in salt condition are subtle, however, both β^{opt} and β^{avg} exhibited a slight increase with the growth of EO number from 20 to 40. We may assume β^{opt} constitutes of two components, contributions from electrostatic free energy $\beta^{elec} = \beta^{pre}$, and from steric free energy β^{st}, thus the difference between β^{opt} and β^{pre} reflect the steric contribution in mixture interaction. The resulted values of β^{st} are 0.17, -0.21, and -0.36 for mixture with 20, 30, and 40 EO, respectively. Hydrophilic head area for AOS (a_{hA}) is 0.286 nm^2, and for NPEs (a_{hN}) with 20, 30, and 40 EO are 0.625, 0.894, and 0.999 nm^2, respectively. It is clear that enlarging the difference between AOS/NPE head area, a much greater steric contribution is envisioned, thus the synergism between AOS-NPE mixture becomes stronger.

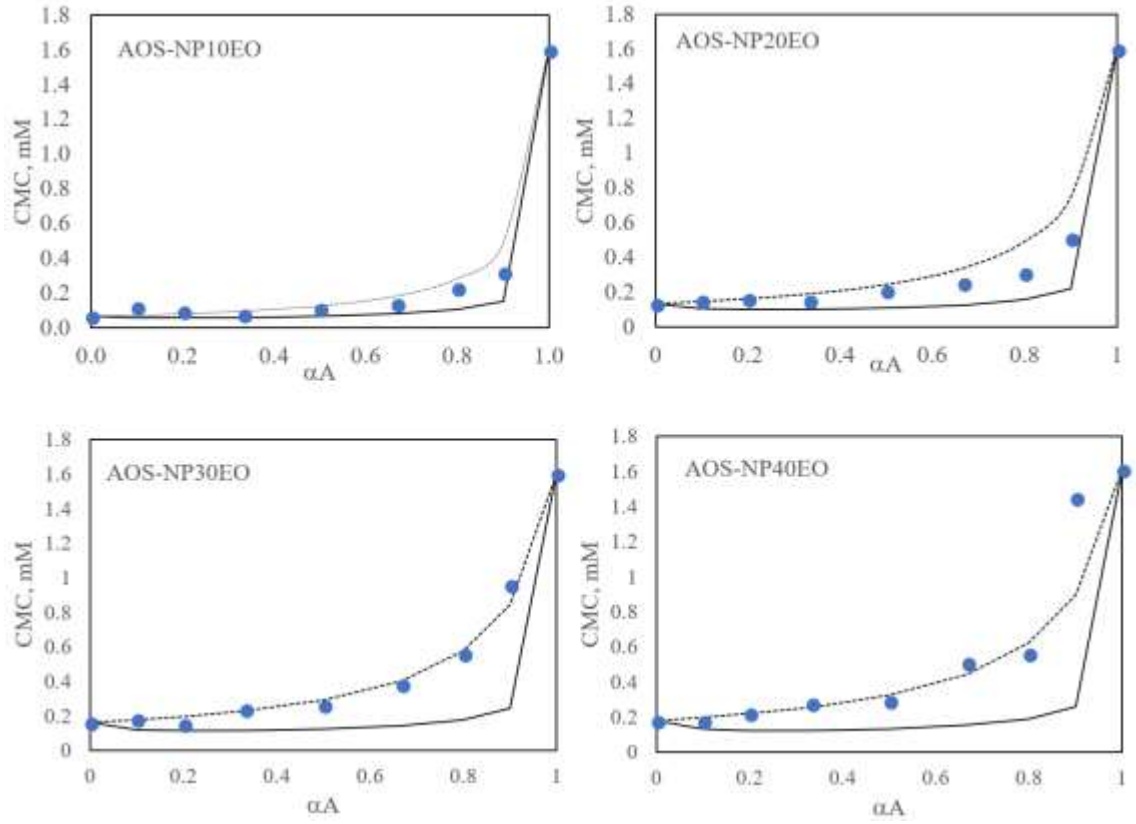

Figure 4.5. CMC vs mole fraction of AOS, α_A, for binary mixed systems in DI. Dashed lines represent ideal mixing values, solid lines represent CMC predicted from PB theory with $\beta^{pred} = -4.97$, and symbols represent experimental values

Figure 4.5, and Figure 4.6 present the CMC variation as a function of α_A in DI as well in 0.5 M NaCl solution. In DI cases, CMC predicted from PB theory is noticeable off from the measured data, likely due to overestimation of interaction parameter. In comparison, ideal model provides a fairly reasonable prediction, especially in the mixture of AOS-NP30EO, where the best fitted β^{opt} is close to zero. It is obvious that nonionic surfactant plays an important role in mixed micelles. For instance, in AOS-NP10EO system, only 0.1 mole fraction of NP10EO in the mixture rendered a drastic reduction on CMC from 1.602 mM to 0.320 mM. Nevertheless, The CMC_M values for all binary mixture systems did not exceedingly drop below those exhibited by the pure NPE surfactants alone. Compared to DI cases, PB theory presented a better prediction on mixture CMC in 0.5 M salt solution than ideal model. The measured CMC values for all binary systems with salt added are pronounced lower than those estimated from ideal mixing rule, clearly revealing the synergistic interactions. The synergism between AOS and NPE is more evident in respect to mixed micelle formation [43], e.g. in AOS-NP40EO scenario, CMC of all binary systems are lower than that of either individual AOS or NP40EO.

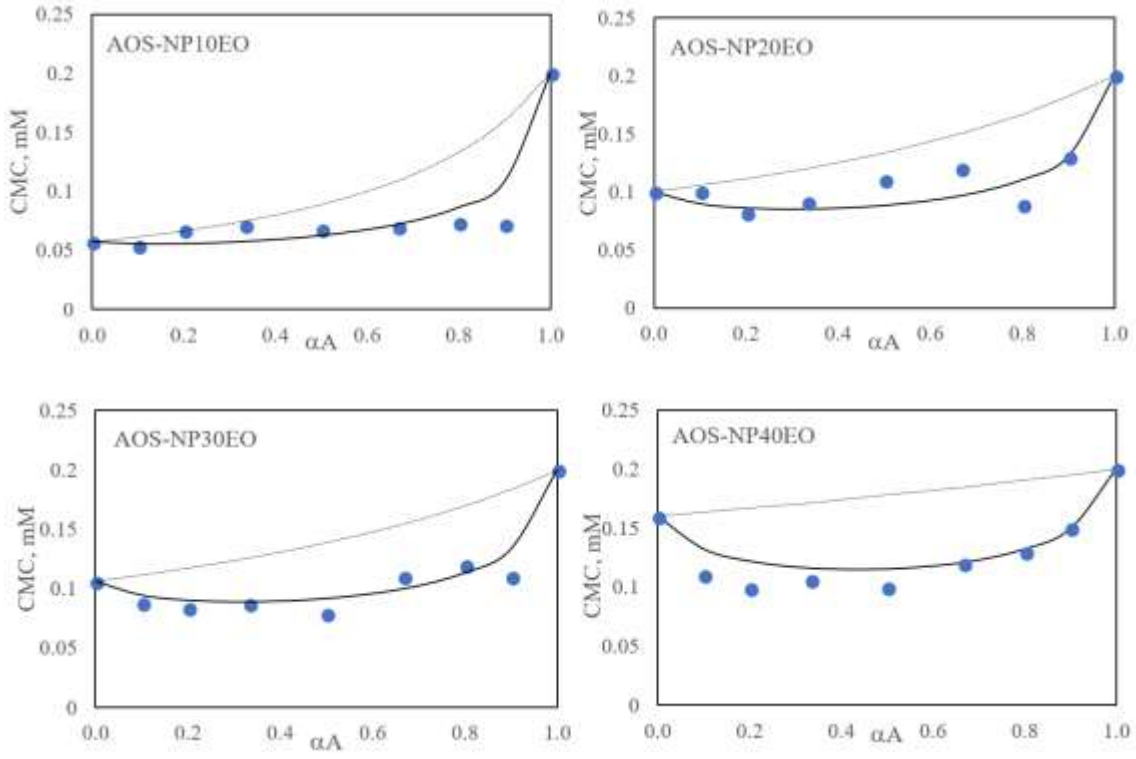

Figure 4.6. CMC vs mole fraction of AOS, α_A for binary mixed systems in 0.5 M NaCl solution. Dashed lines represent ideal values, solid lines represent CMC predicted from PB theory with $\beta^{pred} = -1.75$, and symbols represent experimental values.

4.4 Conclusions

Binary anionic-nonionic surfactant mixtures are of great interest due to their excellent properties in reducing CMC, improving surface/interface activity, strengthening oil solubilizing ability, and cutting chemical costs. In this study, binary mixtures of alpha olefin sulfonate (AOS) and nonylphenol polyethylene glycol ethers (NPE) with a wide range of EO chain length were examined comprehensively by various experimental methods as well as different theoretical treatments. We have observed that CMC values of all binary systems fall between those of the pure constituent surfactants without additional electrolytes. However, with presence of swamping amount of electrolytes, CMC could be lower than that of single nonionic surfactant, indicating strong synergistic

interaction. Addition of AOS increases cloud points for all NPE surfactants tested in both DI and 0.5 M NaCl solutions. Mixture micelle size exhibited complex change depending on the salt concentration, EO chain length and mixture composition.

Based on regular solution theory of Rubingh, and molecular thermodynamic theory of Pavvada and Blankschtein, interaction parameter β calculated for all binary systems are negative, which further confirmed synergistic interaction prevailing in mixed AOS-NPE surfactants. In DI, NPEs are dominant in the mixed micelles as lower micelle fraction of AOS, X_A, against bulk fraction, α_A, has been observed for all AOS-NPE mixtures; with rise in EO numbers, a reduction on synergistic interaction was inferred from decrease in both absolute value of Gibbs energy of micellization ΔG_{Ma} and average interaction parameter β_{avg}. On the other hand, β_{avg} become more negative with increase in surfactant EO groups in elevated salt presence, suggesting rise in synergistic interactions. With swamping amount of salt, AOS shows lower activity in AOS-NP10EO mixture micelles than in bulk solution; while with longer EO chains, AOS are enriched in mixture micelles rather than bulk solution at lower α_A, but exhibit greater activity in bulk solution than in micelles at higher α_A.

This work revealed the impacts of EO length on binary surfactants mixtures, especially, contrary contribution on the scale of synergistic interaction at different electrolytes conditions has been observed for the first time, which is of great significance in understanding the aggregation behavior of mixed surfactants, and therefore facilitating development of superior surfactant formulation with maximized synergistic efficiency for enhanced oil recovery at high salinity reservoirs.

Acknowledgement

The authors thank Institute for Applied Surfactant Research (IASR) to pursue the work.

Reference

[1] M.J. Rosen, J.T. Kunjappu, Surfactants and interfacial phenomena, John Wiley & Sons2012.

[2] M.J. Rosen, Q. Zhou, Surfactant− surfactant interactions in mixed monolayer and mixed micelle formation, Langmuir 17(12) (2001) 3532-3537.

[3] Q. Zhou, M.J. Rosen, Molecular interactions of surfactants in mixed monolayers at the air/aqueous solution interface and in mixed micelles in aqueous media: the regular solution approach, Langmuir 19(11) (2003) 4555-4562.

[4] T. Joshi, J. Mata, P. Bahadur, Micellization and interaction of anionic and nonionic mixed surfactant systems in water, Colloids and Surfaces A: Physicochemical and Engineering Aspects 260(1-3) (2005) 209-215.

[5] J. Penfold, I. Tucker, R. Thomas, E. Staples, R. Schuermann, Structure of mixed anionic/nonionic surfactant micelles: experimental observations relating to the role of headgroup electrostatic and steric effects and the effects of added electrolyte, The Journal of Physical Chemistry B 109(21) (2005) 10760-10770.

[6] C. Hu, R. Li, H. Yang, J. Wang, Properties of binary surfactant systems of nonionic surfactants C12E10, C12E23, and C12E42 with a cationic gemini surfactant in aqueous solutions, J Colloid Interface Sci 356(2) (2011) 605-13.

[7] M.E. Haque, A.R. Das, A.K. Rakshit, S.P. Moulik, Properties of mixed micelles of binary surfactant combinations, Langmuir 12(17) (1996) 4084-4089.

[8] T.P. Goloub, R.J. Pugh, B.V. Zhmud, Micellar Interactions in Nonionic/Ionic Mixed Surfactant Systems, J Colloid Interface Sci 229(1) (2000) 72-81.

[9] S. Ghosh, A. Das Burman, G.C. De, A.R. Das, Interfacial and self-aggregation of binary mixtures of anionic and nonionic amphiphiles in aqueous medium, J Phys Chem B 115(38) (2011) 11098-112.

[10] K. Szymczyk, B. Jańczuk, The adsorption at solution–air interface and volumetric properties of mixtures of cationic and nonionic surfactants, Colloids and Surfaces A: Physicochemical and Engineering Aspects 293(1-3) (2007) 39-50.

[11] S. Lu, J. Wu, P. Somasundaran, Micellar evolution in mixed nonionic/anionic surfactant systems, J Colloid Interface Sci 367(1) (2012) 272-9.

[12] L. Zhu, S. Feng, Synergistic solubilization of polycyclic aromatic hydrocarbons by mixed anionic–nonionic surfactants, Chemosphere 53(5) (2003) 459-467.

[13] K. Yang, L. Zhu, B. Xing, Enhanced soil washing of phenanthrene by mixed solutions of TX100 and SDBS, Environmental Science & Technology 40(13) (2006) 4274-4280.

[14] Y.-j. Guo, J.-x. Liu, X.-m. Zhang, R.-s. Feng, H.-b. Li, J. Zhang, X. Lv, P.-y. Luo, Solution property investigation of combination flooding systems consisting of gemini–non-ionic mixed surfactant and hydrophobically associating polyacrylamide for enhanced oil recovery, Energy & Fuels 26(4) (2012) 2116-2123.

[15] A. Bera, K. Ojha, A. Mandal, Synergistic effect of mixed surfactant systems on foam behavior and surface tension, Journal of Surfactants and Detergents 16(4) (2013) 621-630.

[16] J. Hines, R. Thomas, P.R. Garrett, G. Rennie, J. Penfold, Investigation of mixing in binary surfactant solutions by surface tension and neutron reflection: anionic/nonionic and zwitterionic/nonionic mixtures, The Journal of Physical Chemistry B 101(45) (1997) 9215-9223.

[17] Z.H. Ren, J. Huang, Y. Luo, Y.C. Zheng, P. Mei, L. Lai, Y.L. Chang, Micellization behavior of binary mixtures of amino sulfonate amphoteric surfactant with different octylphenol polyoxyethylene ethers in aqueous salt solution: Both cationic and hydrophilic effects, Journal of Industrial and Engineering Chemistry 36 (2016) 263-270.

[18] A. Sahu, S. Choudhury, A. Bera, S. Kar, S. Kumar, A. Mandal, Anionic–Nonionic Mixed Surfactant Systems: Micellar Interaction and Thermodynamic Behavior, Journal of Dispersion Science and Technology 36(8) (2014) 1156-1169.

[19] C. Chen, M.J. Kadhum, M.C. Mercado, B. Shiau, J.H. Harwell, Surfactant-Only Stabilized Dispersions of Multiwalled Carbon Nanotubes in High-Electrolyte-Concentration Brines, Energy & Fuels 30(11) (2016) 8952-8961.

[20] J.D. Hines, Theoretical aspects of micellisation in surfactant mixtures, Current opinion in colloid & interface science 6(4) (2001) 350-356.

[21] M.A. Abed, A. Saxena, H.B. Bohidar, Micellization of alpha-olefin sulfonate in aqueous solutions studied by turbidity, dynamic light scattering and viscosity measurements, Colloids and Surfaces A: Physicochemical and Engineering Aspects 233(1-3) (2004) 181-187.

[22] R. Farajzadeh, R. Krastev, P.L.J. Zitha, Foam films stabilized with alpha olefin sulfonate (AOS), Colloids and Surfaces A: Physicochemical and Engineering Aspects 324(1-3) (2008) 35-40.

[23] D.N. Rubingh, Mixed micelle solutions, Solution chemistry of surfactants, Springer1979, pp. 337-354.

[24] P.M. Holland, D.N. Rubingh, Mixed Surfactant Systems, 501 (1992) 2-30.

[25] H. Maeda, A simple thermodynamic analysis of the stability of ionic/nonionic mixed micelles, Journal of colloid and interface science 172(1) (1995) 98-105.

[26] S. Puvvada, D. Blankschtein, Theoretical and experimental investigations of micellar properties of aqueous solutions containing binary mixtures of nonionic surfactants, The Journal of Physical Chemistry 96(13) (1992) 5579-5592.

[27] S. Puvvada, D. Blankschtein, Thermodynamic description of micellization, phase behavior, and phase separation of aqueous solutions of surfactant mixtures, The Journal of Physical Chemistry 96(13) (1992) 5567-5579.

[28] M. Schick, Surface films of nonionic detergents—I. Surface tension study, Journal of Colloid Science 17(9) (1962) 801-813.

[29] R. Triolo, L. Magid, J. Johnson Jr, H. Child, Small-angle neutron scattering from aqueous micellar solutions of a nonionic surfactant as a function of temperature, J. Phys. Chem.;(United States) 86(19) (1982).

[30] T. Shikata, M. Okuzono, N. Sugimoto, Temperature-Dependent Hydration/Dehydration Behavior of Poly(ethylene oxide)s in Aqueous Solution, Macromolecules 46(5) (2013) 1956-1961.

[31] E. Florin, R. Kjellander, J.C. Eriksson, Salt effects on the cloud point of the poly (ethylene oxide)+ water system, Journal of the Chemical Society, Faraday Transactions 1: Physical Chemistry in Condensed Phases 80(11) (1984) 2889-2910.

[32] C.-l. Ren, W.-d. Tian, I. Szleifer, Y.-q. Ma, Specific Salt Effects on Poly(ethylene oxide) Electrolyte Solutions, Macromolecules 44(6) (2011) 1719-1727.

[33] M. Schick, S. Atlas, F. Eirich, MICELLAR STRUCTURE OF NON-IONIC DETERGENTS1, The Journal of Physical Chemistry 66(7) (1962) 1326-1333.

[34] A. Shiloach, D. Blankschtein, Measurement and prediction of ionic/nonionic mixed micelle formation and growth, Langmuir 14(25) (1998) 7166-7182.

[35] A. Shiloach, D. Blankschtein, Predicting micellar solution properties of binary surfactant mixtures, Langmuir 14(7) (1998) 1618-1636.

[36] K.S. Sharma, S.R. Patil, A.K. Rakshit, K. Glenn, M. Doiron, R.M. Palepu, P. Hassan, Self-aggregation of a cationic− nonionic surfactant mixture in aqueous media: tensiometric, conductometric, density, light scattering, potentiometric, and fluorometric studies, The Journal of Physical Chemistry B 108(34) (2004) 12804-12812.

[37] J.H. Clint, Micellization of mixed nonionic surface active agents, Journal of the Chemical Society, Faraday Transactions 1: Physical Chemistry in Condensed Phases 71 (1975) 1327-1334.

[38] P. Molyneux, C. Rhodes, J. Swarbrick, Thermodynamics of micellization of N-alkyl betaines, Transactions of the Faraday Society 61 (1965) 1043-1052.

[39] H. Maeda, A thermodynamic analysis of charged mixed micelles in water, The Journal of Physical Chemistry B 109(33) (2005) 15933-15940.

[40] A. Trawiſska, E. Hallmann, K. MŁdrzycka, The effect of alkyl chain length on synergistic effects in micellization and surface tension reduction in nonionic gemini (S-10) and anionic surfactants mixtures, Colloids and Surfaces A: Physicochemical and Engineering Aspects 506 (2016) 114-126.

[41] D.F. Evans, B. Ninham, Ion binding and the hydrophobic effect, The Journal of Physical Chemistry 87(24) (1983) 5025-5032.

[42] C. Sarmoria, S. Puvvada, D. Blankschtein, Prediction of critical micelle concentrations of nonideal binary surfactant mixtures, Langmuir 8(11) (1992) 2690-2697.

[43] A. Trawińska, E. Hallmann, K. Mędrzycka, Synergistic effects in micellization and surface tension reduction in nonionic gemini S-10 and cationic RTAB surfactants mixtures, Colloids and Surfaces A: Physicochemical and Engineering Aspects 488 (2016) 162-172.

Chapter 5 Oil-induced highly viscoelastic wormlike micellar solutions of extended surfactant sodium alkyl alkoxy sulfate

Abstract

In this study the rheological properties of an extended surfactant, a sodium alkyl alkoxy sulfate ($C8–(PO)_4–(EO)_1–SO_4Na$) are extensively investigated as a function of the presence of various paraffinic oils and under a range of salt conditions. The addition of as small as 3 vol% alkane into the surfactant formulations (2 wt%) promotes a sudden shift in viscoelastic behaviors, e.g. solution viscosity jumps 5 orders of magnitude. Oscillatory-shear (frequency sweep) measurements are performed on the viscoelastic samples and solid-like behaviors ($G' > G''$) are observed for all solubilized oil samples in the entire frequency region (0.01-100 rad/s). Commonly, alkanes are believed to be encapsulated in the core of micelles, leading to a radial growth of the cylindrical part of the wormlike micelle resulting in a drop in end-cap energy(E_C) and micelle length; in this study, however, the high zero-shear viscosity and plateau G' reveal that solubilized oil induces the axial growth of wormlike micelle, consistent with the long relaxation time observed for solubilized oil samples (G', G'' cross over is not obtained within a frequency region of 0.01-100 rad/s). The viscosity of oil solubilized samples eventually decreases with an increase of incorporated oil volume. When the volume of solubilized oil is held constant, (6 vol%), the viscosity increases when the counterions concentration rises but the formulation stays within the Winsor Type III region. We hypothesize that this "abnormal oleo-responsive" viscoelastic behavior is related to a spacer of intermediate hydrophilicity, i.e., polypropylene oxide segment, being inserted between the C_8

hydrophobic tail and hydrophilic head (the ethoxylated sulfate segment) of the extended surfactant. The addition of oil extends the PO groups and enlarges the tail length, which would result in an increasing end cap energy of worms, thus give rise to a favorable longitudinal growth of wormlike micelles.

5.1 Introduction

Wormlike micelles are elongated, semi-flexible surfactant aggregates which exhibit remarkable rheological properties. Above a critical concentration c*, wormlike micelles entangle into a transient network and become viscoelastic, similar to a solution of flexible polymers.[1, 2] In contrast to polymers, wormlike micelles are dynamic systems that constantly break and recombine, therefore they are often referred to as "living polymers". For wormlike micelles, the spontaneous curvature of the end caps is higher than the curvature along the cylindrical body. The growth is therefore a consequence of the system minimizing the excess free energy by reducing the number of end caps. Over the past few decades, Wormlike micelles have drawn considerable interest both from a theoretical viewpoint as well as for industrial and technological applications. Understanding the viscoelasticity of wormlike micelles is important for the design and the development of industrial products where the high viscosity and elastic properties are exploited, such as fracture fluids in oil fields, drag reduction agents, home care, personal care and cosmetic products.

Wormlike micelles are highly responsive to multiple factors, such as light, temperature, pH, CO_2, hydrocarbons, etc.[3] For oilfield application, the responsiveness to hydrocarbons is of particular importance because that large amounts of hydrocarbons will lead to a drop of viscosity of wormlike micellar solutions by several orders of magnitude and a complete

loss of viscoelastic properties.[4] Typically, addition of oil influences the growth of wormlike micelles differently dependent on the type of oils being added. Aromatic hydrocarbons are often solubilized at or near the micellar corona, as a result induces the growth of wormlike micelles in length and, hence, the viscosity enhancement.[4, 5] On the opposite, alkane oil are normally solubilized inside the micellar cores, instead of contribute to the entangled worms, they lead to a disruption of wormlike micelles and their transition to microemulsion droplets.[6] As seen before, 0.5 wt% dodecane is able to render a drastic drop in viscosity of wormlike micellar solution up to 5 orders of magnitude.[7] Increasing the alkyl chain of ester oils has seen worsen the longitudinal micellar growth into worms.[8] Reservoir hydrocarbon typically contains a large portion of paraffinic oils, to generate wormlike micelles resistant to paraffins therefore is of great significance for reservoir applications.

Extended surfactants are a class of surfactants containing intermediate polarity molecules, such as polypropylene oxides (POs) and/or polyethylene oxides (EOs), which are inserted between the hydrocarbon tail and hydrophilic head. Benefited from their unique structure, extended surfactants will extend the length of the surfactant tail further into the oil phase without losing water solubility, thereby providing a smoother transition between oil and water phases and leading to a thickening interfacial region.[9, 10] It has been observed, extended surfactants could form much larger middle phase (Winsor III microemulsion) compared to conventional surfactant without PO and EO groups.[11]

In this work, the rheological property of a micellar solution consisting of extended surfactant C8–$(PO)_4$–$(EO)_1$–SO_4Na ($C_8P_4E_1$) was extensively studied. Wormlike micelles were evidenced at salt level above 15 wt%, and at $C_8P_4E_1$ concentration above

4 wt%. Impact of paraffinic oil was then investigated by solubilizing certain concentration of oils into the 2 wt% $C_8P_4E_1$ solution at Winsor III region, the oil-free solution behaves like Newtonian fluid with viscosity of 0.005 Pa.s. Contrary to common oleo-responsive wormlike micelles, addition of oil could drastically increase the viscosity as well as elasticity of $C_8P_4E_1$ solution. Impact of the oil volume, counterion type, and counterion concentration were also examined. Our hypothesis is that, incorporating oil to the spacer layer where PO groups reside can extend the PO groups and enlarge the tail length. This would result in an increasing end cap energy of worms, thus give rise to a favorable longitudinal growth of wormlike micelles. This paper, to the best of our knowledge, is the first work that extensively studied the rheological property of extended surfactant, also the first work that evidenced the abnormal paraffinic oil-induced growth of wormlike micelles.

5.2 Experiments

5.2.1 Materials

The extended surfactant C8–$(PO)_4$–$(EO)_1$–SO_4Na ($C_8P_4E_1$) used in this study was provided by Sasol North America Inc., Lake Charles, LA as a 32.3% active solution. A synthetic isoparaffinic hydrocarbon solvent, Isopar^{TM} -L (>98% C_{11}-C_{13}) was provided by ExxonMobil Chemical Company, Houston, TX. Octane (>99.5%), decane (>98%), dodecane (>99%), sodium chloride, potassium chloride, magnesium chloride, and calcium chloride dihydrate ($CaCl_2{\cdot}2H_2O$) were purchased from Sigma Aldrich. All the chemicals were used as received.

5.2.2 Phase behavior of microemulsions

Phase behavior test was performed in flat-bottom glass vials with Teflon-lined screw caps. Equal volume of 2 wt% surfactant solution and oil (5 mL each) were added into the vial with different electrolytes concentration. All test tubes were first gently hand-shaken for 20 seconds, and subsequently kept in a water bath at 25 ^{o}C to allow equilibration. After the systems reached equilibrium, the resulted interfacial tension between the excess water and excess oil phases of microemulsions was measured at 25 ^{o}C with a M6500 Spinning Drop Tensiometer (Grace Instrument, Houston, TX). The detailed method has been documented by Witthayapanyanon et al [10].

5.2.3 Rheological measurements

Rheological measurements were performed on a Discovery Hybrid Rheometer (DHR-2, TA Instruments) with a temperature-controlling Peltier unit and a sample cover to minimize evaporation. For highly viscous and viscoelastic samples, a cone − plate geometry with 40 mm diameter and 2° cone angle was used, whereas for low-viscous samples, the experiments were performed with concentric cylinders (bob diameter 27.98 mm, cup diameter 30.33 mm). Samples for rheological measurements were vortex mixed and equilibrated for 10 minutes in the measurement cell prior to investigation. Two types of rheological measurements were performed: steady shear-rate viscosity measurements and oscillatory shear measurements. In oscillatory shear measurements, the stress amplitude was chosen in the linear viscoelastic regime as determined by dynamic stress sweep measurements to ensure that the storage modulus (G') and the loss modulus (G'') are independent of the applied stress. Measurements were carried out in duplicates or

triplicates for each sample, with very good reproducibility. The results reported here are examples of typical data obtained, not averages.

5.3 Results and discussions

5.3.1 Rheology of oil-free $C_8P_4E_1$ surfactant solution

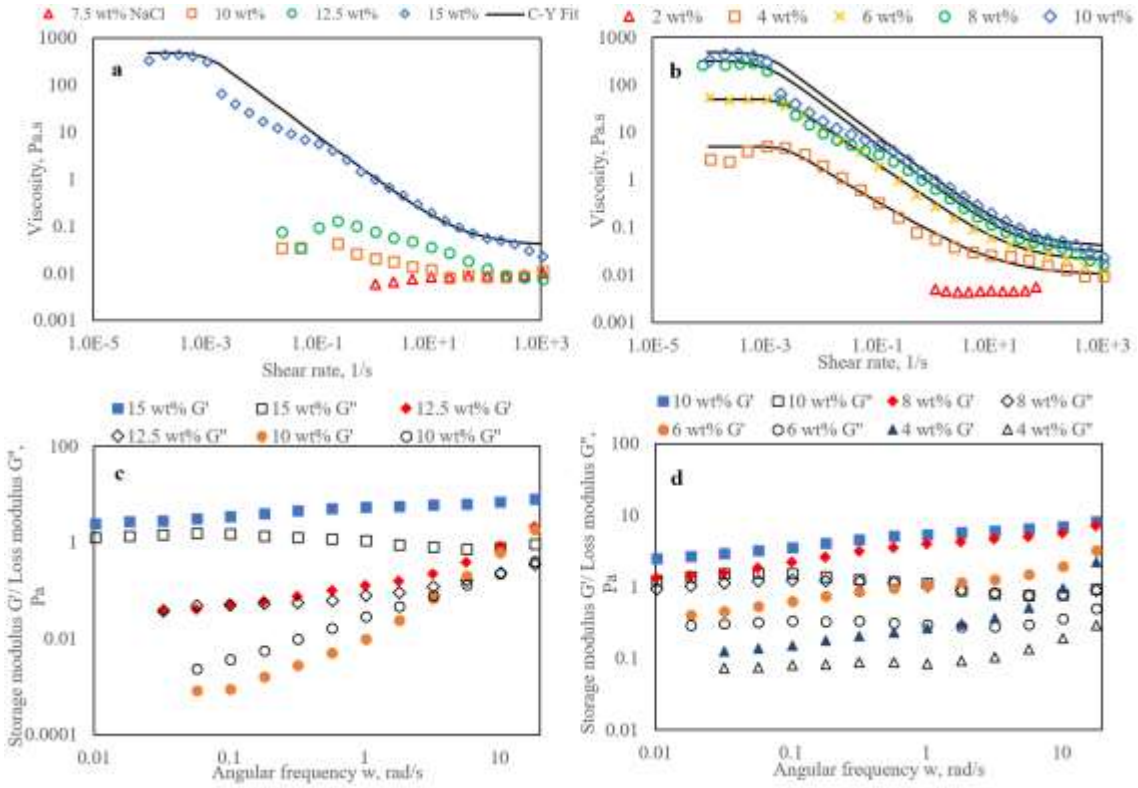

Figure 5.1. Steady shear viscosity as a function of shear rate for (a) 10 wt% $C_8P_4E_1$ solution at various concentration of salt, (b) various concentration of $C_8P_4E_1$ solution with 15 wt% salt. Variation of storage modulus G' (filled symbols) and loss modulus G'' (open symbols) as a function of oscillatory shear frequency for (c) solutions of 10 wt% $C_8P_4E_1$ at various concentration of salt, (d) various concentration of $C_8P_4E_1$ solution with 15 wt% salt.

It is well known that wormlike micelles entangle into a transient network, imparting remarkable viscoelastic properties to the surfactant solutions once the surfactant is above a system-dependent concentration, referred to as the overlap concentration. The growth of wormlike micelles can also be promoted by the addition of co-surfactants or other low-

molecular weight additives, such as short chain alcohols, counterions, salts and oppositely charged surfactants.[8] Firstly, we investigated the impact of salt on the rheology of surfactant solutions at a constant $C_8P_4E_1$ concentration of 10 wt%.

Flow curves were fitted to the Carreau-Yasuda model,

$$\eta(\dot{\gamma}) = \eta_\infty + (\eta_0 - \eta_\infty)[1 + (\lambda\dot{\gamma})^a]^{\frac{n-1}{a}} \quad (5.1)$$

where η_0 is the zero-shear-rate viscosity and η_∞ the infinite-shear rate viscosity. λ is the relaxation time, i.e., the reciprocal of critical shear rate $\dot{\gamma}_c$. For $\dot{\gamma} < \lambda^{-1}$, the Carreau–Yasuda fluid exhibits, essentially, a Newtonian behavior with the viscosity η_0, while for higher shear rates its viscosity drops to $\eta_\infty < \eta_0$. The Carreau– Yasuda model contains two constants: the power-law index $n < 1$ that characterizes the degree of shear-thinning of the model and the constant a that sets the size and curvature of the crossover region between the Newtonian and shear-thinning behavior.

As can be seen in Figure 5.1.a, at salinity of 7.5 wt%, $C_8P_4E_1$ solution behaves like Newtonian fluid; viscosity is 0.009 Pa.s independent of the shear rate. With 10 wt% and 12.5 wt% salt, $C_8P_4E_1$ solutions exhibited rise in viscosity with reducing of shear rate when 100 $s^{-1} > \dot{\gamma} > 0.1$ s^{-1}, but maximum viscosities only around 0.1 Pa.s at $\dot{\gamma} < 0.1$ s^{-1} suggesting the absence of entangled wormlike micelles; for $\dot{\gamma} > 100$ s^{-1}, viscosity leveled off again at 0.009 Pa.s. At higher salt concentration of 15 wt%, the zero-shear viscosity η_0 (determined by Carreau-Yasuda model) reached 480 Pa.s, almost five orders of magnitude higher than that of the 7.5 wt% scenario, undoubtedly manifested the change in the microstructure of the $C_8P_4E_1$ solution. Above a critical shear rate $\dot{\gamma}_c$ of 0.001 s^{-1}, the rheological behavior then becomes shear-thinning, as a consequence of alignment of the wormlike chains in the shear flow.[12]

At no or low salt condition, electrostatic repulsive force between identically charged surfactant head groups stop them from approaching each other too closely at the micelle/water interface. As a result, the micelle maintained a relatively rigid configuration, e.g., spherical packing structure. The micelle geometry can be estimated by critical packing parameter, CP, which is defined as $v/(a_s l_c)$,[13] where v is the volume of the lipophilic chain having maximum effective length l_c, and a_s is the effective area per molecule at the surfactant–water interface. For CP < 1/3, spherical aggregates are expected; for 1/3 < CP < 1/2, surfactants would assemble into rodlike (or wormlike) micelles; whereas for CP > 1/2, lamellar structures should form spontaneously. PO groups reside between hydrophobic tail and hydrophilic head group of C8–$(PO)_4$–$(EO)_1$–SO_4Na molecule; the insertion of such functional groups led to a remarkably bulkier effective head area. For instance, head area of surfactant C_{12}–EO–SO_4Na is reported as 0.44 nm^2 in 0.1 M (0.58 wt%) NaCl solution,[14] while from Gibbs adsorption isotherm (Figure D1 in Appendix D), effective head area of C8–$(PO)_4$–$(EO)_1$–SO_4Na was determined as 1.39 nm^2 in deionized water, and 0.68 nm^2 in 5 wt% NaCl solution, undoubtedly manifesting the contribution from PO groups. Compare PO and EO, the former one behaves more lipophilic,[10] attributed more to the tail rather than the surfactant head. The total number of carbon atoms in the tail chain is 20 (C8-$(PO)_4$). There are only 4 oxygen atoms in the tail (compared to 20 carbon atoms), therefore in terms of tail geometry, we can safely ignore the impact of oxygen atoms. Tail volume is then approximated by $v = 27.4 + 26.9n\ Å^3$, and tail length by $l_c \leq 1.5 + 1.265n\ Å$,[14] where n is the number of carbon atoms of the chain embedded in the micellar core, i.e., 20 in $C_8P_4E_1$. Calculated result is summarized in Table 5.1.

Table 5.1. $C_8P_4E_1$ head area and critical packing parameter at different NaCl concentrations

NaCl, wt%	a_s, nm^2	CP
0	1.392	0.15
5	0.681	0.31
10	0.531	0.39
15	0.479	0.44

CP of $C_8P_4E_1$ falls into the spherical micelle region at salt concentration $\leq$ 5 wt%. While with increase of additional electrolytes to 10 wt%, electrostatic repulsion was largely screened due to compression of electrical double layer. A consequent smaller head area thus led to a larger packing parameter, and rodlike micelle formed in this region. While maximum solution viscosity was only 0.1 Pa.s at 10 wt%, as observed in Figure 5.1.a, which indicates that rodlike micelles were not able to entangle into a transient network due to unfavorable length growth. With further increase of salt to 15 wt%, micelles then grew into 'polymer-like' elongated and flexible aggregates, namely wormlike micelles. In this region, the spontaneous curvature of the end caps is higher than the curvature along the cylindrical body, such length growth is favored for the system to minimize the excess free energy by reducing the number of end caps.[1]

Evolution of microstructure in the solution was also supported by the change of storage modulus (G') and loss modulus (G'') in oscillatory frequency measurement. As shown in Figure 5.1.c, liquid-like behavior ($G' < G''$) was observed at salt concentration of 10 wt%; with increase of salt level to 12.5 wt%, $C_8P_4E_1$ solution shows liquid like behavior in the low-frequency region ($\omega < 0.1$ rad/s), whereas solid-like behavior ($G' > G''$) in the high-frequency region ($\omega > 0.1$ rad/s); with further increase salt to 15 wt%, solid-like behavior was dominant for the whole range of frequency measured. Besides, G' at 15 wt% salt

shows weak dependence on frequency, only slightly changing from 2.5 Pa to 7.2 Pa across three decades, further confirmed the buildup of microstructure.

At constant salt concentration of 15 wt%, effect of $C_8P_4E_1$ concentration was further investigated. As shown in Figure 5.1.b, Newtonian behavior was observed with a viscosity of 0.005 Pa.s at low $C_8P_4E_1$ concentration of 2 wt%. At $C_8P_4E_1 \geq 4$ wt%, shear viscosities exhibited three sections, a high plateau in low shear rate region ($\dot{\gamma} < 0.005$ s^{-1}), a shear thinning behavior at intermediate shear rate (200 $s^{-1} > \dot{\gamma} > 0.005$ s^{-1}), and a second low viscosity plateau at $\dot{\gamma} > 200$ s^{-1}. The zero-shear viscosity is summarized in Table 5.2. With increase in $C_8P_4E_1$ concentration, a rise in zero-shear viscosity reflected the one-dimensional micellar growth. Figure 5.1.d depicts the variation of G′ and G″ as a function of shear frequency. Solid-like behavior (G′ > G″) was observed for $C_8P_4E_1$ concentrations between 4-10 wt% in the entire frequency measured.

Table 5.2. Zero-shear viscosity of $C_8P_4E_1$ solution at 15 wt% salinity

$C_8P_4E_1$ concentration	η_0
wt %	Pa.s
2	0.005
4	4.5
6	52
8	320
10	480

According to Cates model,[15] stress relaxation in the entangled wormlike micellar solutions is governed by two main processes, 1) reptation, i.e., reptilelike motion of the micelle along a tube, and 2) reversible chain scission, i.e., micelle breaking and recombination through exchange of monomers with other micelles. The relaxation time thus depends on two characteristic time parameters, reptation time τ_{rep} and breaking time

τ_{br}. For a sufficiently entangled system, where reptation is much slower than breaking ($\tau_{br} \ll \tau_{rep}$), also known as fast breaking limit, several scission and recombination events take place within the reptation time scale. The viscoelastic behavior of such system follows the Maxwell model of viscoelastic fluids with a single relaxation time, τ_R. For a typical Maxwellian viscoelastic fluid, G'' is symmetric near its peak and G' crosses G'' at this peak. The reciprocal of the crossover frequency is τ_R, which is given mathematically by $\tau_R = (\tau_{br}\tau_{rep})^{1/2}$.

However, in Figure 5.1.c and d, it is evident that G' and G'' responses do not follow that of a Maxwell fluid, i.e., the sample does not have a single relaxation time, but instead has a spectrum of relaxation times.[16] Besides, according to scaling law,[15] dependence of viscosity on surfactant concentration in fast breaking regime obeys $\eta_0 \sim C^{3.7}$. While take the zero-shear viscosity in Figure 5.1.b as an example, the dependence obeys $\eta_0 \sim C^{5.4}$, which is more consistent with scaling parameter for "unbreakable" regime, that $\eta_0 \sim C^{5.7}$. The "unbreakable" regime, namely, reptation occurs fast enough, so that the micelles do not break and recombine many times during τ_{rep}. Therefore, reptation is the principal mechanism of stress relaxation. Since reptation time scales with micellar length, $\tau_{rep} \sim L^3$, low τ_{rep} indicates insufficient contour length of worms.

5.3.2 Microemulsion phase behavior

A microemulsion is a thermodynamically stable dispersion of oil-in-water (Winsor I) or water-in-oil (Winsor II), in contrast to a regular or macroemulsion, which is a kinetically stabilized, non-equilibrium dispersion. The Winsor III microemulsion contains roughly equal volumes of oil and water, where a bilayer or planar microstructure is assumed. The semi-empirical model, hydrophilic-lipophilic deviation (HLD), correlates the effect of

formulation variables such as surfactant type, oil type, temperature and added electrolyte on formation of a Winsor III microemulsion. Negative, zero, or positive HLD values suggest the formation of Winsor Type I, Type III or Type II microemulsions, respectively.[10, 17, 18]

For ionic surfactants, the HLD equation is

$$HLD = \ln(S) - k \cdot EACN + Cc - f(A) - \alpha_T \Delta(T) \quad (5.2)$$

where S is the salinity of the system in grams of electrolyte per 100 ml, $EACN$ is the equivalent alkane carbon number of the oil phase, k is an empirical constant, and Cc is a constant characterizing the hydrophilicity/lipophilicity of the surfactant. Values of k and Cc for $C_8P_4E_1$ are previously reported as 0.053, and -2.47, respectively.[18] $f(A)$ is a function of added alcohol, α_T is an empirical constant, and $\Delta(T)$ is the temperature deviation from a reference temperature of 25 °C. At our experimental condition, 25 °C, without addition of alcohol, the HLD equation can be simplified as,

$$HLD = \ln(S) - k \cdot EACN + Cc \quad (5.3)$$

Optimum salinity S^*, is the salt level where by definition $HLD = 0$ and an optimum Type III microemulsion ($V_o = V_w$) is realized. V_o is the volume of oil in the microemulsion and V_w is the volume of water. Solubilization parameter is defined as the maximum amount of oil (water) solubilized in the microemulsion per unit amount of surfactant, SPo = V_{oil} / m_S (SPw = V_{water} / m_S).

Salinity scan was carried out for 2 wt% $C_8P_4E_1$ solutions with different oils and electrolytes. Figure 5.2 shows representative Winsor III microemulsions of $C_8P_4E_1$ and oil Isopar at different NaCl levels. As can be seen, translucent middle phase

microemulsions are in equilibrium with clear excess oil and water phases. Optimum salinity S^*, of $C_8P_4E_1$/Isopar/NaCl system was determined by interfacial tension measurement. For instance, in Figure 5.3, a minimum interfacial tension of 0.003 mN/m was obtained between excess oil and water at 19.0 wt% salinity, in line with identical solubilization parameters of oil and water in microemulsion phase. Optimum salinity of $C_8P_4E_1$/NaCl solutions with different paraffinic oil or $C_8P_4E_1$/Isopar systems with various type of electrolytes are summarized in Table 5.3.

Figure 5.2. Winsor III microemulsion of 2 wt% $C_8P_4E_1$/Isopar at NaCl concentration from 18.4 - 19.9 wt%

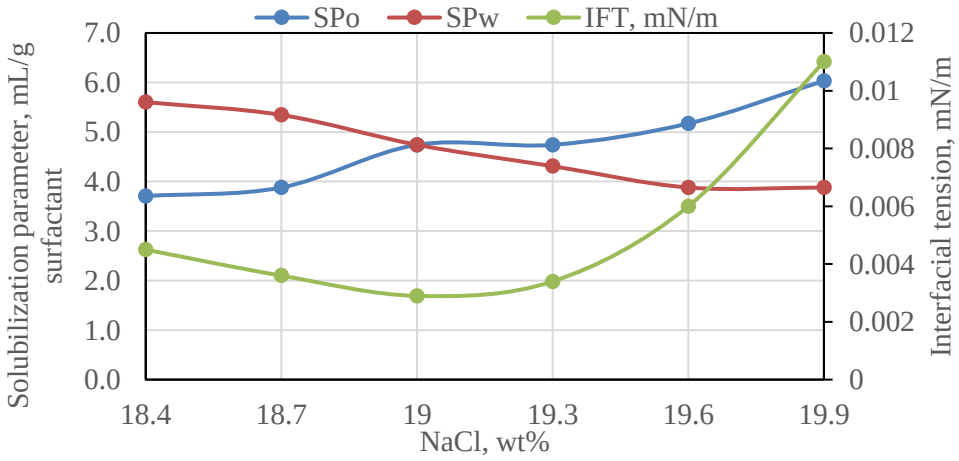

Figure 5.3. Solubilization parameter and interfacial tension between excess oil and water phases for $C_8P_4E_1$/Isopar/NaCl formulation. Optimum salinity is 19.0 wt%

Table 5.3. Optimum salinity (S^*)

$C_8P_4E_1$/NaCl			$C_8P_4E_1$/Isopar	
Oil	EACN	S^* (wt%)	Electrolyte	S^* (wt%)
Octane	8	16.3	NaCl	19.0
Decane	10	18.4	KCl	17.7
Dodecane	12	19.3	CaCl2	20.0
Isopar	11.4*	19	MgCl2	21.7

*EACN of Isopar: calculated based on HLD equation

5.3.3 Rheology of $C_8P_4E_1$ surfactant solution with oil

It is interesting to note, vortex mixing 2 wt% $C_8P_4E_1$ saline solution with a fraction of oil, which formed Winsor III microemulsion at 1:1 volume ratio, can promote a highly viscous solution as shown in Figure 5.4. The homogeneous soft-gel like solution is apparently different from common microemulsion systems, which typically have viscosity ranging from few cP to tens of cP.[19] The viscous solution could be formed with oil of wide volume fraction and at different NaCl concentrations, but only within the Winsor III range. Rheology measurements were carried out to further understand these viscous formulations.

Figure 5.4. Viscous emulsion formed by 3 vol% of Isopar with 2 wt% $C_8P_4E_1$ solution at 19 wt% NaCl.

As seen in Figure 5.5.a, oil-free $C_8P_4E_1$ solution (2 wt%) exhibited a typical Newtonian fluid behavior with viscosity of 0.005 Pa.s. Addition of oil Isopar has dramatic

enhancement in viscosity of the $C_8P_4E_1$ solutions. As mere as 3 vol% Isopar added could induce a highly viscous network and performance. The viscosity approaches a plateau at low shear rate; zero-shear viscosity of 2373 Pa.s is obtained using the Carreau-Yasuda model. The resulted $C_8P_4E_1$ solution behaved shear thinning above a critical shear rate around 0.001 s^{-1}. The viscosity curve seems plateau at shear rate above 100 s^{-1} but a small leap was also seen for some cases before the onset of second plateau. The reason of the viscosity disturbance is believed due to shear banding. Shear banding is a transition between a homogeneous and a non-homogeneous state of flow, the latter being characterized by a "separation" of the fluid into macroscopic regions (bands) of different shear rates.[20, 21] Shear banding transition has been widely observed for wormlike micellar solutions, which is associated with a plateau in the stress versus shear rate curve, as seen in Figure D2 (Appendix D). With increasing solubilized oil volume in the $C_8P_4E_1$ solution, a slow decrease on the steady shear viscosity was seen. Nevertheless, the zero-shear viscosity (η_o) of the oil-induced wormlike micellar solutions has increased at least 4 orders of magnitude (260 Pa.s in 24 vol% oil) compared to the oil-free $C_8P_4E_1$ solution.

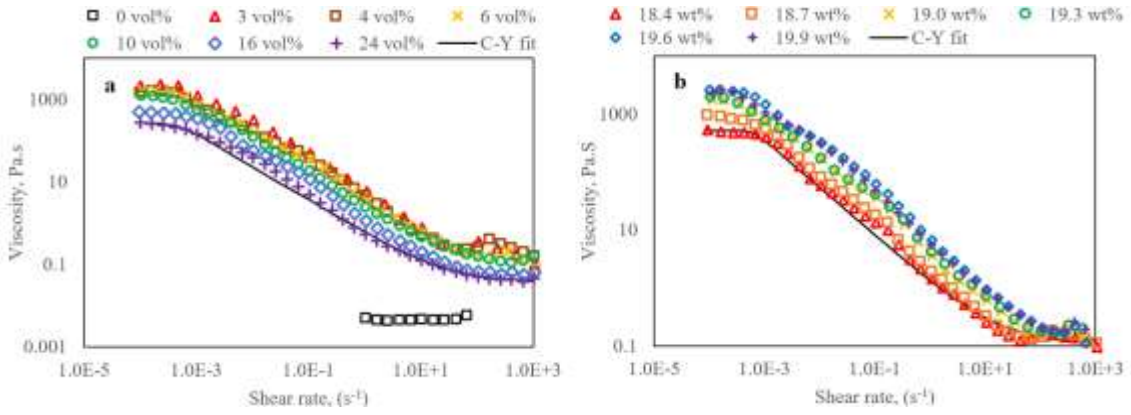

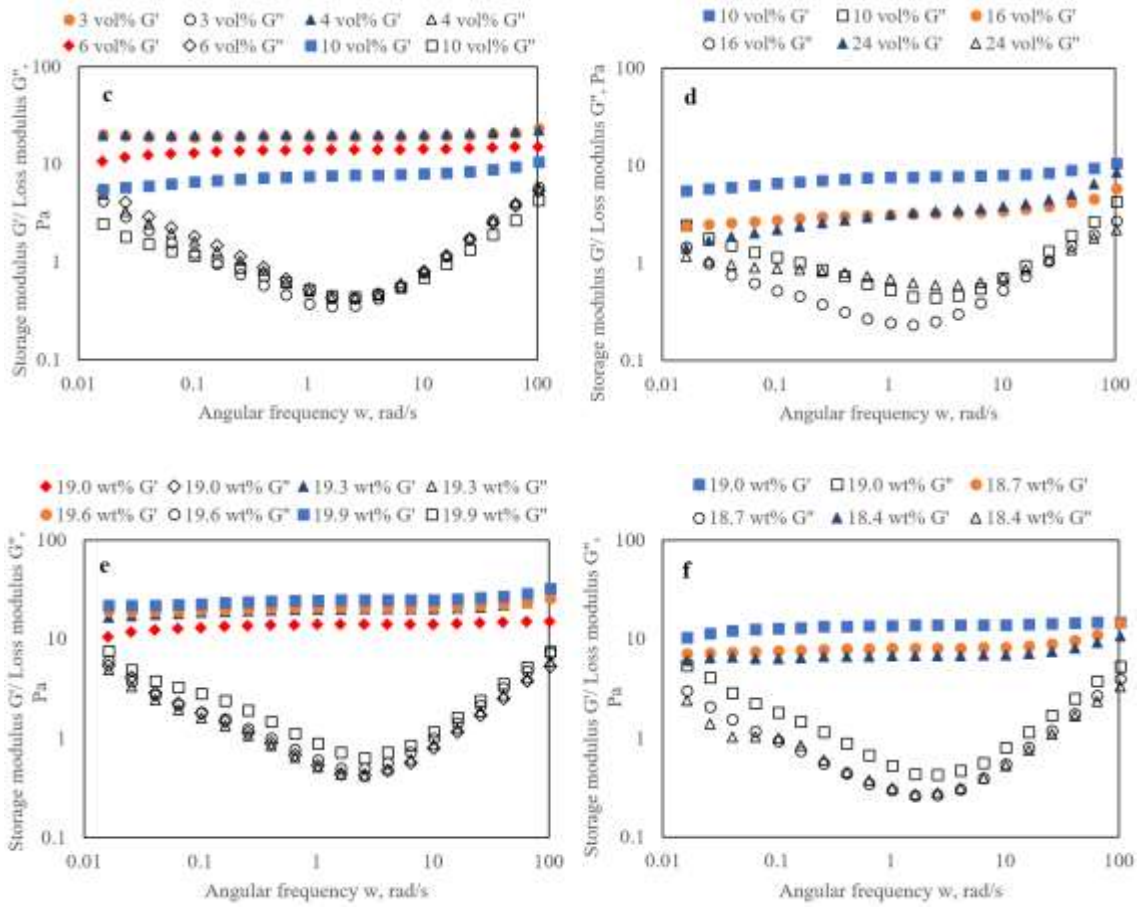

Figure 5.5. Steady shear viscosity as a function of shear rate for (a) 2 wt% $C_8P_4E_1$ solution with various volume of Isopar at optimum salinity of 19 wt% salt, (b) 2 wt% $C_8P_4E_1$ solution with 6 vol% of Isopar at different salinity. Carreau-Yasuda model fit only show in 24 vol% Isopar and 18.4 wt% salt scenarios to present data with clarity. Variation of storage modulus G' (filled symbols) and loss modulus G'' (open symbols) as a function of oscillatory shear frequency for (c and d) solutions of 2 wt% $C_8P_4E_1$ at 19 wt% salt with various volume of Isopar, (e and f) solutions of 2 wt% $C_8P_4E_1$ with 6 vol% of Isopar at different salt concentration.

Figure 5.5.b shows the influence of the salinity change on the viscosity of oil solubilized $C_8P_4E_1$ solutions (6 vol% oil). It should be note that all the salinities presented in Figure 5.5.b are still within the Winsor III microemulsion range. Three segments were observed, a viscosity plateau at low shear rate; shear thinning behavior at intermediate shear rate; and a second viscosity plateau at high shear rate. The viscosity behavior is similar to a typical shear viscosity curve of a polymer melt, as polymers undergoes entanglement,

disentanglement, and eventually orientate along the flow direction with increase of shear rate.[22] With salinity increase from 18.4 to 19.6 wt%, the zero-shear viscosity goes up from 527 to 2737 Pa.s. While at 19.9 wt% salinity, viscosity has slightly dropped to 2509 Pa.s. Figure 5.5.c, d exhibit the variation of G′ and G″ as a function of shear frequency for $C_8P_4E_1$ solutions with oil concentration between 3 vol% and 24 vol%. G' exhibited clear plateaus among all the scenarios tested, while G'' showed a funnel shape with minimum between 1 rad/s and 10 rad/s. For instance, in $C_8P_4E_1$ solution with 3 vol% oil, plateau modulus, G_0, was 20 Pa, with G''_{min} of 0.36 Pa occurred at 1.58 rad/s. No cross-over point for G' and G'' was seen in the frequency range investigated, i.e., 0.01-100 rad/s. Solution with 4 vol% oil behaves as stiff as the solution with 3 vol% oil, with same plateau G_0 recorded at 20 Pa. A decrease in G_0 was seen with increase of solubilized oil concentration > 4 vol% into the $C_8P_4E_1$ solution. Nevertheless, solid-like behaviors (G′ > G″) were observed for all oil concentrations examined. The rather high viscosities (>200 Pa.s), and distinct plateaus of G' indicated the entangled networks of wormlike micelles. Figure 5.5.e, f exhibit the variation of dynamic shear moduli at various salinity levels. Similarly, solid-like behaviors (G′ > G″) were observed for all salt concentrations examined without a cross-over point between 0.01-100 rad/s. With rise in the salt concentration from 18.4 to 19.9 wt%, a growth in G_0 is observed from 7.0 to 25.7 Pa.

The dominance of G′ over G″ implied unique elasticity of oil-solubilized $C_8P_4E_1$ solutions. While contrary to a typical elastic gel system, which in essence does not relax, i.e., its relaxation time t_R (and in turn, its zero-shear viscosity η_o) is infinite,[16] the authors believe the relaxation time of oil solubilized $C_8P_4E_1$ solution should be a finite, yet quite high value. In the rheology measurement, oil solubilized solution did not show a yield

stress, which is a characteristic of typical gels and the reason for their infinite viscosity at stagnant situation. Instead, a finite zero-shear viscosity was recorded. Also observing the trend of G' and G'' in the oscillatory graph, G'' is believed to rise with further reduction in shear frequency, and eventually give rise to a cross between G' and G'' at frequency < 0.01 rad/s. In turn, an extremely high (> 100s) rather than infinite relaxation time is expected for such gel-like solutions.

As suggested by Dreiss, the inverse of the critical shear rate γ_c gives an estimate of the longest micellar structural relaxation time τ_R.[1] In oil solubilized $C_8P_4E_1$ solution, the shear thinning did not appear until shear rate around 4 - 6 $\times 10^{-4}$ s^{-1}, which in turn gives τ_R around 2000 s, obviously exceeding the range of measurements; in the oil-free solution, γ_c is observed around 1-2 $\times 10^{-3}$ s^{-1}, resulting in τ_R around 500 - 1000 s. In comparison, a typical relaxation time has been reported around 0.1-10 s,[2, 4] of wormlike micellar solution such as sodium laury ether sulfate (SLES), and potassium oleate.

For typical wormlike micellar solutions conforming to Maxwell model, e.g., cetylpyridinium chloride, and hexadecyltrimethylammonium bromide (CTAB), breaking time τ_{br} has been measured around 0.01-0.1s.[23, 24] τ_{br} > 10 s was reported for highly viscoelastic (gel-like) wormlike micellar solution, typically formed with surfactant acquiring an overall tail length of C22 (erucyl tail) or longer.[25] Rheological properties of erucyl tail surfactant has been previously investigated with erucyl bis(hydroxyethyl) methylammonium chloride (EHAC), erucyl dimethyl amidopropyl betaine (EDAB), and 3-(-Nerucamidopropyl-N,N-dimethyl ammonium) propane sulfonate (EDAS).[25-27] It is common that G' shows a plateau extending up to $\omega \sim 0.01$ rad/s at the low end, and G' > G'' at entire frequency range by a factor of 10 or more. The long C22 tail was believed

to increase hydrophobicity of surfactant dramatically, so that it is unfavorable for C22 surfactant to diffuse through water, either out of a micelle or into another one, therefore leading to several orders of magnitude higher τ_{br}. The extended tail of $C_8P_4E_1$ has in total 20 carbon atoms, though it is smaller than a C22 tail, the breaking of $C_8P_4E_1$ micelles would be a relatively unfavorable process compared to shorter alkyl chain wormlike micelle, e.g., CTAB, thus we can safely assume a τ_{br} = 10 s for $C_8P_4E_1$, similar as erucyl tail surfactant.

Reptation time τ_{rep} of entangled worms have been estimated from 10^3 to 10^5 s.[16, 25] We assume τ_{rep} of 10^4 s for $C_8P_4E_1$, and according to $\tau_R = (\tau_{br}\tau_{rep})^{1/2}$ in Maxwell model, τ_R is therefore calculated around 316 s. This calculated value is close to the τ_R of EDAB observed in dynamic rheological test, around 200-300 s.[25] Compared to a typical relaxation time of 10 s encountered in wormlike micellar solution, the high relaxation time of EDAB was attributed to a rather long contour length and consequent long reptation time (as $\tau_{rep} \sim L^3$), as well as a larger breaking time.[16]

Study indicated EDAB micellar solutions are, however, extremely oleo-responsive;[28] as little as 0.1% toluene could result in a significant disruption of the network and a decrease in zero-shear viscosity of around 100-fold. Effect of alkane was inspected for wormlike micellar solution of EHAC. Addition of hexane above 0.6 wt% (70 mM) was able to disrupt the plateau modulus, indicating the breaking of the wormlike structure.[29]

Compare 3 vol% oil solubilized $C_8P_4E_1$ solution and oil-free solution, higher zero-shear viscosity (2373 Pa.s vs. 0.005 Pa.s) and plateau modulus G_0 (20 Pa) unquestionably indicates that solubilized oil induces the growth of wormlike micelle. The primary composition of Isoapr L is essentially a synthetic isoparaffinic hydrocarbon, which

contains very low levels of aromatic composition. The equivalent alkane carbon number (EACN) of Isoapr L was determined about 11.4, in other words, it behaves approximate hendecane and dodecane. As opposed to typical alkane oils, which were reportedly solubilized in the core of surfactants micelles thus to shorten the wormlike micelle, the authors believe Isopar oil may be solubilized at the spacer layer where PO groups reside. Presence of POs provide a smooth transition zone between the extremely hydrophilic sulfate headgroup and extremely lipophilic alkyl tail in the interface.

In the Winsor III regime, the surfactant has approximately equal affinity to both water and oil. As seen in Figure 5.3, 1:1 ratio of oil and water were solubilized by $C_8P_4E_1$ at optimum salinity therefore lead to a planar (bilayer) structure. Our hypothesis is that, in the oil solubilized wormlike micellar formulation, $C_8P_4E_1$ micelle may incorporate insufficient oil into the core, thus solubilized oil was not able to swell the micelle core, and lead to a planar structure, i.e., reduce curvature to 0. Instead, oil probably bond to the spacer layer where PO groups reside. Incorporating of oil into PO groups reveals two-fold impacts, first, fully extend the length of PO groups thus enlarge the tail length; second, truncate the cross-section area of head group, because agglomerated PO groups would otherwise contribute to a bulkier head group, as seen in Gibbs adsorption calculation. Since increase in tail length and decrease in head area would oppose each other in the denominator term in critical packing parameter, $CP = v/(a_s l_c)$, a net effect of these two may have trivial change on packing factor, which is approximate to that of oil-free micelles between 1/3 to 1/2.

On the other hand, the change in formation energy of end caps can provide an alternative to evaluate the micelle evolution. As suggested by May and Ben-Shaul,[30] the free energy per surfactant can be expressed by,

$$f = \gamma a \left(1 - \frac{a_0}{a}\right)^2 + f_c \tag{5.4}$$

where γ is the effective surface tension between the hydrophobic core and the surrounding solution, which is often approximated by the water-alkane surface tension $\gamma \approx 0.12\, k_B T/\dot{A}^2$; a is the surface area per surfactant molecule; a_0 is the optimum headgroup area which resulted in a minimum packing free energy;[13] and f_c is the chain contribution to the molecular packing free energy, which is a constant, independent of the aggregation geometry according to the convention that hydrophobic core of amphiphilic aggregates is liquidlike.

For a semi-spherical end cap, $a_{sph} = 3\mathrm{v}/\mathrm{l}_c$, the number of surfactant molecules in one end cap can be approximated by,

$$N = \frac{2\pi {l_c}^2}{a_{sph}} \tag{5.5}$$

The excess energy per molecule in the end cap is suggested by Shibaev,[7]

$$\Delta f = f_{sph} - f_{cyl} \approx \gamma a_{sph} \left(1 - \frac{a_0}{a_{sph}}\right)^2 \tag{5.6}$$

Then the energy cost E_c of a single end cap (half of scission energy) is expressed as,

$$E_c = N\Delta f \approx 2\pi\gamma {l_c}^2 \left(1 - \frac{a_0}{a_{sph}}\right)^2 \tag{5.7}$$

We assume here, solubilizing small volume of oil into the PO groups only extends the length of PO groups therefore length of the tail but does not change the volume of the

hydrophobic tail, in other words, solubilized oil takes the empty space previously inaccessible to alkyl chain due to steric hindrance resulted from bulk PO groups, i.e., $v = \frac{a_{sph} l_c}{3} = const.$ Above equation is therefore rewritten as,

$$E_c \approx 2\pi\gamma {l_c}^2 \left(1 - \frac{a_0 l_c}{3v}\right)^2 \tag{5.8}$$

In forming spherical micelle in the end cap, a_0 satisfies the condition, $a_0 > 3v/l_c$; in turn, $l_c > 3v/a_0$. Differentiate above equation,

$$dE_c/dl_c = 4\pi\gamma l_c(1 - \frac{a_0 l_c}{3v})(1 - \frac{2a_0 l_c}{3v}) \tag{5.9}$$

Obviously, when $l_c > 3v/a_0$, we have,

$$\begin{cases} 1 - \frac{a_0 l_c}{3v} < 0 \\ 1 - \frac{2a_0 l_c}{3v} < 0 \end{cases} \tag{5.10}$$

Thus, $dE_c/dl_c > 0$, indicating that E_c is monotonically rising with increase in l_c. According to mean-field theory,[15] the average contour length $\bar{\mathrm{L}}$ is related to surfactant volume fraction C, end cap energy E_c, as well as temperature T by,

$$\bar{\mathrm{L}} \sim C^{0.5} exp(E_c/k_B T) \tag{5.11}$$

Obviously, higher end cap energy would lead to a longer contour length. In other words, solubilizing even smaller volume of oil in PO groups, would effectively enlarge the length of surfactant tail, truncate the headgroup area, and lead to a greater end cap excess energy, thus growth of wormlike micelle is favored.

It is necessary to iterate here, above estimation of E_c is only viable for solubilizing small volume of oil. With larger volume of solubilized oil, however, a hydrocarbon core (sphere droplet) would form inside the micelle and lead to a swelling end cap. The calculation of

E_c of a swelling end cap can be found elsewhere.[7] In short, swelling of end cap would decrease interfacial curvature of micelles and lead to the reduction of the scission energy $2E_c$, therefore growth of wormlike micelle would be restrained.

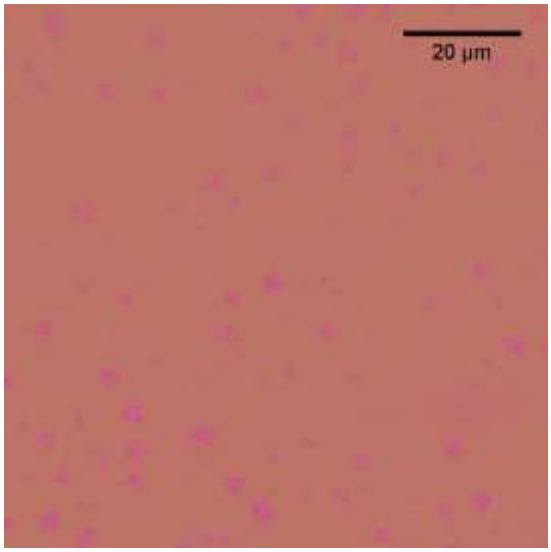

Figure 5.6. Fluorescence image of oil solubilized wormlike micellar solution of 2 wt% $C_8P_4E_1$ with 4 vol% Isopar at 19 wt% salinity. Isopar was dyed by Nile red, as illustrated by magenta color in the image. Giant oil droplets are seen with size ranging from 2-4 μm.

Figure 5.6 is a fluorescence image obtained from confocal microscopy for 2 wt% $C_8P_4E_1$ with 4 vol% Isopar at 19 wt% salinity. Isopar was dyed by Nile Red as indicated by the magenta color in the image. It is needed to be note, resolution of confocal microscopy is limited around 100 nm scales, thus it is unable to differentiate the wormlike structure of the sample. Nevertheless, it is effective to visualize the giant oil droplets may evolve in the solution. Some oil droplets are seen sparsely distributed in Figure 5.6, with size ranging from 2-4 μm. The presence of oil droplets indicates that reduced end cap energy (due to incorporating oil into the core) eventually lead to giant oil in water dispersion, which obviously impeded the rise of viscosity, also may be a probable reason for the shear banding observed in steady shear viscosity. Fu et al.[31] observed that large oil droplets

embedded in the three-dimensional droplet network leading to apparent viscoelasticity enhancement, when blend 10 vol% tetradecyl trimethyl ammonium laurate solution with 90 vol% of paraffin oil at intermediate salt concentration. Obviously in our study, the volume of introduced oil was too low to logjam a densely packed three-dimensional network.

As mentioned previously, the wormlike $C_8P_4E_1$ solution was only induced by solubilized oil in Winsor III regime. What does this indicate? In the system other than Winsor III microemulsion, surfactant molecule has unbalanced affinity between oil and water phase. For instance, in Winsor I region, surfactant has stronger water-surfactant interaction than oil-surfactant interaction. Water molecules hydrated to the head groups (-EO-SO4Na) are sufficient to maintain a rigid micellar interface with a positive curvature. On the other hand, oil-surfactant interaction is relatively weaker. PO groups therefore behaves less lipophilic compared to that in Winsor III region, and agglomerated POs would assume rather than extended structure. Instead of contributing to an enlarged tail, solubilized oil would be directly incorporated into micelle core, thus growing of wormlike micelle is not anticipated. From dynamic light scattering (Figure D3 in Appendix D), hydrodynamic diameter of oil swollen micelle was determined around 30-50 nm in Winsor I microemulsion, (octane solubilized by 2 wt% $C_8P_4E_1$ at 13.3-14.4 wt% NaCl), which is obviously larger than twice of fully extended surfactant length (approximate 3 nm) of $C_8P_4E_1$ molecule assuming a tail to tail spherical micelle.

In Figure 5.5.c-f, it is evident, plateau modulus G_0 decreases with increase in solubilized oil volume, while increases with rise in the salt concentration in the Winsor III region. In

terms of worm structure, G_0 is related to the network mesh size of the entangled wormlike micelle ξ by,

$$G_0 = \frac{k_B T}{\xi^3} \tag{5.12}$$

A rise in G_0 indicates the decrease in ξ, in other words, network structure becomes increasingly tighter. This is consistent with the observation of zero-shear viscosity, that η_o reduces with rise in solubilized oil volume but increases with growth of salinity. ξ is related to the persistence length of the micelles, l_p, and the entanglement length l_e, the average distance along the micelles between two entanglement points in the micellar networks by,

$$l_e = \frac{\xi^{5/3}}{l_p^{2/3}} \tag{5.13}$$

The persistence length, l_p, typically ranges from 20 to 50 nm as determined through scattering techniques.[1] Shibaev et al.[7] observed that l_p is almost independent of solubilized oil volume, and Oelschlaeger et al.[32] stated that l_p is rather independent over the change of ionic strength. Thus, we can safely assume l_p is a constant, 30 nm, in our oil solubilized $C_8P_4E_1$ wormlike micelles. The change in the average contour length $\bar{L}$ relative to entanglement length l_e is estimated directly from the rheological data using,[15]

$$\frac{\bar{L}}{l_e} \approx \frac{G_0}{G''_{min}} \tag{5.14}$$

where G''_{min} is the value of the loss modulus at the high frequency minimum. The ratio $\frac{\bar{L}}{l_e}$ defines the average number of entanglements per micelle. ξ, l_e, and $\bar{L}$ are calculated based on the measured rheological data.

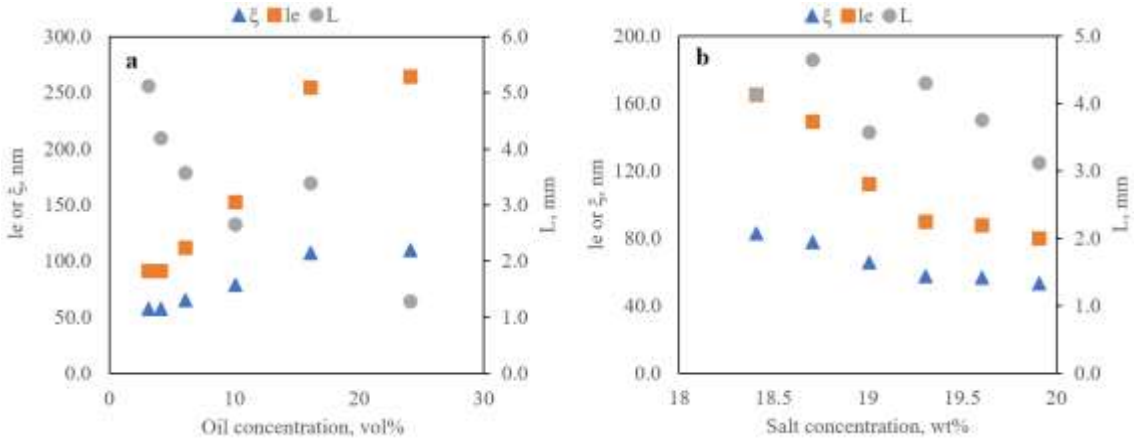

Figure 5.7. Dependence of the network mesh size ξ, entanglement length l_e, and average contour length of micelles $\bar{L}$ on a. Isopar concentration (constant salt concentration 19 wt%) and b. salt concentration (constant oil concentration 6 vol%) for 2 wt% $C_8P_4E_1$ solution at 25 °C.

As can be seen in Figure 5.7, with rise in the concentration of solubilized oil above 3 vol%, both network mesh size ξ, and entanglement length l_e increased, indicating less frequency for worms to get entangled. A reduction on contour length of wormlike micelle from 5.1 to 1.3 μm is seen with oil volume growing from 3 to 24 vol%. While with rise in the salt concentration in the micellar solution, both network mesh size ξ, and entanglement length l_e decreased, which means the network structure becomes increasingly stiffer. The change in contour length was less obvious, slightly fluctuating within 4.6 and 3.1 μm. It is needed to note, the contour length of $C_8P_4E_1$ solution was estimated as high as 5 μm, which is around an order of magnitude higher than a typical value of 100-500 nm, being reported for wormlike micelles, such as sodium dodecyl

sulfate (SDS), SLES, and CTAB.[1, 2, 32] Details of the characteristic parameters for wormlike micelles are summarized in Table 5.4.

Table 5.4. Characteristic parameters obtained from rheological measurements. Group A varying NaCl concentration in 2 wt% C8P4E1 solution with 6 vol% Isopar; Group B varying concentration of Isopar in 2 wt% C8P4E1 solution with 19 wt% NaCl; Group C varying concentration of C8P4E1 with 6 vol% Isopar and 19 wt% NaCl; Group D varying cations (at respective optimum concentration) in 2 wt% C8P4E1 solution with 6 vol% Isopar; Group E varying oils (6 vol%) in 2 wt% C8P4E1 solution with NaCl at respective optimum salinity.

Group	NaCl, wt%	G_0, Pa	η_0, Pa.s	G''_{min}	L/le	ξ, nm	le, nm	L, um
A	18.4	7.0	527	0.28	25	84	166	4.2
	18.7	8.4	986	0.27	31	79	150	4.7
	19	14.3	1895	0.44	33	66	112	3.6
	19.3	20.7	2026	0.44	47	58	91	4.3
	19.6	21.7	2737	0.51	43	57	89	3.8
	19.9	25.7	2509	0.66	39	54	81	3.1
	Isopar, vol%	G_0, Pa	η_0, Pa.s	G''_{min}	L/le	ξ, nm	le, nm	L, um
B	3	20.0	2373	0.36	55.6	59	93	5.1
	4	20.8	1663	0.44	47.3	58	91	4.3
	6	14.3	1895	0.44	32.5	66	112	3.6
	10	8.0	1309	0.46	17.4	80	154	2.7
	16	3.5	532	0.24	14.6	106	244	3.6
	24	3.2	272	0.61	5.2	109	256	1.3
	C8P4E1, wt%	G_0, Pa	η_0, Pa.s	G''_{min}	L/le	ξ, nm	le, nm	L, um
C	1.5	11.5	1154	0.31	37	71	126	4.7
	2	14.3	1895	0.44	33	66	112	3.6
	3	24.9	3625	0.63	40	55	82	3.2
	4	19.6	4262	0.7	28	59	94	2.6
	6	22.2	3198	0.94	24	57	87	2.1
	cation	G_0, Pa	η_0, Pa.s	G''_{min}	L/le	ξ, nm	le, nm	L, um
D	K^+	3.2	336	0.15	21	109	256	5.5
	Na^+	14.3	1895	0.44	33	66	112	3.6
	Ca^{2+}	8.8	678	0.28	31	78	146	4.6
	Mg^{2+}	11.5	2443	0.27	43	71	126	5.4
	oil	G_0, Pa	η_0, Pa.s	G''_{min}	L/le	ξ, nm	le, nm	L, um
E	octane	5.0	420	0.24	21	94	200	4.2
	decane	12.2	2337	0.31	39	70	122	4.8
	Isopar	14.3	1895	0.44	33	66	112	3.6
	dodecane	7.8	1016	0.18	43	81	156	6.8

Our hypothesis that formation of wormlike micelles in oil solubilized $C_8P_4E_1$ solution is due to the extending of PO groups at optimum Winsor III condition, in essence it is a characteristic of surfactant itself. External physical conditions, such as cations species (impact on head), and solubilized oil (impact on alkyl tail) are not the critical factors governing the formation of wormlike micelles, as long as the packing geometry stands, and oil-surfactant-water interaction is balanced (optimum Winsor III microemulsion). The steady shear viscosity, and dynamic shear moduli of 2 wt% $C_8P_4E_1$ solution with constant concentration of various oils (6 vol%), namely, octane, decane, Isopar, and dodecane; and the effect of different cations, such as Na^+, K^+, Ca^{2+}, and Mg^{2+}, as well as the impact of $C_8P_4E_1$ concentration on the rheological behavior are thus examined. The results are shown in Figure D4 (Appendix D), with critical rheological and structural parameters listed in Table 5.4.

Divalent cations, Mg^{2+} (2.28 mol/kg) and Ca^{2+} (1.8 mol/kg) are more effective to create Winsor III microemulsions of $C_8P_4E_1$ compared to monovalent cations Na^+ (3.25 mol/kg) and K^+ (2.38 mol/kg). Three segments were also observed in shear viscosity for $C_8P_4E_1$ wormlike solutions with different cations. Increase in zero-shear viscosity (both absolute increment as well as increase per mole of cation) was seen following $K^+ < Ca^{2+} < Na^+ < Mg^2$. For K^+, the viscosity is at relatively lower level compared to other three cations, with a zero-shear viscosity of 336 Pa.s. Addition of Mg^{2+} exhibited the highest viscosity, leveled off at 2443 Pa.s. Cation radii follows a reverse trend, K^+ (133 pm) > Ca^{2+} (99 pm) > Na^+ (95 pm) > Mg^{2+} (65 pm). The change on viscosity is attributed to the strength of interaction between surfactant headgroups and metal cations, that the cation with smaller radius may not only be adsorbed in the interface of the micelles, but also embed around

the headgroups. Therefore, smaller cations will compress the area of surfactant headgroups to a great extent and enhance micellar growth.[33]

Among the 4 species of oils, octane induced $C_8P_4E_1$ wormlike solutions exhibits apparently lower viscosity compared to other three oils. The shear viscosity as well as the plateau modulus follows octane < dodecane < Isopar ≈ decane. In terms of shear viscosity and G', Isopar and decane almost overlap with each other, except that Isopar reached a plateau in the low shear rate with a viscosity about 1895 Pa.s, whereas decane has not yet leveled off at the shear rate as low as 0.0001 s^{-1} (the zero-shear viscosity of decane is simply obtained by averaging last 3 data points in the low shear rate). In the microemulsion phase behavior (not shown), octane generates thicker middle phase compared to other three oil, implying stronger oil-$C_8P_4E_1$ interaction. In comparison with other oils tested, molecular structure of octane is identical to the alkyl chain of $C_8P_4E_1$. This will lead to a favorable interaction (miscible) between tail of $C_8P_4E_1$ and octane, thus octane molecules are more likely to diffuse to the interior of the micelle instead of bonding to the POs, and less tail extension is understandable.

Fixing the amount of solubilized oil (6 vol% Isopar) by varying the concentration of $C_8P_4E_1$ is helpful to figure out the optimum ratio of oil/surfactant, where the highest viscosity and modulus may occur. As $C_8P_4E_1$ concentration increase from 1.5 wt% to 3.0 wt%, rise in both η_0 and G_0 manifest a stiffer network of wormlike micelles. While increase $C_8P_4E_1$ concentration from 4 wt% to 6 wt%, both η_0 and G_0 show reduction. The optimum ratio of oil/surfactant is thus calculated around 1.3-1.7 mL/g (3.0-4.1 molecules of Isopar per molecule of $C_8P_4E_1$), which is obviously less than the optimum solubilization parameter in Winsor III microemulsion, 4.8 mL/g. Again, this confirms

insufficient solubilized oil may only bond to POs thus give rise to the growth of wormlike micelles rather than swell the core. At $C_8P_4E_1$ concentration < 3 wt%, a higher ratio 2.6-3.4 mL/g indicating more oil may be solubilized into core therefore reduce the end cap energy and impede the build-up of viscosity and storage modulus. With 6 wt% $C_8P_4E_1$, ratio of oil/surfactant is lower, 0.9 mL/g. In this case, oil was fully solubilized into POs to achieve maximum number of extended POs, i.e., maximum worms. The decrease of viscosity is possible due to the branching of worms at high concentration. The branches provide intermicellar junctions, which can effectively slide along the micellar body thus serve as stress-release points. The resulting multi-connected network therefore displays a reduced viscosity compared to entangled micelles.[1, 2, 34, 35]

5.3.4 Implications in reservoir application

Oil-induced (or oleo-resistant) viscoelastic behavior are of great importance for oilfield applications, such as fracking fluid, and surfactant slug in tertiary recovery. In terms of the fracking fluid, adopting surfactant-based viscoelastic fluid have some priorities over traditional polymer-based viscoelastic fluid, 1. avoid the use of crosslink breaker which is typically needed to degrade polymer gels; 2. ease pore blocking normally occurred in polymer gels due to their gigantic molecular structure; 3. the most important advantage of our oil-induced viscoelastic fluid, because it is reformed from Winsor III microemulsion, collapse of worms would improve the microscopic displacing efficiency due to ultralow interfacial tension between oil and water phase.

Figure 5.8. Proppant carrying performance of viscoelastic fluid. a. 3 pounds per gallon (0.36 g/mL) of ceramic proppants in 2 wt% $C_8P_4E_1$ solution right after agitation, specific gravity of proppant in left cylinder (black) is 3.2, in right cylinder (gray) is 2.5, both proppants are 20/40 mesh size; b-d, 3 pounds per gallon (0.36 g/mL) of ceramic proppants in viscoelastic fluid (2 wt% $C_8P_4E_1$ with 3.0 vol% oil) right after agitation, after 12 hours of heating at 50 ºC, and after 24 hours of heating at 50 ºC, respectively.

Figure 5.8 illustrated the proppant carrying performance of viscoelastic fluid. Ceramic proppants (3 pounds per gallon, specific gravity 2.5-3.2) settled down right after agitation in the oil-free $C_8P_4E_1$ solution. While in the oil-induced viscoelastic fluid, proppants were suspended homogeneously after agitation, and good suspendability was maintained after 24 hours of heating at 50 ºC. Besides, oil-induced viscoelastic fluid could also be used in other areas where fine particles need to be suspended, for instance, in stabilizing and transporting zero valent iron (ZVI) particles in environmental remediation work. Figure

5.9 compared the suspendability of ZVI in both $C_8P_4E_1$ solution and $C_8P_4E_1$ viscoelastic fluid. Samples become completely black after mixing 4 grams of ZVI with 10 mL of dispersant solution (yielding mass concentration of ZVI 26 wt%). To facilitate sedimentation of particles, samples were centrifuged at 537 relative centrifugal force (RCF) for 10 minutes. It can be seen in Figure 5.9 b, in oil-free $C_8P_4E_1$ solution (0.005 Pa.s) ZVI precipitated at the bottom of the vial completely. While in oil-induced viscoelastic fluid, ZVI were well suspended after centrifugation because of high viscosity originated from entangled worms network. It is needed to be note, the viscoelastic fluid in Figure 5.8 andFigure 5.9 contains only 2 wt% $C_8P_4E_1$ and 3 vol% oil. To achieve the best suspendability, the concentration of $C_8P_4E_1$ as well as ratio between $C_8P_4E_1$ and oil could be optimized as shown in previous section.

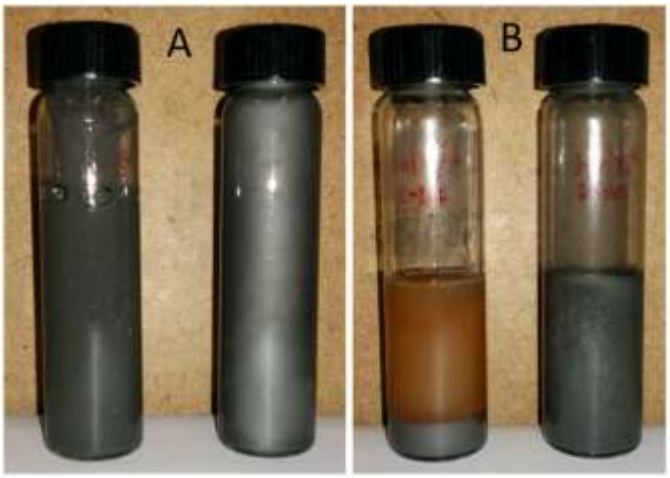

Figure 5.9. Suspendability of zero valent iron particles (2 μm) by viscoelastic fluid. a. samples right after vortex mixing; b, samples after 10 minutes of centrifugation at 537 relative centrifugal force (RCF). Left vial, 26 wt% of zero valent iron in 2 wt% $C_8P_4E_1$ solution; right vial, 26 wt% of zero valent iron in viscoelastic fluid (2 wt% $C_8P_4E_1$ with 3.0 vol% oil).

As for the tertiary recovery chemical slug, the oil-induced viscoelastic fluid provides not only exceptional microscopic displacing efficiency but also favorable macroscopic sweep

efficiency, compared to typical surfactant-only slug. In this endeavor, we tested the potential serving of oil-induced viscoelastic fluid as tertiary recovery surfactant slug via laboratory sand pack experiments. Figure 5.10 compares the efficiency of viscoelastic fluid (2 wt% $C_8P_4E_1$ with 5.6 vol% oil) versus surfactant-only slug (2 wt% $C_8P_4E_1$) in residual oil recovery. 0.25 PV viscoelastic slug was able to recover 80% of residual oil, as compared to 48% of oil recovery made by the surfactant-only system without polymer injection. With improving both the volumetric sweep efficiency and microscopic displacement efficiency, viscoelastic fluid gave rise to a faster oil breakthrough and larger oil cut in comparison to surfactant-only slug. At 1 PV after chemical slug injected, the oil recovery is 77% with viscoelastic recipe vs. 10 % in surfactant-only case. The detailed comparison of injection scenarios with different slug size and solubilized oil concentrations can be found in Figure D5 (Appendix D). In general, the advantage of the viscoelastic formulation is a single-step process offering both the ultra-low interfacial tension and highly favorable rheological characteristic of the displacing agent, thus, it has potential in providing a better alternative over the existing surfactant/polymer or micellar/polymer process.

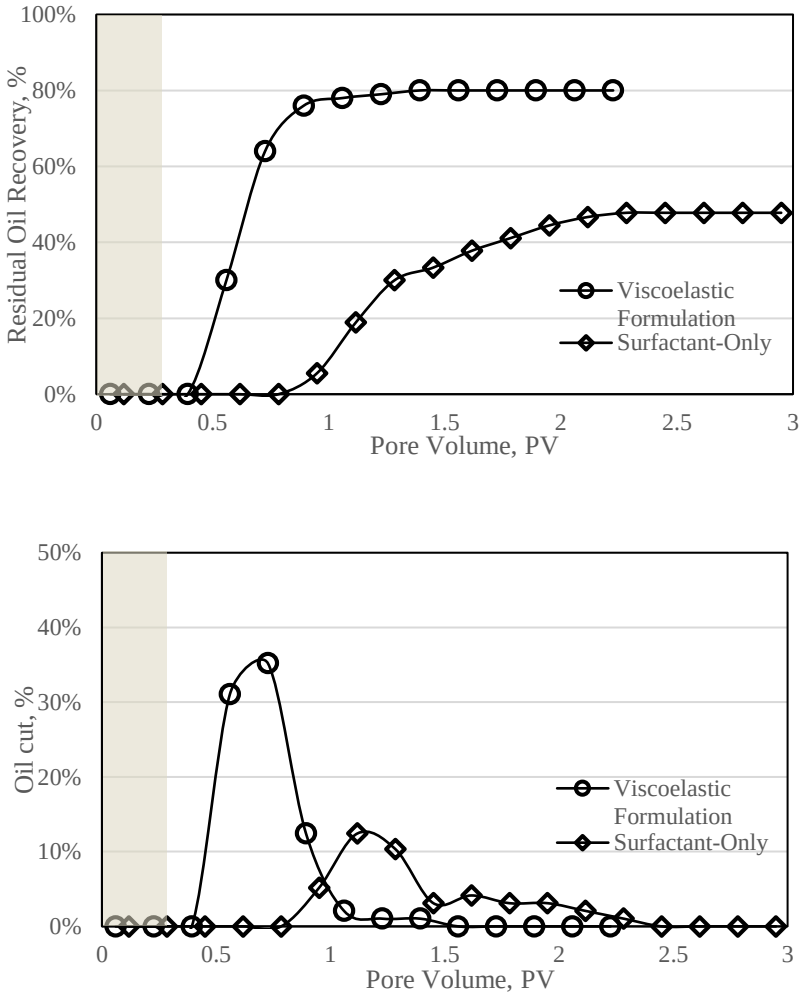

Figure 5.10. Residual oil recovery profile of injecting 0.25 PV oil-induced viscoelastic fluid versus surfactant-only slug. Oil-induced viscoelastic fluid contains 5.6 vol% of oil, i.e., 35 vol% of oil solubilized in the middle phase microemulsion. Shaded area indicates the injection of chemical slug.

5.4 Conclusion

In this work, the rheological property of a micellar solution consisting of extended surfactant C8–$(PO)_4$–$(EO)_1$–SO_4Na ($C_8P_4E_1$) was extensively studied. Addition of as small as 3 vol% alkane into the $C_8P_4E_1$ formulations (2 wt%) promotes a sudden rise in viscoelastic behaviors, e.g. solution viscosity jumps 5 orders of magnitude. Oscillatory-shear (frequency sweep) measurements were performed on the viscoelastic samples and

solid-like behaviors (G' > G'') were observed in the entire frequency region (0.01-100 rad/s). Highly viscoelastic fluids were able to be formed via varying oil volume, type of counterion, and counterion concentration. Contrary to common oleo-responsive wormlike micelles, addition of paraffinic oil into $C_8P_4E_1$ solution within Type III system apparently give rise to a favorable longitudinal growth of wormlike micelles. Our hypothesis is that, incorporating oil to the spacer layer where PO groups reside can extend the PO groups and enlarge the tail length, thus result in an increasing end cap energy and promote longitudinal growth of worms. This paper, to the best of our knowledge, is the first work that extensively studied the rheological property of extended surfactant, also the first work that evidenced the phenomena of paraffinic oil-induced growth of wormlike micelles. The discovery of this "abnormal oleo-responsive" viscoelastic behavior is of great significance in practical applications, such as oilfield fracking fluids, home care products, cosmetics, and drug delivery agents. Last but not least, this oil-induced viscoelastic behavior is not unique for $C_8P_4E_1$, we have observed such behavior in other surfactants as well. A detailed study on oil-induced wormlike micelles in respect to the impacts of surfactant alkyl tail length, PO size, as well as the head types, i.e., cationic, anionic, and nonionic surfactants, will be documented in a separate paper soon.

Acknowledgement

The authors would like to thank Dr. Tingting Gu for conducting confocal microscopy at Samuel Roberts Noble Microscopy Laboratory (University of Oklahoma).

Reference

1. Dreiss, C. c. A., Wormlike micelles: where do we stand? Recent developments, linear rheology and scattering techniques. *Soft Matter* **2007,** 3, (8), 956.

2. Parker, A.; Fieber, W., Viscoelasticity of anionic wormlike micelles: effects of ionic strength and small hydrophobic molecules. *Soft Matter* **2013,** 9, (4), 1203-1213.

3. Chu, Z.; Dreiss, C. A.; Feng, Y., Smart wormlike micelles. *Chem Soc Rev* **2013,** 42, (17), 7174-203.

4. Shibaev, A. V.; Molchanov, V. S.; Philippova, O. E., Rheological Behavior of Oil-Swollen Wormlike Surfactant Micelles. *J Phys Chem B* **2015,** 119, (52), 15938-46.

5. Kumar, S.; Bansal, D.; Kabir-ud-Din*, Micellar growth in the presence of salts and aromatic hydrocarbons: influence of the nature of the salt. *Langmuir* **1999,** 15, (15), 4960-4965.

6. Sharma, S. C.; Acharya, D. P.; Aramaki, K., Viscoelastic micellar solutions in a mixed nonionic fluorinated surfactants system and the effect of oils. *Langmuir* **2007,** 23, (10), 5324-5330.

7. Shibaev, A. V.; Tamm, M. V.; Molchanov, V. S.; Rogachev, A. V.; Kuklin, A. I.; Dormidontova, E. E.; Philippova, O. E., How a viscoelastic solution of wormlike micelles transforms into a microemulsion upon absorption of hydrocarbon: new insight. *Langmuir* **2014,** 30, (13), 3705-14.

8. Afifi, H.; Karlsson, G.; Heenan, R. K.; Dreiss, C. A., Structural transitions in cholesterol-based wormlike micelles induced by encapsulating alkyl ester oils with varying architecture. *J Colloid Interface Sci* **2012,** 378, (1), 125-34.

9. Salager, J.-L.; Antón, R. E.; Sabatini, D. A.; Harwell, J. H.; Acosta, E. J.; Tolosa, L. I., Enhancing solubilization in microemulsions—state of the art and current trends. *Journal of surfactants and detergents* **2005,** 8, (1), 3-21.

10. Witthayapanyanon, A.; Harwell, J. H.; Sabatini, D. A., Hydrophilic-lipophilic deviation (HLD) method for characterizing conventional and extended surfactants. *J Colloid Interface Sci* **2008,** 325, (1), 259-66.

11. Witthayapanyanon, A.; Phan, T. T.; Heitmann, T. C.; Harwell, J. H.; Sabatini, D. A., Interfacial properties of extended-surfactant-based microemulsions and related macroemulsions. *Journal of surfactants and detergents* **2010,** 13, (2), 127-134.

12. Croce, V.; Cosgrove, T.; Dreiss, C. A.; King, S.; Maitland, G.; Hughes, T., Giant micellar worms under shear: a rheological study using SANS. *Langmuir* **2005,** 21, (15), 6762-6768.

13. Israelachvili, J. N., *Intermolecular and surface forces*. Academic press: 2011.

14. Rosen, M. J.; Kunjappu, J. T., *Surfactants and interfacial phenomena*. John Wiley & Sons: 2012.

15. Cates, M. E.; Fielding, S. M., Rheology of giant micelles. *Advances in Physics* **2006,** 55, (7-8), 799-879.

16. Raghavan, S. R.; Feng, Y., Wormlike Micelles: Solutions, Gels, or Both? In *Wormlike Micelles*, 2017; pp 9-30.

17. Acosta, E. J.; Bhakta, A. S., The HLD-NAC Model for Mixtures of Ionic and Nonionic Surfactants. *Journal of Surfactants and Detergents* **2008,** 12, (1), 7-19.

18. Budhathoki, M.; Hsu, T.-P.; Lohateeraparp, P.; Roberts, B. L.; Shiau, B.-J.; Harwell, J. H., Design of an optimal middle phase microemulsion for ultra high saline brine using hydrophilic lipophilic deviation (HLD) method. *Colloids and Surfaces A: Physicochemical and Engineering Aspects* **2016,** 488, 36-45.

19. Kiran, S. K.; Acosta, E. J., Predicting the morphology and viscosity of microemulsions using the HLD-NAC model. *Industrial & Engineering Chemistry Research* **2010,** 49, (7), 3424-3432.

20. Croce, V.; Cosgrove, T.; Maitland, G.; Hughes, T.; Karlsson, G., Rheology, cryogenic transmission electron spectroscopy, and small-angle neutron scattering of highly viscoelastic wormlike micellar solutions. *Langmuir* **2003,** 19, (20), 8536-8541.

21. Berret, J.-F., Rheology of wormlike micelles: equilibrium properties and shear banding transitions. In *Molecular gels*, Springer: 2006; pp 667-720.

22. Aho, J.; Boetker, J. P.; Baldursdottir, S.; Rantanen, J., Rheology as a tool for evaluation of melt processability of innovative dosage forms. *Int J Pharm* **2015,** 494, (2), 623-42.

23. Oelschlaeger, C.; Waton, G.; Candau, S., Rheological behavior of locally cylindrical micelles in relation to their overall morphology. *Langmuir* **2003,** 19, (25), 10495-10500.

24. Faetibold, E.; Waton, G., Dynamical properties of wormlike micelles in the vicinity of the crossover between dilute and semidilute regimes. *Langmuir* **1995,** 11, (6), 1972-1979.

25. Kumar, R.; Kalur, G. C.; Ziserman, L.; Danino, D.; Raghavan, S. R., Wormlike micelles of a C22-tailed zwitterionic betaine surfactant: from viscoelastic solutions to elastic gels. *Langmuir* **2007,** 23, (26), 12849-12856.

26. Raghavan, S. R.; Kaler, E. W., Highly viscoelastic wormlike micellar solutions formed by cationic surfactants with long unsaturated tails. *Langmuir* **2001,** 17, (2), 300-306.

27. Chu, Z.; Feng, Y.; Su, X.; Han, Y., Wormlike micelles and solution properties of a C22-tailed amidosulfobetaine surfactant. *Langmuir* **2010,** 26, (11), 7783-91.

28. McCoy, T. M.; Valiakhmetova, A.; Pottage, M. J.; Garvey, C. J.; Campo, L.; Rehm, C.; Kuryashov, D. A.; Tabor, R. F., Structural Evolution of Wormlike Micellar Fluids Formed by Erucyl Amidopropyl Betaine with Oil, Salts, and Surfactants. *Langmuir* **2016,** 32, (47), 12423-12433.

29. Siriwatwechakul, W.; LaFleur, T.; Prud'homme, R. K.; Sullivan, P., Effects of organic solvents on the scission energy of rodlike micelles. *Langmuir* **2004,** 20, (21), 8970-8974.

30. May, S.; Ben-Shaul, A., Molecular packing in cylindrical micelles. *SURFACTANT SCIENCE SERIES* **2007,** 140, 41.

31. Fu, Y.; Liang, D.; Abdunaibe, A.; Li, H.; Yan, H.; Wang, H., Viscoelasticity enhancement induced by salts for highly concentrated oil-in-water (O/W) emulsions. *Colloids and Surfaces A: Physicochemical and Engineering Aspects* **2017,** 513, 280-286.

32. Oelschlaeger, C.; Suwita, P.; Willenbacher, N., Effect of counterion binding efficiency on structure and dynamics of wormlike micelles. *Langmuir* **2010,** 26, (10), 7045-53.

33. Mu, J.-H.; Li, G.-Z.; Jia, X.-L.; Wang, H.-X.; Zhang, G.-Y., Rheological properties and microstructures of anionic micellar solutions in the presence of different inorganic salts. *The Journal of Physical Chemistry B* **2002,** 106, (44), 11685-11693.

34. Trickett, K.; Eastoe, J., Surfactant-based gels. *Advances in colloid and interface science* **2008,** 144, (1-2), 66-74.

35. Rogers, S. A.; Calabrese, M. A.; Wagner, N. J., Rheology of branched wormlike micelles. *Current Opinion in Colloid & Interface Science* **2014,** 19, (6), 530-535.

Chapter 6 Conclusions and recommendations

Overall, this dissertation examined potential alternatives in conventional surfactant flooding process, via injecting nanoparticle-surfactant blends or single slug surfactant-based viscoelastic slug to improve ultimate oil recovery.

Chapter 2 and 3 proposed of using carbonaceous nanoparticles, e.g., multiwalled carbon nanotubes (MWNTs) and carbon blacks as surfactant carriers in reservoir applications. Competitive adsorption of surfactant on nanoparticles was seen beneficial to decrease adsorptive loss on porous medium at equilibrium concentration below critical micelle concentration (CMC). Binary anionic-nonionic surfactants mixture at a proper ratio were proved exceptional disperse agent for nanoparticles and their transport in porous media in mimic reservoir condition. Microemulsion phase behavior confirmed the spontaneous release of surfactants from carrier surface to oil/water interface. Nanoparticles-amended surfactant formulations achieved faster and higher tertiary oil recovery than surfactant-only formulation. Chapter 4 illuminated the reversed binary micellar interactions between anionic surfactant alpha olefin sulfonate (AOS) and nonionic surfactant nonylphenol polyethylene glycol ether (NPEs) with/without the addition of electrolytes. In the absence of additional electrolytes, NPEs exhibited substantially higher activity in micelles than bulk solution; with growth of EO groups, shrinkage on the scale of synergistic interaction was evidenced. In contrary, with swamping amount of electrolytes, synergistic interactions enlarged with the rise of EO groups, and AOS activity in mixed micelles was found depending on both EO length and bulk mole fraction (α_A). Chapter 5 discovered an oil-induced viscoelastic wormlike micellar solution of an extended surfactant. Contrary to typical oleo-responsive wormlike micelles, that worms break with addition

of oil, solubilized oil was seen able to shift the oil-free Newtonian micellar solution to an exceptional viscoelastic fluid. This unique formulation was reformed form Winsor III microemulsion, which acquired capacity in improving both the volumetric sweep efficiency and microscopic displacement efficiency. Residual oil recovery test proved its potential of serving as an alternative in surfactant flooding process.

Advantages of nanoparticles-amended surfactant formulations as well as surfactant-based viscoelastic fluid over conventional surfactant slug were well demonstrated in this work. Here some future studies are recommended to better understand the mechanisms behind these advanced technologies as well as to pave the way for potential field applications.

1. So far, stability of MWNT dispersions are largely dependent on laboratory phase behavior studies. A quantitative tool that describes the interaction between these cylindrical nanosized particles is of critical importance to predict the colloidal stability in aqueous media. The future work is suggested to improve the current mathematical model DLVO theory, by incorporating particles geometry consideration, i.e., cylindrical structure, thus to assist in designing a well-dispersed colloidal system.
2. It has been observed, that release of surfactants from nano-carrier surface may worsen the stability of nano-carrier, and lead to possible formation damage. Thus, later study is aimed to tailor the surface of carbonaceous nanoparticle by introducing functional groups to improve colloidal stability of nanoparticles in aqueous media. These groups should be able to provide stability for dispersed nanoparticles after surfactants are released from their surface, thus to ensure the transport of nanoparticles, especially in tight rock matrix.

3. The interfacial interaction of binary surfactant mixtures, e.g., air/water interface, are of great significance in designing a successful foam flooding pattern, in that synergistic interactions in mixed surfactants would lead to less chemical consumptions and project costs. Although micellar interaction between binary components are well studied both theoretically and experimentally, a profound understanding of interfacial interaction is somewhat neglected. Based on Rubingh's regular solution theory, Rosen and coworkers modified this simple model to describe the interfacial interactions of a binary system. However, this modified model failed to capture the variation of interaction between NPE-AOS mixtures with respect to the size of EO groups (not documented in this dissertation). It is thus suggested to advance understanding of the mechanism of interfacial interactions under the impact of surfactants structure, and to develop a simple model in the future to assist in designing/optimizing the foam flooding formula.
4. Oil-induced (oil-resistant) wormlike micellar solution has potential serving in reservoirs applications. The future work is recommended to comprehensively examine the feasibility of using oil-induced viscoelastic fluid as fracking fluids. Besides, it is suggested to study the impact of adding other surfactants on the rheological behavior of viscoelastic fluids. A synergistic system would be beneficial to reduce the chemical consumptions and project costs.

Appendix A

Table A1. Structures of surfactants

Abbreviation	Generic name	Trade name	Molecular Weight	Hydrophilic-lipophilic balance (HLB)	Critical Micelle Concentration, mg/L	Structure
$C_{12-13}(PO)_4SO_4Na$	Branched Alkyl Propoxy Sulfates	Alfoterra 123-4s	527			$CH_3(CH_2)_{11-12}O(C_3H_6O)_4SO_3Na$
$C_{12-13}(PO)_8SO_4Na$	Branched Alkyl Propoxy Sulfates	Alfoterra 123-8s	759			$CH_3(CH_2)_{11-12}O(C_3H_6O)_8SO_3Na$
SDDPDS	Sodium Dodecyl Diphenyl Oxide Disulfonate	Calfax DB-45	542		70 @25 °C in 0.1M NaCl	$C_{12}H_{25}O(C_6H_4SO_3Na)_2$
$C_{12}(EO)_3SO_4Na$	Sodium Laureth Sulfate	Steol CS-460	420		74	$CH_3(CH_2)_{10}CH_2(OCH_2CH_2)_3OSO_3Na$
$C_{12}EOSO_4Na$	Sodium Laureth Sulfate	Steol CS-130	332		167	$CH_3(CH_2)_{10}CH_2(OCH_2CH_2)OSO_3Na$
NP10EO	Nonylphenol Ethoxylates	Surfonic N-100	660	13.3	50	$C_9H_{19}C_6H_4(OCH_2CH_2)_{10}OH$
NP20EO	Nonylphenol Ethoxylates	Surfonic N-200	1100	16		$C_9H_{19}C_6H_4(OCH_2CH_2)_{20}OH$
NP30EO	Nonylphenol Ethoxylates	Surfonic N-300	1540	17.1		$C_9H_{19}C_6H_4(OCH_2CH_2)_{30}OH$
NP40EO	Nonylphenol Ethoxylates	Surfonic NB-407	1980	17.8		$C_9H_{19}C_6H_4(OCH_2CH_2)_{40}OH$
LA41EO	Linear Alcohol Ethoxylates	Tergitol 15-s-40	2004	18	2200	$C_{11-15}H_{23-31}O(CH_2CH_2O)_{41}H$

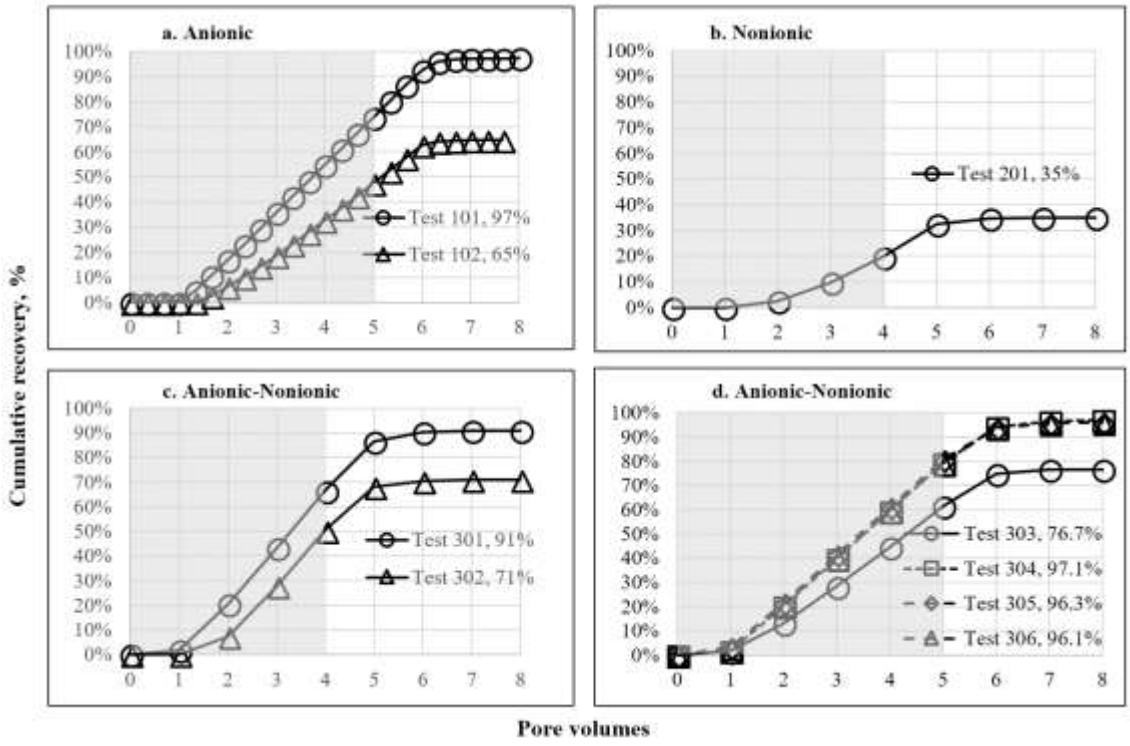

Figure A1. Cumulative recovery vs. pore volumes (shaded area is dispersion injection period) a. Test 101(95 mg/L MWNT with 6 mM IOS, 2.4 mM C12(EO)3SO4Na in DI) and Test 102 (37 mg/L MWNT with 12 mM IOS, 4.8 mM C12(EO)3SO4Na in 5 wt% brine) in 2'' Ottawa sand packs; b. Test 201 (75 mg/L MWNT with 1.25 mM NP40EO in API brine) in 1'' Ottawa sand pack; c. Test 301 in 1'' Ottawa sand pack and Test 302 in 1'' Berea sand pack (77 mg/L MWNT with 6 mM IOS and 1.25 mM NP40EO in API brine); d. Test 303-306 in 1'' Ottawa sand packs (MWNT concentration was 72, 73, 73, and 75 mg/L respectively; surfactants were 1 mM NP40EO with 2, 4, 6, and 8 mM $C_{12,13}(PO)_8SO_4Na$ respectively in API brine)

Appendix B

Table B1. Hydrodynamic diameter of dispersed MWNT and CB with different surfactant formulations in 3 wt% brine by dynamic light scattering (DLS). Formulation 1. 1000 mg/L NP30EO, 2. 1000 mg/L NP30EO with 1000 mg/L AOS, 3. 1000 mg/L NP40EO, 4. 1000 mg/L NP40EO with 1000 mg/L AOS.

Batch		Diameter, nm	Polydispersity	Diameter, nm	Polydispersity
	Formulation	Initial		Day 3 (50 °C)	
	1	162	0.196	217	0.211
MWNT	2	229	0.214	421	0.290
	3	165	0.172	175	0.200
	4	190	0.213	254	0.251
	Formulation	Initial		Day 3 (60 °C)	
	1	124	0.142	124	0.153
CB	2	124	0.110	129	0.137
	3	121	0.166	127	0.186
	4	126	0.129	128	0.108

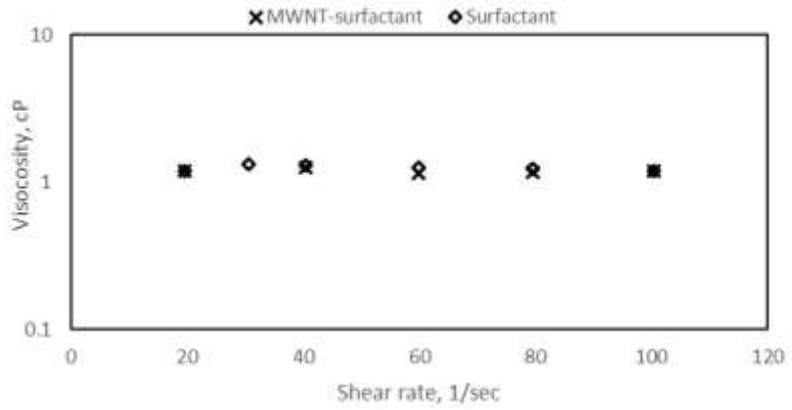

Figure B1. Viscosity of surfactant only and MWNT-surfactant formulation as a function of shear rate.

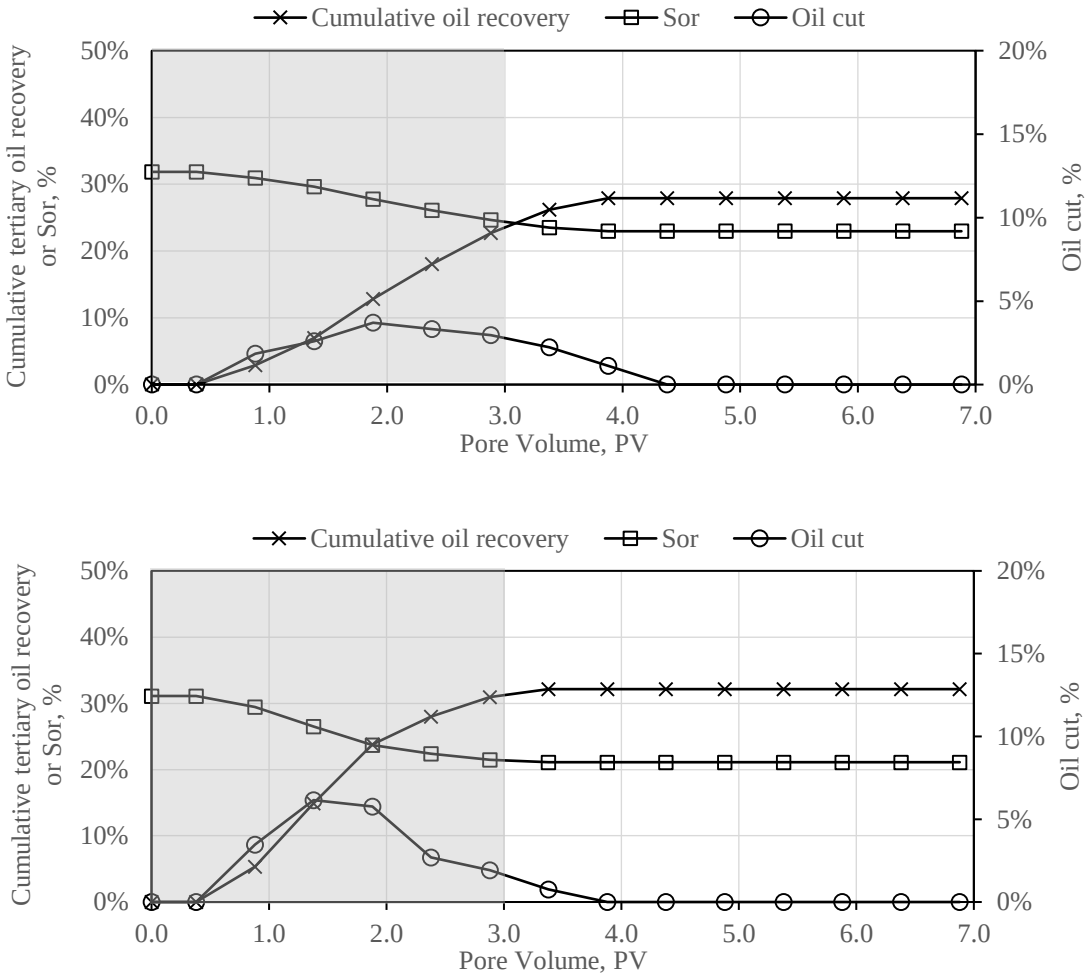

Figure B2. Tertiary oil recovery after injection of 3 PVs chemical slug (shaded area) in 0.1 wt% NaCl solution at 25 ºC. Top, Surfactant-only NP10EO slug at concentration of 0.1 wt%, initial Sor was 31.9%, and cumulative oil recovery was 27.9%; Bottom, 0.1 wt% NP10EO slug with 200 mg/L CB, initial Sor was 31.1%, and cumulative oil recovery was 32.1%

Appendix C

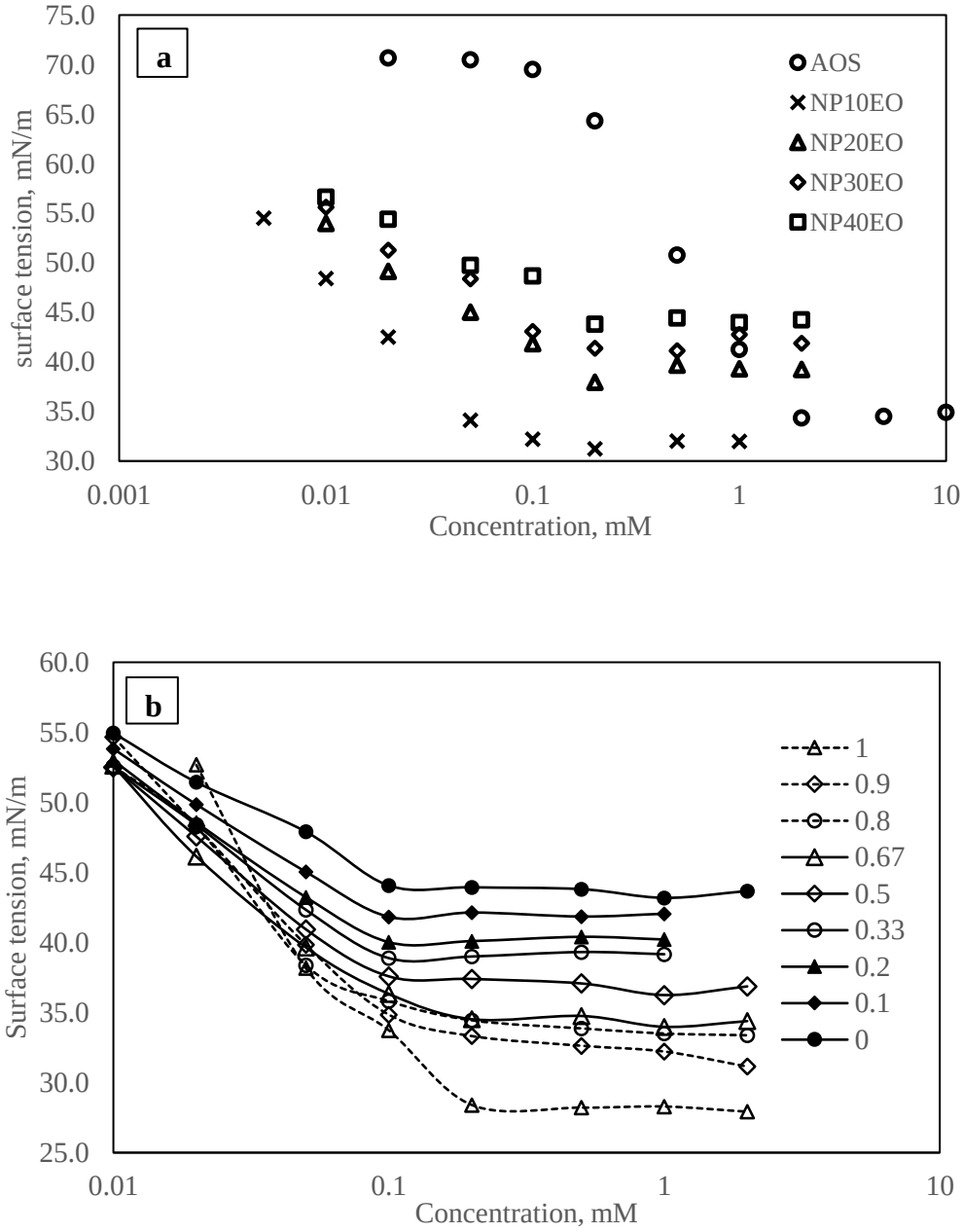

Figure C1. Surface tension vs surfactant concentration at 25ºC (a) individual surfactant in DI; (b) binary mixture of AOS and NP30EO in 0.5 M NaCl with legend indicating fraction of AOS.

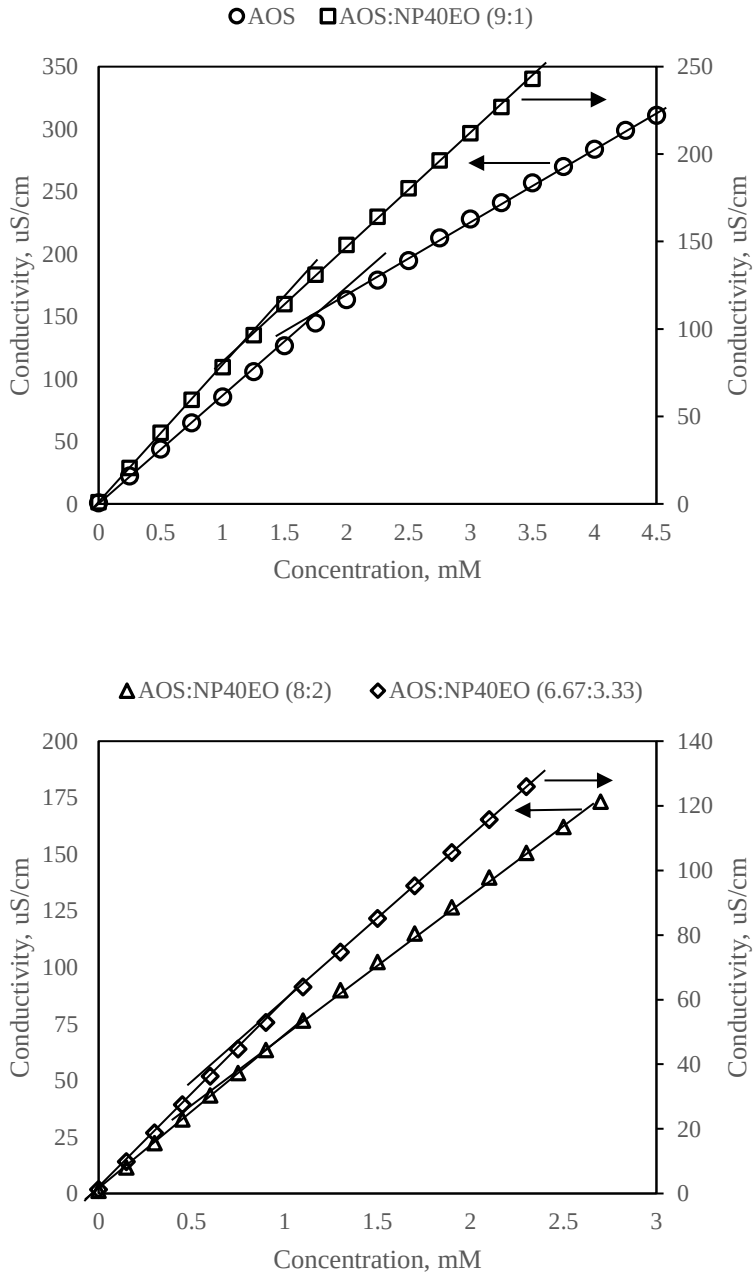

Figure C2. Conductivity vs surfactant concentration at 25ºC in DI.

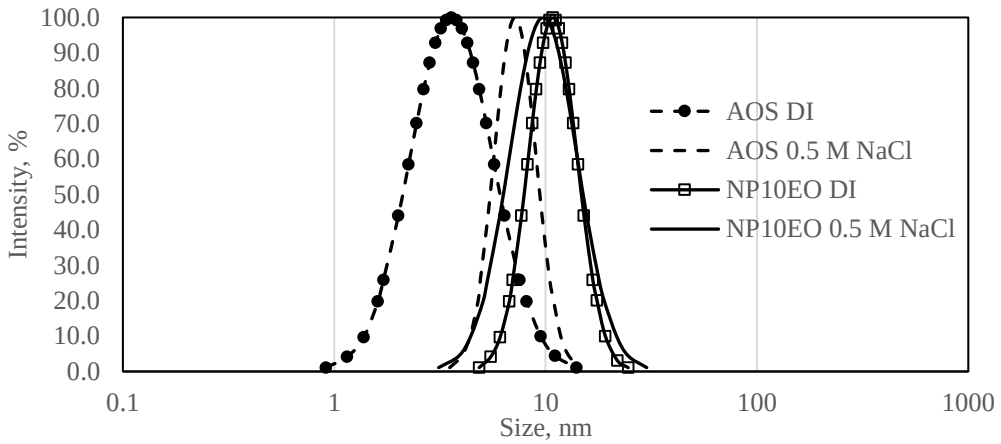

Figure C3. Size distribution by intensity of individual surfactant AOS, NP10EO in DI and 0.5 M NaCl solution.

Appendix D

The surfactant head area is estimated graphically from a plot of Gibbs adsorption isotherm using Gibbs adsorption equation,

$$\Gamma = -\frac{1}{2.303nRT}\left(\frac{\partial\gamma}{\partial log C}\right)_T$$

$$a_s = \frac{10^{21}}{N_A\Gamma}$$

where Γ is surface excess concentration in mM/m^2, R, universal gas constant 8.314J/mol-K, T temperature in K, γ surface tension in mN/m, C is surfactant concentration in mol/L, a_s is area per molecule at the interface in nm^2, and N_A is Avogardo's number. n is the number of species of ions that arise from dissociation of surfactant, and its value largely depends on electrolytes, e.g. n is 1 for monomeric surfactant in the presence of a swamping (elevated) amount of electrolytes; n is taken as 2 represents for monomeric surfactant without extra electrolytes.

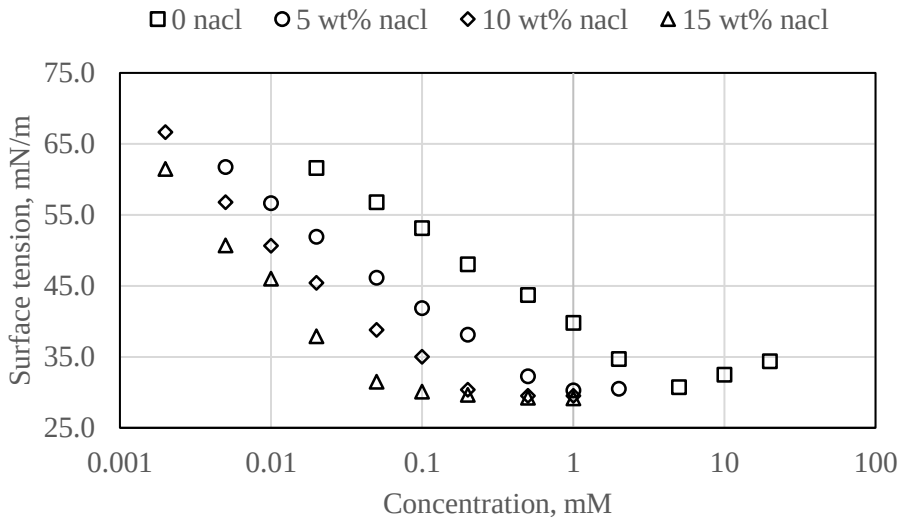

Figure D1. Variation of surface tension with respect to concentration of $C_8P_4E_1$ solution at different salinities.

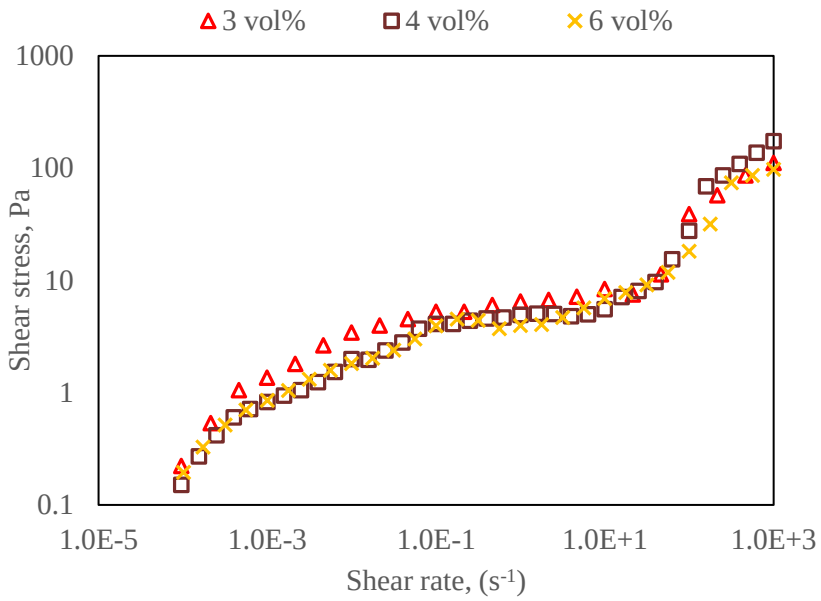

Figure D2. Shear stress as a function of shear rate for 2 wt% $C_8P_4E_1$ solution with 3-6 vol% of Isopar at optimum salinity of 19 wt% salt.

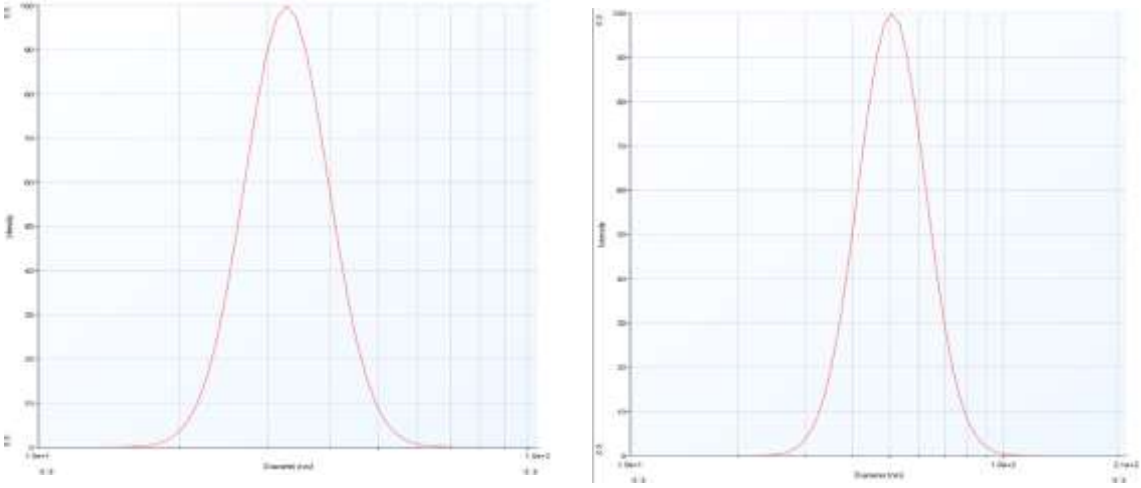

Figure D3. Dynamic light scattering hydrodynamic diameter of Winsor I microemulsion, octane in 2 wt% $C_8P_4E_1$ solution at salt level 13.3 wt% (left), and 14.4 wt% (right).

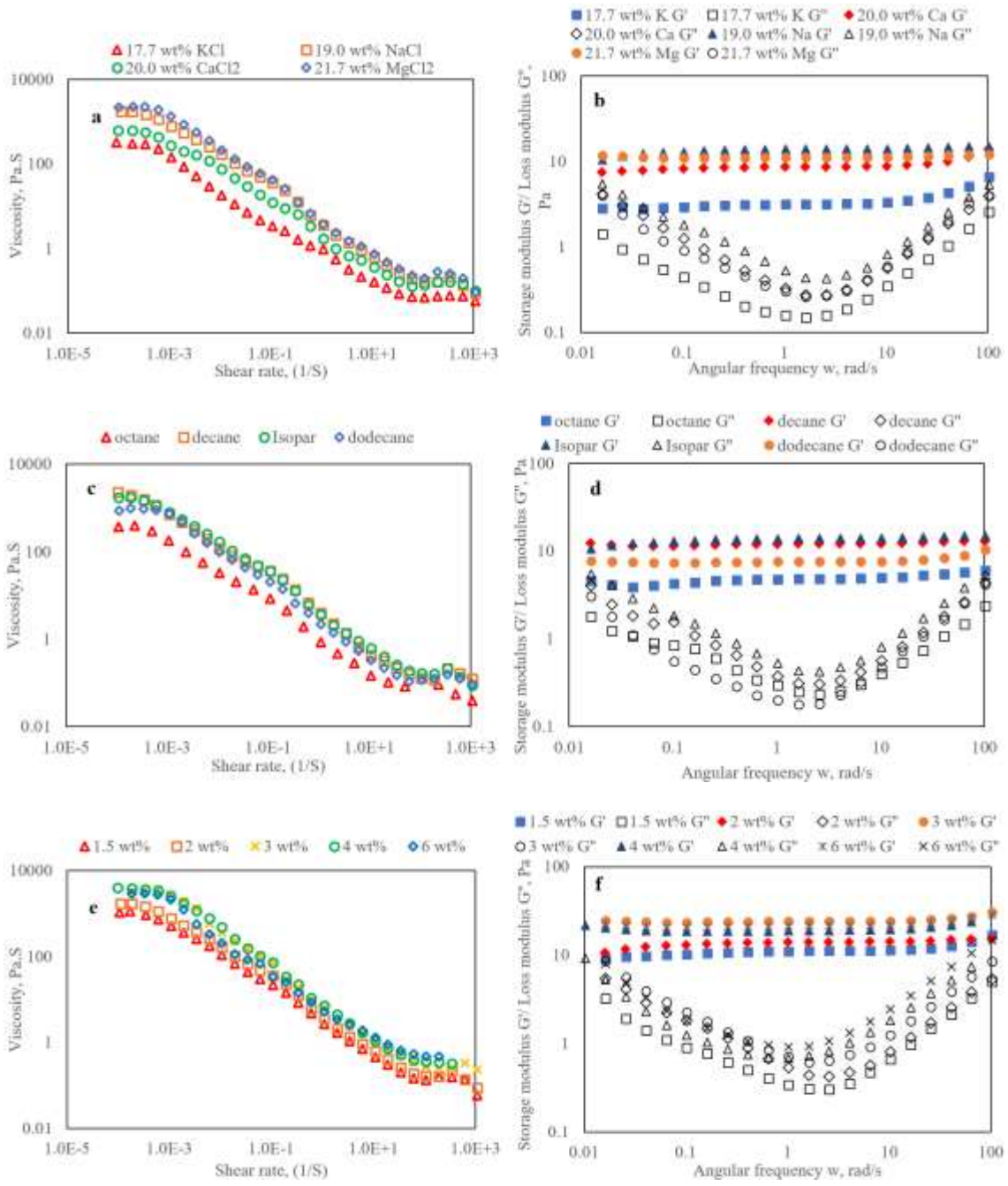

Figure D4. Steady shear viscosity as a function of shear rate for (a) 2 wt% $C_8P_4E_1$ solution with 6 vol% of Isopar and different salt at their optimum salinities (NaCl 19.0 wt%, KCl 17.7 wt%, CaCl2 20.0 wt%, MgCl2 21.7 wt%), (c) 2 wt% $C_8P_4E_1$ solution with 6 vol% of various oil at their optimum salinities (octane 16.3 wt%, decane 18.4 wt%, Isopar 19.0 wt%, dodecane 19.3 wt%), (e) various concentration of $C_8P_4E_1$ solution with 6 vol% of Isopar at 19 wt% salt. Variation of storage modulus G' (filled symbols) and loss modulus G'' (open symbols) as a function of oscillatory shear frequency for (b) 2 wt% $C_8P_4E_1$ solution with 6 vol% of Isopar and different salt at their optimum salinities, (d) 2 wt% $C_8P_4E_1$ solution with 6 vol% of

various oil at their optimum salinities, (f) various concentration of $C_8P_4E_1$ solution with 6 vol% of Isopar at 19 wt% salt.

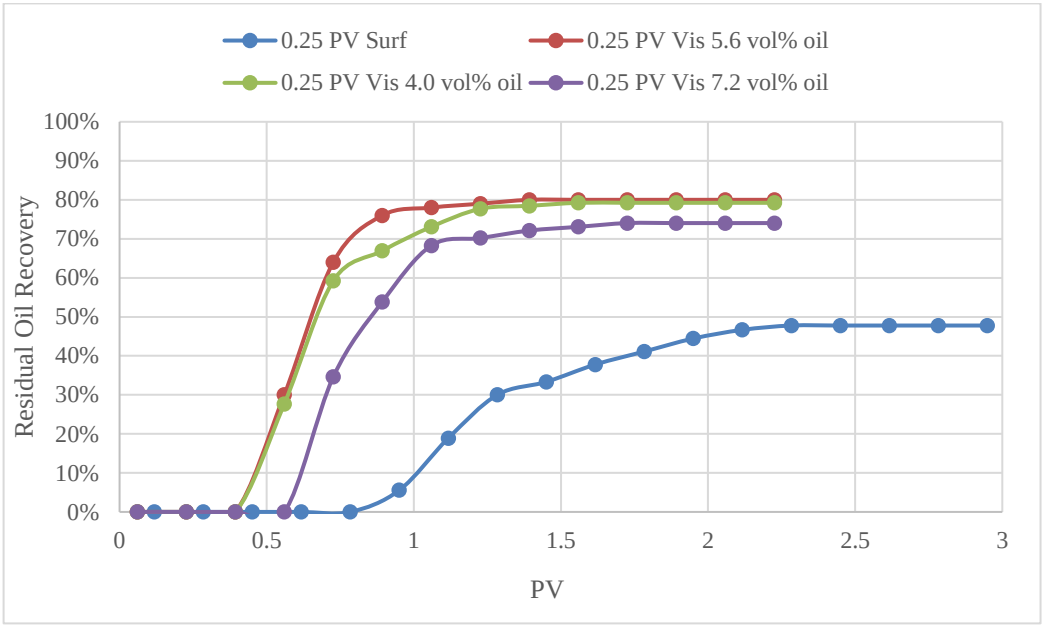

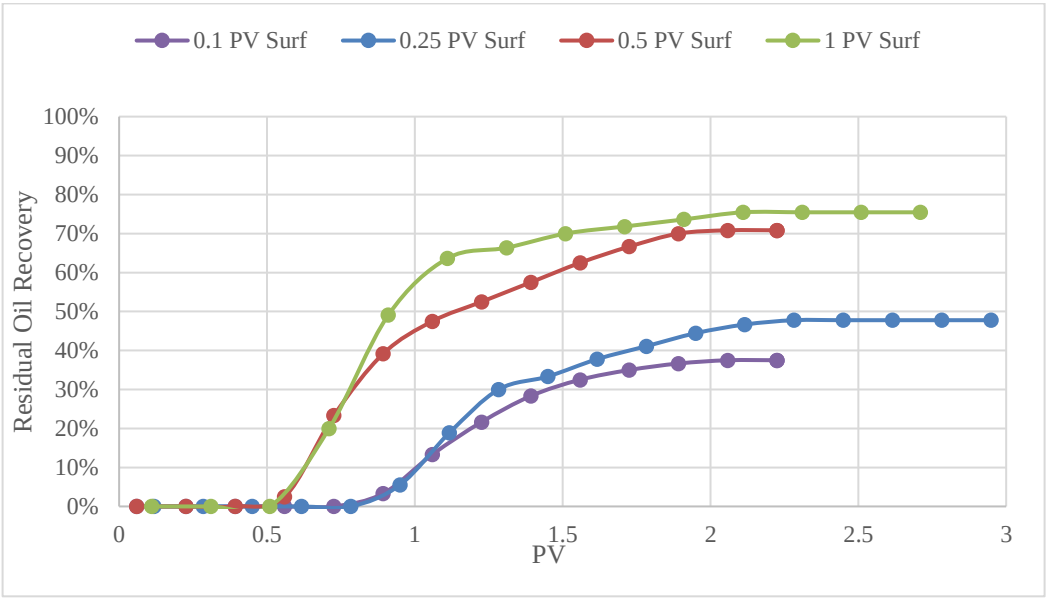

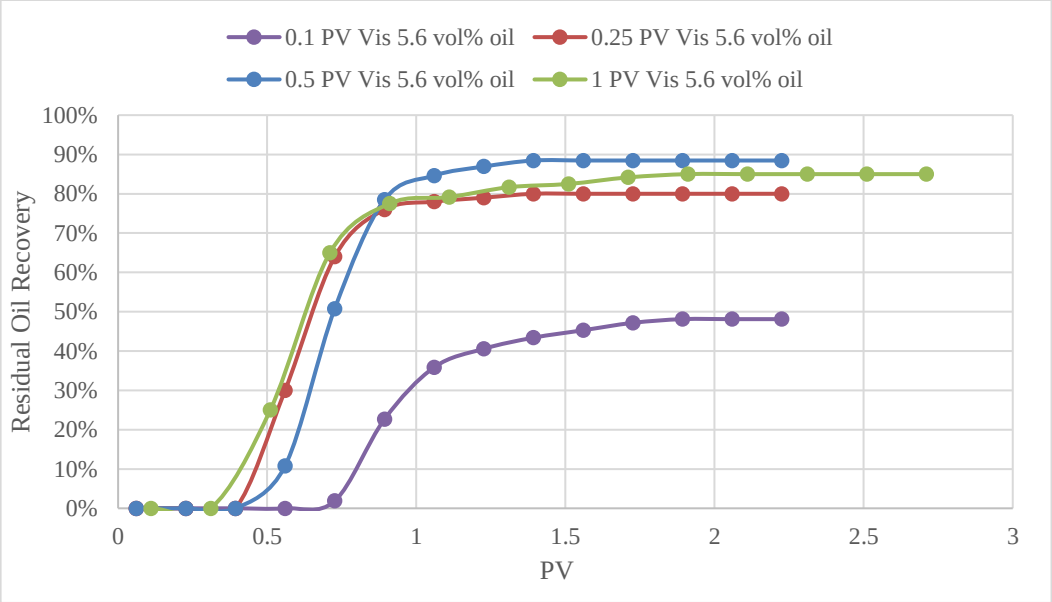

Figure D5. Impact of chemical slug size and solubilized oil concentration in viscoelastic fluid on residual oil recovery. Surf for 2 wt% $C_8P_4E_1$ surfactant-only slug, and Vis for 2 wt% $C_8P_4E_1$ viscoelastic fluid slug.